IEEE Access
Multidisciplinary | Rapid Review | Open Access Journal

Received October 5, 2021, accepted October 13, 2021, date of publication October 15, 2021, date of current version October 26, 2021.

Digital Object Identifier 10.1109/ACCESS.2021.3120803

Low Voltage Distribution Networks Modeling and Unbalanced (Optimal) Power Flow: A Comprehensive Review

IBRAHIM ANWAR IBRAHIM[1,2], (Member, IEEE), AND M. J. HOSSAIN[3], (Senior Member, IEEE)

[1]School of Engineering, Macquarie University, Sydney, NSW 2109, Australia
[2]CSIRO Energy Centre, Mayfield West, NSW 2300, Australia
[3]School of Electrical and Data Engineering, University of Technology Sydney, Sydney, NSW 2007, Australia

Corresponding author: Ibrahim Anwar Ibrahim (ibrahim.a.ibrahim@hdr.mq.edu.au; ibrahim.a.ibrahim@ieee.org)

ABSTRACT The rapid increase of distributed energy resources (DERs) installation at residential and commercial levels can pose significant technical issues on the voltage levels and capacity of the network assets in distribution networks. Most of these issues occur in low-voltage distribution networks (LVDNs) or near customer premises. A lack of understanding of the networks and advanced planning approaches by distribution network service providers (DNSPs) has led to rough estimations for maximum DERs penetration levels that LVDNs can accommodate. These issues might under- or over-estimate the actual hosting capacity of the LVDNs. Limited available data on LVDNs' capacity to host DERs makes planning, installing, and connecting new DERs problematic and complex. In addition, the lack of transparency in LVDNs' data and information leads to model simplifications, such as ignoring the phase imbalance. This can lead to grossly inaccurate results. The main aim of this paper is to enable the understanding of the true extent of local voltage excursions to allow more targeted investment, improve the network's reliability, enhance solar performance distribution, and increase photovoltaic (PV) penetration levels in LVDNs. Therefore, this paper reviews the state-of-the-art best practices in modeling unbalanced LVDNs as accurately as possible to avoid under- or over-estimation of the network's hosting capacity. In addition, several PV system modeling variations are reviewed, showing their limitations and merits as a trade-off between accuracy, computational burden, and data availability. Moreover, the unbalanced power flow representations, solving algorithms, and available tools are explained extensively by providing a comparative study between these tools and the ones most commonly used in Australia. This paper also presents an overview of unbalanced optimal power flow representations with their related objectives, solving algorithms, and tools.

INDEX TERMS Power distribution networks, phase unbalanced, power flow, mathematical optimization, inverter control, smart grid.

I. INTRODUCTION

The increased installation of low-carbon technologies, (e.g., solar photovoltaic (PV) systems, electric vehicles (EVs), storage batteries, and heat pumps), affects power systems' development and operations. These technologies are mostly integrated into the distribution networks, and they can be flexible and controlled remotely. Besides, the customers' behaviour is more visible with the increased use of smart meters, which provide more granular data. Usually, the distribution networks are managed by the distribution network service providers (DNSPs) using a passive 'fit-and-forget' approach. Because of the increased use of low-carbon technologies and data available from smart meters, DNSPs realize that they can take more active approaches to effectively manage and operate the distribution networks. These active approaches require support tools for decision making which facilitate the coordination between all the connected devices in the distribution networks, such as inverters, battery systems, and on-load tap changers, among others.

The associate editor coordinating the review of this manuscript and approving it for publication was Akin Tascikaraoglu.

Advanced distribution management systems (ADMSs) are a promising platform for developing decision support tools. ADMSs can deploy the gathered data from the DNSPs' subsystems and use them for coordinating the operation of the connected devices in the distribution networks [1]. DNSPs will enhance the power quality and availability of the energy sources and manage the costs by deploying ADMSs. State estimation can also be one of the key tools in reliable and safe transmission systems [2].

Accordingly, accurate models for the low-voltage distribution networks' (LVDNs') models are required for (i) assisting in estimating the hosting capacity of the existing assets, in future planning and upgrading the infrastructure to accommodate the new loads, and in the integration of the distributed energy resources (DERs); (ii) modeling the impact of low-carbon technologies; and (iii) mitigating the growth scenarios of integrating these low-carbon technologies. The investment in upgrading the existing infrastructure in the LVDNs is very high; therefore, precise models are targeted to inform planning the infrastructure development. Until recently, modeling the LVDNs was compromised as the data available to characterize the load data were limited, even without connecting the DERs. Comprehensive measurement of the data was constrained as there are many loads connected to the LVDNs, and the voltage monitoring equipment has few locations at which to be connected. A lack of computer capability also restricted the quality of power flow (PF) simulations to process big data. Nowadays, some of the limitations in accurate modeling of LVDNs have been resolved [3]. The computers' capability is much better in terms of processing power, and more monitoring equipment, such as smart meters, is installed to track the behaviour of the loads. The availability of data with accurate models of the LVDNs can, for example, allow optimization of the voltage level in the substation, which increases its capacity, with the voltages at the loads' side still operating within limits [4], [5].

A further difficulty in modeling the LVDNs is that the assumptions utilized in modeling the transmission systems are not applicable. In transmission systems, the load is assumed to vary smoothly with time and is thus highly aggregated. This load can be forecasted from the daily load profile. It is also assumed that the imbalance between the three phases is minimal, which is not applicable in modeling LVDNs as the loads are arbitrarily connected between phases, creating highly unbalanced cases. Moreover, the harmonics distortion is assumed to be relatively low even in LVDNs, but with the increased use of power electronics converters, this is no longer the case. Finally, the PV systems' planning was assumed to be carried out for the worst-case scenario, in which there existed the highest possible generation from PV systems and the lowest expected demand. However, in reality, the probability of these two extreme scenarios occurring at the same time is rare; therefore, the planning of the PV systems may be oversized, creating further power quality issues in the feeder [3].

Transparency in the data and models will lead to accurate development of the tools and technologies for decarbonization [5]. Therefore, the tools and knowledge that have been utilized for planning should be subject to scrutiny. Open access to the tools, models, and data will reduce research effort and development duplication, increasing the quality of research outputs, and their legitimacy and credibility [5], [6]. Accordingly, several developers offered their distribution network simulation tools and models as open accessible for all researchers and engineers, such as the Open Distribution System Simulator (OpenDSS) [7] and Gridlab-D. However, distribution-focused generalizations about optimal power flow (OPF) are still currently evolving, and their development faces some significant challenges.

According to the literature review, it is concluded that (i) LVDNs require new techniques, technologies, and tools to facilitate the rapid development of the network; (ii) the new technologies can play a crucial role in saving expenses, but they may drive the system nearer to its limits; (iii) DNSPs' target is to reach a level of quality and reliability of supply or exceed it; and (iv) DNSPs are looking for solutions to enable high PV penetration levels without breaching the network limits and without any extra investments. Here, to achieve the points mentioned above, efficient decision-making tools aimed to take into account the technical and physical limits of the LVDNs are required. In this paper, the mathematical models are reviewed of the components for representing and optimizing the LVDNs which require automating decision-making. Several review and survey research works are published in this field, including [1], [8]–[10]. In addition, the impacts of PV systems on the LVDNs along with the traditional and non-traditional solutions to reduce these impacts and increase the PV penetration levels in LVDNs are reviewed. Several review and survey research works are also published in this field, including [11]–[13].

This paper focuses on (i) the mathematical modeling of LVDNs including their main components, such as lines, transformers, generators, loads, PV systems, and inverters; (ii) distributed optimization and control of the PV systems using smart inverter techniques; (iii) the translation of the mathematical models of LVDNs' components into a well-defined mathematical optimization problem; (iv) unbalanced PF representations based on the π-equivalent line model with several solving algorithms and tools; (v) several objectives related to the OPF problems with several solving algorithms and tools; (vi) the impacts of high PV penetration levels on LVDNs, the limitations of enabling high PV penetration levels, and the traditional and non-traditional solutions; and (vii) the research gaps and research directions that are addressed in this paper to enable high PV penetration levels together with solving the common DNSPs' concerns. Some research topics are not considered in this paper, such as distributed controllers with potential improvements in communication coordination systems, their computational requirements, and cybersecurity. Moreover,

meta-heuristic-based optimization methods to solve the (O)PF by proposing alternative solutions instead of traditional optimization algorithms are not considered in this paper.

The rest of this paper is organized as follows: Section II covers the best practices to model the components in LVDNs, including notation and preliminaries in Subsection II-A, the foundations of modeling LVDNs in Subsection II-B, scalars and matrix variables in modeling LVDNs in Subsection II-C, variable bounds in Subsection II-D and the models of the components in Subsection II-E. Here, the models of the components discussed in this paper include the bus model, line model, transformers and ideal tap changer models, loads, generators, PV systems (i.e., inverters, smart inverter controls, and PV modules), and shunts. In addition, the delta- and wye-connection configurations of loads, generators, and PV systems, as well as Kirchhoff's current law (KCL), are described in this section. Moreover, the accuracy of the aforementioned models and the importance of unbalanced modeling to represent the LVDNs as accurately as possible are outlined in Subsection II-G.

In addition, Section III comprises a description of the unbalanced PF equation models, algorithms used to solve the PF equations, and the available tools (e.g., software and packages) to represent and solve the distribution unbalanced PF equations. In this, Subsection III-A is a discussion of the branch flow model and the bus injection model for several coordinate LVDNs. Subsection III-B consists of an explanation of the meta and concert algorithms used for solving PF equations, including Newton-based methods, the fixed-point iteration method as meta algorithms, and the backward-forward sweep algorithm, continuation (predictor-corrector Euler homotopy) algorithm, current injection algorithm, and holomorphic embedding algorithm as concert algorithms. Subsection III-C covers the software and packages available to represent and solve unbalanced PF equations. This includes DIgSILENT PowerFactory, PSS/Sincal, CYMDIST, Open Distribution System Simulator (OpenDSS), GridLAB-D, and Open Platform for Energy Networks (OPEN). In addition, the subsection concludes with a summary and comparisons of the reviewed PF tools.

The unbalanced OPF in LVDNs is described in Section IV, which includes the most common objectives, algorithms, relaxation and approximation, and tools that are utilized to solve OPF problems. Here, Subsection IV-A lists the commonly used objectives for solving OPF equations, including network losses, generation cost, cost of consumption, and others. In addition, Subsection IV-B covers the common algorithms that are used to solve OPF problems, including interior point algorithms and sequential quadratic programming algorithms. The relaxation and approximation to solve non-convex OPF problems are discussed in Subsection IV-C. Also, Subsection IV-D consists of a summary of the most commonly used tools for handling optimization problems in unbalanced distribution networks, such as Open-DSOPF and PowerModelsDistribution, and a summary and comparisons of the reviewed OPF tools. Finally, the main findings, research gaps, and the research opportunities covered in this paper are summarized in Section V.

II. MODELING LVDNs

The distribution network is a part of the power system; it is located between the large-scale transmission system and the residential, commercial, and industrial end-users. The distribution network contains two voltage levels, in the medium-voltage (MV) and low-voltage (LV) networks. The general structure and main components of an electric power system can be illustrated in Figure 1. Traditionally, the components of the distribution system are modeled in an inelegant way. Previously, modeling the generation and transmission system components has met many challenges for designing and operating purposes. Nowadays, power plants are becoming more prominent in the system, and transmission takes place through large interconnected networks. Therefore, these sizeable interconnected networks' operation and design have attracted researchers to develop more advanced models and tools for analyzing and operating such systems. However, the distribution systems still deliver power to the ultimate user's meter with limited analysis of the actual amount provided, or none [14].

Accordingly, LVDNs are typically designed to be oversized. The integration of several renewable energy resources rapidly increases the alert for operating LVDNs at their maximum capacity. This alert is the critical drive to accurately model the LVDNs to calculate the exact maximum capacity and efficiently operate the LVDNs within operating limits. In general, the LVDNs start from the step-down distribution substation from MV level to LV level, while it may be fed directly from the sub-transmission lines. However, a high-voltage (HV) transmission line can feed the LVDNs directly without a sub-transmission system. The structure of LVDNs varies based on the DNSPs. Each step-down distribution substation will deliver the power to one or more primary feeders. Radial feeding is the most common type used in LVDNs [15].

The LVDN feeder is inherently imbalanced because of the loading of several unequal single-phase loads or DERs connected arbitrarily on the feeder. The non-equilateral spacing between the three-phase overhead and underground line conductors also introduces an additional imbalance into the network. Several PF tools, which are used to analyze and study transmission systems' behaviour, are not adequate for the LVDNs because these tools assume that the LVDN is perfectly balanced, which is modeled by its components being in a single-phase equivalent system. Therefore, these tools show poor convergence for application to radial LVDNs. To ensure accurate PF analysis, the accurate characterizing of the LVDNs is needed, which can be done by modeling the three-phase models of the components as accurately as possible. Importantly, accurate PF analysis of the LVDNs determines the system's existing operating conditions and simplifies future development by applying ''what if'' scenarios [14]. Accordingly, the key concepts in modeling the

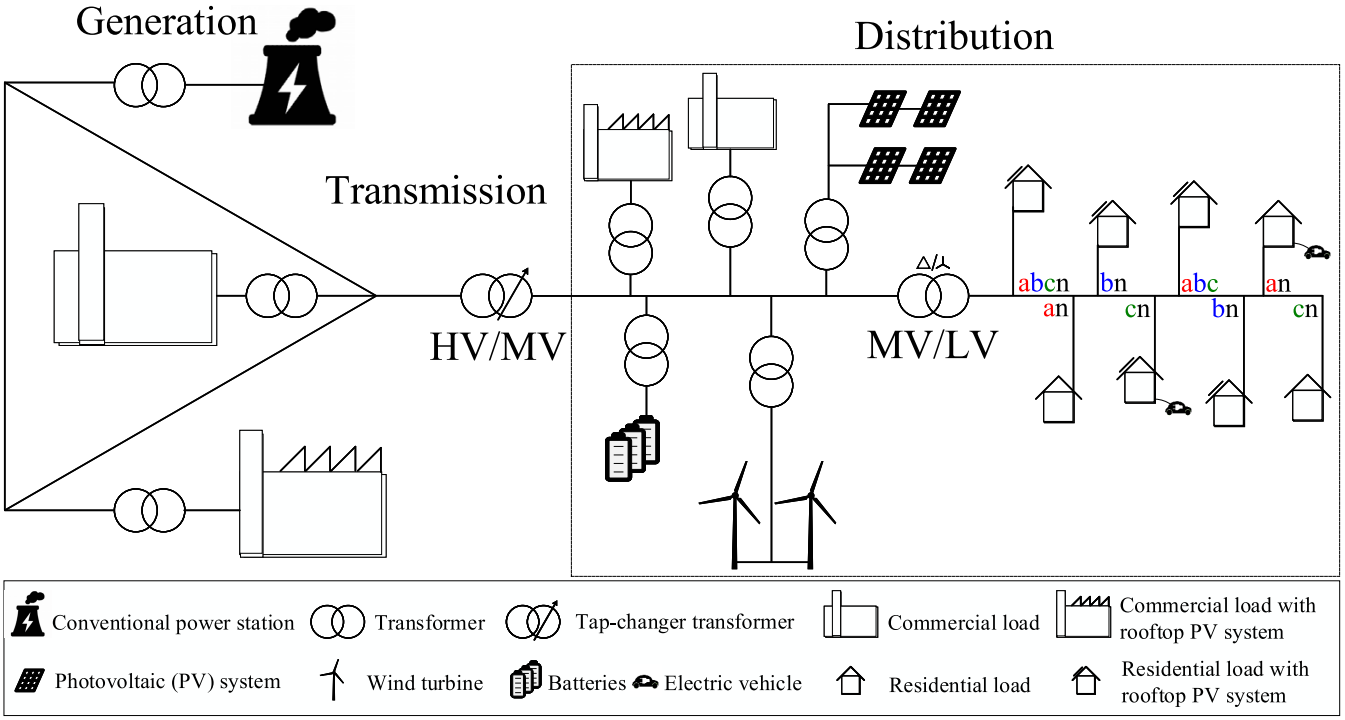

FIGURE 1. A one-line diagram of a distribution network as part of the power system.

components in LVDNs are reviewed in this paper. These are expanded in a discussion of optimization models. However, the accuracy of modeling the LVDNs is investigated and reviewed in-depth in [3].

In this context, this paper focused in reviewing the simple and accurate models for the components of LVDNs as well as have the ability to be generalized. The simplicity here means easy to get the model's parameters from the datasheet and has the compatibility to work with (O)PF model. Complex models such as machine learning models are required huge historical data for training and they are geographical dependent. Therefore, the machine learning- and meta-heuristic-based modeling methods are not considered in this paper.

A. NOTATION AND PRELIMINARIES

The core variables to represent the unbalanced LVDNs are current, impedance and voltage. These variables are defined as a range of matrix, vector and scalar parameters related to grid buses and lines. In general, the network is multi-phase and radial. In addition, a substation bus exists in the network, and is assumed to have a fixed voltage. Accordingly, the one-line diagram of a generic LVDN can be represented as shown in Figure 2.

Based on Figure 2, Table 1 lists the typography and mathematical notation used; Table 2 defines sets and indices; Table 3 defines parameters; and Table 4 defines typical engineering variables.

Here, we used $\leqslant$ and $\geqslant$ for vectors and matrices to indicate element-wise inequality, while we used $\succeq$ for matrix positive semi-definiteness.

B. FOUNDATIONS OF LVDNs MODELING

An accurate line model is an essential requirement for modeling the LVDNs as precisely as possible. If the neutral wire is unconnected to the ground, the ground path can be excluded from the model. This is possible in the case of a sheath conductor which is included in the cable bundle [16]. If a fault exists, and the eddy currents are neglected, then no current will flow inside the sheath. This leads to excluding it from the impedance matrix. The cable is normally buried; therefore, the assumption can be made that no additional impedance contributions exist due to eddy currents induced in the ground. By considering the above assumptions, the line impedance matrix can be reduced from a 4×4 form to a 3×3 form—the impedance terms corresponding to the three phases. Thus, the 3×3 impedance matrix is considered as a phase impedance matrix [3].

On the other hand, if the neutral wire connects to the ground, the ground path is to be included in the impedance matrix. Thus, the current in each phase is established by the line to neutral voltage in the loads. Here, for calculating the neutral and ground current, further assumptions are required. The Kron reduction resolves this issue by assuming a perfect short-circuit between the neutral wire and ground wire. By applying this assumption to the circuit impedance matrix, a 3×3 phase impedance matrix will result. The self-impedances and mutual impedances as sub-matrix can be calculated from the 3×3 impedance matrix between phase conductor circuits and the neutral wire [17]. Here, Carson's equations can be applied to obtain the values of the mutual- and self-impedance for a set of wires, using the wire geometry

TABLE 1. Typography and mathematical notation.

$\mathbf{X}$	vector or matrix variable
X	scalar variable
X^{T}	transpose of matrix $\mathbf{X}$
$X*$	conjugate of $\mathbf{X}$
$X^{\mathrm{H}} = (X*)^{\mathrm{T}}$	conjugate transpose of $\mathbf{X}$
$\circ$	element-wise multiplication
$\oslash$	element-wise division
j	imaginary unit, satisfies $(j)^2 = -1$
$a\angle b$	polar notation of complex number $a.e^{jb}$
$\mathbb{R}^{n\times m}$	set of real $n \times m$ matrices
$\mathbb{C}^{n\times m}$	set of complex $n \times m$ matrices
diag (X)	extract diagonal of $\mathbf{X}$, diag : $\mathbb{C}^{n\times n} \rightarrow \mathbb{C}^{n\times 1}$

TABLE 2. Sets and indices.

Phases	$\varphi, \phi \in \Phi = \{a, b, c\}$
Branches	$l \in \mathcal{L}$
Buses	$n \in \mathcal{N}$
Topology (forward)	$lij \in \mathcal{T}^{\rightarrow} \subseteq \mathcal{L} \times \mathcal{N} \times \mathcal{N}$
Topology (reverse)	$lji \in \mathcal{T}^{\leftarrow} = \{lji \vert lij \in \mathcal{T}^{\rightarrow}\}$
Topology	$lij \in \mathcal{T} = \mathcal{T}^{\rightarrow} \cup \mathcal{T}^{\leftarrow}$
Bus pairs	$ij \in \mathcal{N} = \{ji \vert ij \in \mathcal{T}^{\rightarrow}\} \subseteq \mathcal{N} \times \mathcal{N}$
Loads	$d \in \mathcal{D}$
Load connectivity	$di \in \mathcal{T}^{\text{loads}} \subseteq \mathcal{D} \times \mathcal{N}$
Generators	$gen \in \mathcal{G}$
Generator connectivity	$geni \in \mathcal{T}^{\text{generators}} \subseteq \mathcal{G} \times \mathcal{N}$
PV system	$pv \in \mathcal{PV}$
PV system connectivity	$pvi \in \mathcal{T}^{\text{photovoltaics}} \subseteq \mathcal{PV} \times \mathcal{N}$
Shunts	$h \in \mathcal{H}$
Shunt connectivity	$hi \in \mathcal{T}^{\text{shunt}} \subseteq \mathcal{H} \times \mathcal{N}$

TABLE 3. Parameters.

Bus voltage magnitude min./max. (V)	$\mathbf{V}_i^{\min}, \mathbf{V}_i^{\max} \in \mathbb{R}^{\vert\Phi\vert\times 1}$
Bus phase angle diff. min./max. (rad)	$\mathbf{\Theta}_i^{\min}, \mathbf{\Theta}_i^{\max} \in \mathbb{R}^{\vert\Phi\vert\times 1}$
Branch current rating (A)	$\mathbf{I}_{lij}^{\text{rated}} \in \mathbb{R}^{\vert\Phi\vert\times 1}$
Branch apparent power rating (VA)	$\mathbf{S}_{lij}^{\text{rated}} \in \mathbb{R}^{\vert\Phi\vert\times 1}$
Branch series impedance (Ω)	$\mathbf{z}_l^{\text{s}} \in \mathbb{C}^{\vert\Phi\vert\times\vert\Phi\vert}$
Branch series admittance (S)	$\mathbf{y}_l^{\text{s}} \in \mathbb{C}^{\vert\Phi\vert\times\vert\Phi\vert}$
Branch shunt admittance (S)	$\mathbf{y}_{lij}^{\text{sh}}, \mathbf{y}_{lji}^{\text{sh}} \in \mathbb{C}^{\vert\Phi\vert\times\vert\Phi\vert}$
Bus pair angle diff. min./max. (rad)	$\Theta_{ij}^{\min}, \Theta_{ij}^{\max} \in \mathbb{R}^{\vert\Phi\vert\times 1}$
Bus shunt admittance (S)	$\mathbf{y}_h \in \mathbb{C}^{\vert\Phi\vert\times\vert\Phi\vert}$
Load current rating (A)	$\mathbf{I}_d^{\text{rated}} \in \mathbb{R}^{\vert\Phi\vert\times 1}$
Load active power bounds (W)	$\mathbf{P}_d^{\min}, \mathbf{P}_d^{\max} \in \mathbb{R}^{\vert\Phi\vert\times 1}$
Load reactive power bounds (var)	$\mathbf{Q}_d^{\min}, \mathbf{Q}_d^{\max} \in \mathbb{R}^{\vert\Phi\vert\times 1}$
Generator current rating (A)	$\mathbf{I}_{gen}^{\text{rated}} \in \mathbb{R}^{\vert\Phi\vert\times 1}$
Generator active power bounds (W)	$\mathbf{P}_{gen}^{\min}, \mathbf{P}_{gen}^{\max} \in \mathbb{R}^{\vert\Phi\vert\times 1}$
Generator reactive power bounds (var)	$\mathbf{Q}_{gen}^{\min}, \mathbf{Q}_{gen}^{\max} \in \mathbb{R}^{\vert\Phi\vert\times 1}$
PV system current rating (A)	$\mathbf{I}_{pv}^{\text{rated}} \in \mathbb{R}^{\vert\Phi\vert\times 1}$
PV system active power bounds (W)	$\mathbf{P}_{pv}^{\min}, \mathbf{P}_{pv}^{\max} \in \mathbb{R}^{\vert\Phi\vert\times 1}$
PV system reactive power bounds (var)	$\mathbf{Q}_{pv}^{\min}, \mathbf{Q}_{pv}^{\max} \in \mathbb{R}^{\vert\Phi\vert\times 1}$

and electrical properties of the ground and wires [18], [19]. This can also be extended for multiple neutral models.

Therefore, in modeling the LVDNs, the line impedance matrix is commonly simplified to a 3×3 form using some assumptions to describe the connection between the neutral and ground wires. In this, the line has a multi-grounded neutral setpoints [14]. In particular, the Kron reduction assumes that the voltages between the neutrals and ground are zero at both ends of a line model because the neutral is grounded. The voltage drops in the line are calculated accurately via the 3×3 phase impedance matrix once the currents have been determined. Here, as no assumptions are considered, such as the transposition in terms of the spacing between conductors, the impact of mutual coupling between phases is considered precisely. As a result, this representation renders the most exact line segment modelling [14]. In general,

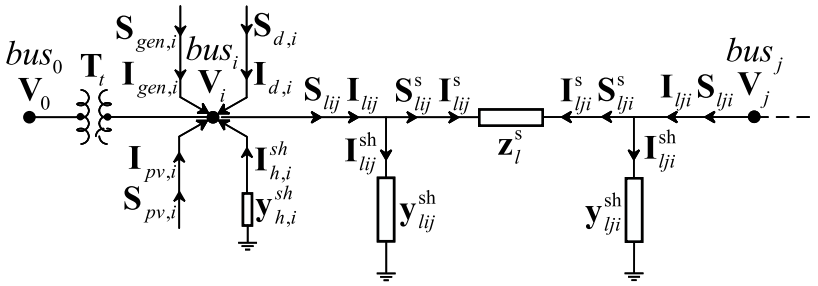

FIGURE 2. A one-line diagram of a generic LVDN.

TABLE 4. Optimization variables.

Bus voltage (V)	$\mathbf{V}_i, \mathbf{V}_j \in \mathbb{C}^{\lvert\Phi\rvert\times 1}$
Branch current (A)	$\mathbf{I}_{lij}, \mathbf{I}_{lji} \in \mathbb{C}^{\lvert\Phi\rvert\times 1}$
Branch series current (A)	$\mathbf{I}^{s}_{lij}, \mathbf{I}^{s}_{lji} \in \mathbb{C}^{\lvert\Phi\rvert\times 1}$
Branch shunt current (A)	$\mathbf{I}^{sh}_{lij}, \mathbf{I}^{sh}_{lji} \in \mathbb{C}^{\lvert\Phi\rvert\times 1}$
Branch power flow (W)	$\mathbf{S}_{lij}, \mathbf{S}_{lji} \in \mathbb{C}^{\lvert\Phi\rvert\times\lvert\Phi\rvert}$
Branch series power flow (W)	$\mathbf{S}^{s}_{lij}, \mathbf{S}^{s}_{lji} \in \mathbb{C}^{\lvert\Phi\rvert\times\lvert\Phi\rvert}$
Branch shunt power flow (W)	$\mathbf{S}^{sh}_{lij}, \mathbf{S}^{sh}_{lji} \in \mathbb{C}^{\lvert\Phi\rvert\times\lvert\Phi\rvert}$
Load current (A)	$\mathbf{I}_d \in \mathbb{C}^{\lvert\Phi\rvert\times 1}$
Load power (W)	$\mathbf{S}_d \in \mathbb{C}^{\lvert\Phi\rvert\times\lvert\Phi\rvert}$
Generator current (A)	$\mathbf{I}_{gen} \in \mathbb{C}^{\lvert\Phi\rvert\times 1}$
Generator power (W)	$\mathbf{S}_{gen} \in \mathbb{C}^{\lvert\Phi\rvert\times\lvert\Phi\rvert}$
PV system current (A)	$\mathbf{I}_{pv} \in \mathbb{C}^{\lvert\Phi\rvert\times 1}$
PV system power (W)	$\mathbf{S}_{pv} \in \mathbb{C}^{\lvert\Phi\rvert\times\lvert\Phi\rvert}$

the length of lines in the LVDNs are so short; therefore, the shunt admittance is so small as to be negligible and thus ignored. However, there are some cases where the lines could be longer than the usual lightly loaded overhead lines. Here, the shunt admittance should be considered into the analysis. Also, the shunt admittance is much higher in underground lines than overhead lines, which should be also considered for an accurate analysis. As the analysis is carried out using the computer, it is more accurate to model the shunt admittance in all the cases for overhead lines and underground lines. Therefore, this takes care of the assumption that the shunt admittance is not necessary [14]. Accordingly, a fundamental unbalanced 3×3 π-model line is illustrated in Figure 3, which summarizes the variables and parameters. Here, all voltages for circuit elements are defined w.r.t. and the ground voltages at both ends ($V_{i,g}$ and $V_{j,g}$) are set to zero.

C. SCALAR AND MATRIX VARIABLES

The series impedance matrix for line l between the buses i and j ($\mathbf{z}^{s}_{l}$) can be defined by a full matrix based on the work in [20], as:

$$\mathbf{z}^{s}_{l} = \mathbf{r}^{s}_{l} + j\mathbf{x}^{s}_{l} = \begin{bmatrix} z^{s}_{l,aa} & z^{s}_{l,ab} & z^{s}_{l,ac} \\ z^{s}_{l,ba} & z^{s}_{l,bb} & z^{s}_{l,bc} \\ z^{s}_{l,ca} & z^{s}_{l,cb} & z^{s}_{l,ac} \end{bmatrix}, \tag{1}$$

where each element consists of a series of resistive and reactive impedance. In physical systems, $\mathbf{r}^{s}_{l} \succeq 0$ and $\mathbf{x}^{s}_{l} \succeq 0$. The series admittance representation of impedance $\mathbf{z}^{s}_{l}$ in line l ($\mathbf{y}^{s}_{l}$) can be represented in matrix notation as:

$$\mathbf{y}^{s}_{l} = \left(\mathbf{z}^{s}_{l}\right)^{-1} = \mathbf{g}^{s}_{l} + j\mathbf{b}^{s}_{l}. \tag{2}$$

where $\left(\mathbf{z}^{s}_{l}\right)^{-1}$ stands for the matrix inverse of $\mathbf{z}^{s}_{l}$. Here, if one conductor or more are missing (e.g., single, or two-conductor connections), then it is valid to use the Moore-Penrose inverse instead.

In addition, the shunt admittance at the beginning and end of line l between buses i and j, respectively, ($\mathbf{y}^{sh}_{lij}$ and $\mathbf{y}^{sh}_{lji}$) can be defined as:

$$\mathbf{y}^{sh}_{lij} = \mathbf{g}^{sh}_{lij} + j\mathbf{b}^{sh}_{lij} = \begin{bmatrix} y^{sh}_{lij,aa} & y^{sh}_{lij,ab} & y^{sh}_{lij,ac} \\ y^{sh}_{lij,ba} & y^{sh}_{lij,bb} & y^{sh}_{lij,bc} \\ y^{sh}_{lij,ca} & y^{sh}_{lij,cb} & y^{sh}_{lij,cc} \end{bmatrix}, \tag{3}$$

$$\mathbf{y}^{sh}_{lji} = \mathbf{g}^{sh}_{lji} + j\mathbf{b}^{sh}_{lji} = \begin{bmatrix} y^{sh}_{lji,aa} & y^{sh}_{lji,ab} & y^{sh}_{lji,ac} \\ y^{sh}_{lji,ba} & y^{sh}_{lji,bb} & y^{sh}_{lji,bc} \\ y^{sh}_{lji,ca} & y^{sh}_{lji,cb} & y^{sh}_{lji,cc} \end{bmatrix}. \tag{4}$$

The shunt admittances can be considered as two different and full matrices, although they are diagonal and have equal values of both sides for typical distribution lines and cables. Furthermore, this allows for re-use of the representation for other elements, such as distribution transformers [20].

The bus voltage at bus i ($\mathbf{V}_i$) can be represented as a vector variable that contains a set of the complex variables for each

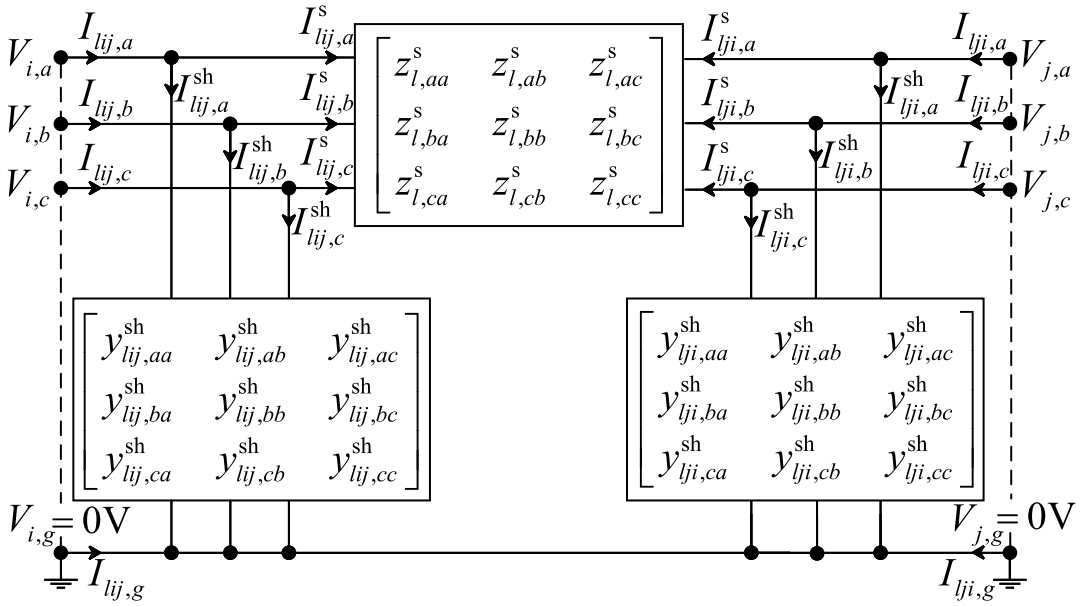

FIGURE 3. Unbalanced 3 × 3 π-model line.

wire based on the work in [21], as:

$$\mathbf{V}_i = \begin{bmatrix} V_{i,a} \\ V_{i,b} \\ V_{i,c} \end{bmatrix} = \begin{bmatrix} V^{\text{mag}}_{i,a} \angle \theta_{i,a} \\ V^{\text{mag}}_{i,b} \angle \theta_{i,b} \\ V^{\text{mag}}_{i,c} \angle \theta_{i,c} \end{bmatrix}. \tag{5}$$

In addition, the flowing current from bus i to bus j ($\mathbf{I}_{lij}$) can be defined as a vector variable for each wire:

$$\mathbf{I}_{lij} = \begin{bmatrix} I_{lij,a} \\ I_{lij,b} \\ I_{lij,c} \end{bmatrix} = \begin{bmatrix} I^{\text{sh}}_{lij,a} \\ I^{\text{sh}}_{lij,b} \\ I^{\text{sh}}_{lij,c} \end{bmatrix} + \begin{bmatrix} I^{\text{s}}_{lij,a} \\ I^{\text{s}}_{lij,b} \\ I^{\text{s}}_{lij,c} \end{bmatrix} = \mathbf{I}^{\text{s}}_{lij} + j\mathbf{I}^{\text{sh}}_{lij}, \tag{6}$$

where $\mathbf{I}^{\text{s}}_{lij}$ defines the current flow in the series elements in the π-model in l from bus i to bus j, therefore, this definition implies $\mathbf{I}^{\text{s}}_{lij} + \mathbf{I}^{\text{s}}_{lji} = 0$ [21], and $\mathbf{I}^{\text{sh}}_{lij}$ stands for the current flow in the shunt elements at the beginning of l from the bus i side.

Accordingly, the complex PF through line l from bus i to bus j defined as the relationship between the voltage at bus i ($\mathbf{V}_i$) and the conjugate transpose of the current flow in line l from bus i to bus j ($\mathbf{I}_{lij}$):

$$\begin{aligned} \mathbf{S}_{lij} &= \mathbf{P}_{lij} + j\mathbf{Q}_{lij} = \mathbf{V}_i \left(\mathbf{I}_{lij}\right)^{\text{H}} \\ &= \begin{bmatrix} S_{lij,aa} & S_{lij,ab} & S_{lij,ac} \\ S_{lij,ba} & S_{lij,bb} & S_{lij,bc} \\ S_{lij,ca} & S_{lij,cb} & S_{lij,cc} \end{bmatrix}. \end{aligned} \tag{7}$$

D. VARIABLE BOUNDS

The voltage magnitudes are limited by minimum and maximum operational limits at each wire [20]. These limits can be represented for the three-phase unbalanced voltages at bus i as:

$$\mathbf{V}^{\min}_i = \begin{bmatrix} V^{\min}_{i,a} \\ V^{\min}_{i,b} \\ V^{\min}_{i,c} \end{bmatrix} \leqslant \begin{bmatrix} |\, V_{i,a} \,| \\ |\, V_{i,b} \,| \\ |\, V_{i,c} \,| \end{bmatrix} \leqslant \begin{bmatrix} V^{\max}_{i,a} \\ V^{\max}_{i,b} \\ V^{\max}_{i,c} \end{bmatrix} = \mathbf{V}^{\max}_i. \tag{8}$$

While the apparent power bounds for $\mathbf{S}_{lij}$ can be represented based on the work in [20], as:

$$0 \leqslant \begin{bmatrix} |\, S_{lij,aa} \,| \\ |\, S_{lij,bb} \,| \\ |\, S_{lij,cc} \,| \end{bmatrix} \leqslant \begin{bmatrix} S^{\text{rated}}_{lij,a} \\ S^{\text{rated}}_{lij,b} \\ S^{\text{rated}}_{lij,c} \end{bmatrix} = \mathbf{S}^{\text{rated}}_{lij}, \tag{9}$$

which can be expressed as:

$$0 \leqslant \begin{bmatrix} |\, S_{lij,aa} \,|^2 \\ |\, S_{lij,bb} \,|^2 \\ |\, S_{lij,cc} \,|^2 \end{bmatrix} \leqslant \begin{bmatrix} \left(S^{\text{rated}}_{lij,a}\right)^2 \\ \left(S^{\text{rated}}_{lij,b}\right)^2 \\ \left(S^{\text{rated}}_{lij,c}\right)^2 \end{bmatrix}. \tag{10}$$

In addition, the magnitudes of current flow in each wire from bus i to bus j should stay within the rated values [20]. The current magnitudes in each wire can be limited as:

$$0 \leqslant \begin{bmatrix} |\, I_{lij,a} \,| \\ |\, I_{lij,b} \,| \\ |\, I_{lij,c} \,| \end{bmatrix} \leqslant \begin{bmatrix} I^{\text{rated}}_{lij,a} \\ I^{\text{rated}}_{lij,b} \\ I^{\text{rated}}_{lij,c} \end{bmatrix} = \mathbf{I}^{\text{rated}}_{lij}. \tag{11}$$

Accordingly, the power bounds for all elements of $\mathbf{S}_{lij} = \mathbf{P}_{lij} + j\mathbf{Q}_{lij}$ are:

$$-\mathbf{V}^{\max}_i \left(\mathbf{I}^{\text{rated}}_{lij}\right)^{\text{T}} \leqslant \mathbf{P}_{lij}, \mathbf{Q}_{lij} \leqslant \mathbf{V}^{\max}_i \left(\mathbf{I}^{\text{rated}}_{lij}\right)^{\text{T}}. \tag{12}$$

Here, the voltage angles for the voltage drop (angle difference) between bus i and bus j are also limited based on the work in [20], as:

$$\begin{bmatrix} -\pi/2 \\ -\pi/2 \\ -\pi/2 \end{bmatrix} \leqslant \underbrace{\begin{bmatrix} \theta_{ij,aa}^{\min} \\ \theta_{ij,bb}^{\min} \\ \theta_{ij,cc}^{\min} \end{bmatrix}}_{\Theta_{ij}^{\min}} \leqslant \begin{bmatrix} \theta_{i,a} - \theta_{j,a} \\ \theta_{i,b} - \theta_{j,b} \\ \theta_{i,c} - \theta_{j,c} \end{bmatrix} \leqslant \underbrace{\begin{bmatrix} \theta_{ij,aa}^{\max} \\ \theta_{ij,bb}^{\max} \\ \theta_{ij,cc}^{\max} \end{bmatrix}}_{\Theta_{ij}^{\max}} \leqslant \begin{bmatrix} \pi/2 \\ \pi/2 \\ \pi/2 \end{bmatrix}. \tag{13}$$

For a relatively balanced voltage phasor, we expected that $\theta_{i,a} - \theta_{i,b} \approx \theta_{i,b} - \theta_{i,c} \approx \theta_{i,c} - \theta_{i,a} \approx 2\pi/3$ [20]. The voltage angle differences among phases at bus i can be limited to enforce the angle balance relative to the expected 120 degrees as:

$$\underbrace{\begin{bmatrix} \theta_{i,aa}^{\min} \\ \theta_{i,bb}^{\min} \\ \theta_{i,cc}^{\min} \end{bmatrix}}_{\Theta_{i}^{\min}} \leqslant \begin{bmatrix} \theta_{i,a} - \theta_{i,a} - 2\pi/3 \\ \theta_{i,b} - \theta_{i,b} - 2\pi/3 \\ \theta_{i,c} - \theta_{i,c} - 2\pi/3 \end{bmatrix} \leqslant \underbrace{\begin{bmatrix} \theta_{i,aa}^{\max} \\ \theta_{i,bb}^{\max} \\ \theta_{i,cc}^{\max} \end{bmatrix}}_{\Theta_{i}^{\max}}. \tag{14}$$

The magnitudes of the load, generator and PV system currents, $|\ \mathbf{I}_d\ |$, $|\ \mathbf{I}_{gen}\ |$ and $|\ \mathbf{I}_{pv}\ |$, respectively, are also limited by the rated current of each unit in the wire that it is connected to as:

$$\begin{bmatrix} |\ I_{d,a}\ | \\ |\ I_{d,b}\ | \\ |\ I_{d,c}\ | \end{bmatrix} \leqslant \begin{bmatrix} I_{d,a}^{\text{rated}} \\ I_{d,b}^{\text{rated}} \\ I_{d,c}^{\text{rated}} \end{bmatrix} = \mathbf{I}_d^{\text{rated}}, \tag{15}$$

$$\begin{bmatrix} |\ I_{gen,a}\ | \\ |\ I_{gen,a}\ | \\ |\ I_{gen,a}\ | \end{bmatrix} \leqslant \begin{bmatrix} I_{gen,a}^{\text{rated}} \\ I_{gen,b}^{\text{rated}} \\ I_{gen,c}^{\text{rated}} \end{bmatrix} = \mathbf{I}_{gen}^{\text{rated}}, \tag{16}$$

$$\begin{bmatrix} |\ I_{pv,a}\ | \\ |\ I_{pv,b}\ | \\ |\ I_{pv,c}\ | \end{bmatrix} \leqslant \begin{bmatrix} I_{pv,a}^{\text{rated}} \\ I_{pv,b}^{\text{rated}} \\ I_{pv,c}^{\text{rated}} \end{bmatrix} = \mathbf{I}_{pv}^{\text{rated}}. \tag{17}$$

The active and reactive powers of generator g ($\mathbf{P}_{gen}$ and $\mathbf{Q}_{gen}$) can be changed according to the amount of real and reactive powers injected or consumed by the DERs [20]. Therefore, the amount of $\mathbf{P}_{gen}$, $\mathbf{Q}_{gen}$ and $\mathbf{S}_{gen}$ are limited as:

$$\mathbf{P}_{gen}^{\min} \leqslant |\ \mathbf{P}_{gen}\ | \leqslant \mathbf{P}_{gen}^{\max}, \tag{18}$$

$$\mathbf{Q}_{gen}^{\min} \leqslant |\ \mathbf{Q}_{gen}\ | \leqslant \mathbf{Q}_{gen}^{\max}, \tag{19}$$

$$|\ \mathbf{S}_{gen}\ | \leqslant \mathbf{S}_{gen}^{\max}. \tag{20}$$

In addition, the PF from a PV system is subject to an apparent PF limit of the inverter [22], which is limited by the nominal inverter's apparent power rating ($\mathbf{S}_{pv}^{\text{rated}}$) as:

$$|\ \mathbf{S}_{pv}\ |^2 = \left(\mathbf{P}_{pv}\right)^2 + \left(\mathbf{Q}_{pv}\right)^2 \leq \left(\mathbf{S}_{pv}^{\text{rated}}\right)^2. \tag{21}$$

Finally, the magnitudes of the shunt currents ($|\ \mathbf{I}_h\ |$) are also limited by the rated current of each shunt in the wire that its connected to, as described in [20]:

$$\begin{bmatrix} |\ I_{h,a}\ | \\ |\ I_{h,b}\ | \\ |\ I_{h,c}\ | \end{bmatrix} \leqslant \begin{bmatrix} I_{h,a}^{\text{rated}} \\ I_{h,b}^{\text{rated}} \\ I_{h,c}^{\text{rated}} \end{bmatrix} = \mathbf{I}_h^{\text{rated}}. \tag{22}$$

E. COMPONENT MODELS

Electrical networks can be subdivided into a set of finite components for modeling their behaviour. These components can be modeled as single- or three-phase units. Three-phase components can be joined in 'wye' configuration (i.e., linked between each phase and the neutral) or 'delta' configuration (i.e., connected between two phases). These components are connected to a set of terminals (3 terminals (i.e., 3-phase and 3 wires system) or 4 terminals (i.e., 3-phase and 4 wires system)) through "lines", which are grouped in a 'bus'. The modeling of the components aims to describe how the variables of current and voltage are related. Therefore, the components are modeled with an associated voltage level, where they either input or withdraw current.

Accordingly, this subsection provides the best practices for modeling the main components in LVDNs with logical assumptions. The main components covered in this subsection are the bus model, line mode, transformer models, loads, generators, PV systems (including the PV inverter, inverter smart controller, and PV modules), and shunts. Finally, the connection configurations of the components mentioned above are also mathematically represented along with the current summation from all these components at bus i using KCL.

1) BUS MODEL

The reference bus ($\mathcal{N}_{\text{ref}}$) can be indexed by 0 and the other buses by $1, 2, \ldots, n$ (e.g., i and j). Let $\mathcal{N} = \{0, 1, \ldots, n\}$, which stands for a set of buses and can be defined as $N^+ = N \backslash \{0\}$ [23]. Therefore, the voltage phasor at reference buses $0 \in \mathcal{N}_{\text{ref}} \subset \mathcal{N}$ is fixed as:

$$\mathbf{V}_0 = \begin{bmatrix} V_{0,a}^{\text{mag}} \angle \theta_{0,a} \\ V_{0,b}^{\text{mag}} \angle \theta_{0,b} \\ V_{0,c}^{\text{mag}} \angle \theta_{0,c} \end{bmatrix}. \tag{23}$$

2) LINE MODEL

A line connects the terminals of two buses, which contains a set of wires. The π model is one of the most used models to characterize the mathematical representation of the currents in a specific wire and induce a voltage in the remaining wires. The π model constructs from a matrix of series impedance and two matrices for the shunt admittance at the beginning and end of the line [14]. Each line l joins a pair of buses i and j. Let $\mathcal{L} = \{0, 1, \ldots, l\}$, which represents a set of lines. Therefore, $(i, j) \in L$, and $i \rightarrow j$ interchangeably. If $i \rightarrow j$ or $j \rightarrow i$, then $i \sim j$. The main idea of the line model is to express the relationships between the complex

voltage phasors (e.g., V_i and V_j) and the injected complex branch power in line l from bus i to bus j ($\mathbf{S}_{lij}$).

The total amount of the current flows in line l from bus i to bus j are formulated in [20], as:

$$\mathbf{I}_{lij} = \mathbf{y}_{lij}^{\text{sh}}\mathbf{V}_i + \mathbf{I}_{lij}^{\text{s}}, \tag{24}$$

and from bus j to i as:

$$\mathbf{I}_{lji} = \mathbf{y}_{lji}^{\text{sh}}\mathbf{V}_j + \mathbf{I}_{lji}^{\text{s}}, \tag{25}$$

where $\mathbf{I}_{lij}^{\text{s}}$ equals to $-\mathbf{I}_{lji}^{\text{s}}$.

In addition, the voltage at the bus j can be obtained by applying Ohm's law in line $lij \in \mathcal{T}^{\rightarrow}$ [20], which is represented in a matrix notation as:

$$\mathbf{V}_j = \mathbf{V}_i - \mathbf{z}_l^{\text{s}}\mathbf{I}_{lij}^{\text{s}}. \tag{26}$$

Here, the current flows from bus i to bus j ($\mathbf{I}_{lij}$) or vice versa ($\mathbf{I}_{lji}$) is split up into series and shunt current in the π-section [20]. The $\mathbf{I}_{lij}$ and $\mathbf{I}_{lji}$ can be split up using KCL as:

$$\mathbf{I}_{lij} = \mathbf{I}_{lij}^{\text{s}} + \mathbf{I}_{lij}^{\text{sh}}, \tag{27}$$

$$\mathbf{I}_{lji} = \mathbf{I}_{lji}^{\text{s}} + \mathbf{I}_{lji}^{\text{sh}}. \tag{28}$$

Therefore,

$$\mathbf{I}_{lij} + \mathbf{I}_{lji} = 0. \tag{29}$$

The voltage angles difference between bus i and bus j can be represented by Θ_{ij}. The value of Θ_{ij} can be limited by $\Theta_{ij}^{\min}$ and $\Theta_{ij}^{\max}$. Thus, the vectors of the element-wise application of the tangent function to $\Theta_{ij}^{\min}$ is defined based on the work in [21], as:

$$\tan\circ(\Theta_{ij}^{\min}) = \begin{bmatrix} \tan(\theta_{ij,a}^{\min}) \\ \tan(\theta_{ij,b}^{\min}) \\ \tan(\theta_{ij,c}^{\min}) \end{bmatrix}, \tag{30}$$

and analogous for $\tan\circ(\Theta_{ij}^{\max})$.

3) TRANSFORMER MODELS

Transformers aim to step up or step down the voltage level based on a number of turns ratio, orientation, and interconnection of the winding magnetic core. Transformers are different than voltage regulators because of their galvanic isolation. In general, the LV transformers are serving a group of customers [24]. In both American and European distribution networks, the LV transformers are connected to MV lines. In the American one, more single-phase MV/LV transformers are used with lower power and supplying fewer users, while in Europe, more three-phase transformers are employed with greater power and supplying more users. Several types of transformer and connection configurations can be used based on the application. More details can be found in [14]. Transformers vary based on their configurations. Three-phase transformers are often used as a wye-wye connection [25]–[27], delta-wye connection [28], or zigzag winding connection. The wye connection side is usually assumed as solidly grounded. Other configurations are also used, such as open-delta windings [29]. Besides, the generic ABCD transformer model can be applied to a broad range of these configurations [25]. The transformers' connection configuration introduces a multiple of 30° phase angle offset between the primary and secondary voltages on top of the normal phase angles between the three-phases (i.e., vector group). Therefore, the neutral point can be grounded.

In European networks, the LV side of the distribution transformer is connected as a wye configuration, and its neutral point is linked to the ground. The neutral is connected to the ground by separated earth electrodes, in the case of overhead cables, or to ground at the substation, in the case of underground cables. An example of such a configuration is explained in [30]. Here, the neutral connection in the transformer side is linked to the ground because the neutrals are given with the connection to every household. Therefore, the delta-wye transformers are the most used configuration for step-down transformers in LVDNs [31]. The delta connection represents the primary side and it is connected to the high voltage level, while the wye connection stands for the secondary side and it is connected to the lower voltage side and assumed to be solidly grounded.

Modeling the LVDNs is typically done based on a reference node where the source voltage is defined [14]. If the LVDNs model contains multiple distribution transformers and their effects on the MV feeder are to be analyzed, it can be assumed that a perfect voltage source represents the secondary side of the primary substation transformer. Therefore, it is assumed that the targeted MV feeder's voltage source is independent of current flowing in the rest of the MV feeders [32]. Other models apply the same assumption by considering the LVDNs as a standalone model; therefore, the LV distribution transformer is modeled as an unregulated voltage source. In [33], a daily profile is employed to define the voltage at the LV distribution transformer's secondary side. Thus, the voltage is assumed to depend on currents in other LV mains linked to the same HV feeder instead of depending on currents in the LV feeder that is modeled. Therefore, the distribution transformer in the LVDNs, when the MV feeder is attached to the LVDN, can be assumed as a constant voltage source, thus neglecting impacts on the load current [14]. Otherwise, the modeling of a physical three-phase delta-wye transformer can be characterized based on two virtual parts by modeling the transformations of the powers and the voltages (i.e., lossless transformer) or by modeling the losses and thermal limits per each winding (i.e., three-phase line segments).

The modelling of a transformer should consider Ampere's law, representing the current flows in the coil to generate the magnetic field, and Faraday's law of induction, representing the relationship between the magnetic flux and voltage [34]. Therefore, there are two main transformer models: the linear transformer model and the ideal transformer model. The linear transformer model is primarily used for communications applications. It uses both sides' impedances

(i.e., coils and reflected impedances) and the impedances for mutual induction. Therefore, the linear transformer model is a fairly complicated model which used phasor analysis and mutual inductance to carry out the analysis. The ideal transformer model is primarily used for power transfer applications. It uses voltages and the number of coil turns, which requires a few different assumptions to be made that are never wholly accurate, but they give a general idea about how the transformer will operate. These assumptions are (i) the coefficient of coupling is assumed to equal 1, coefficient of coupling varies between 0 and 1, 0 means that there is no mutual inductance between the two coils and they are completely independent from each other, and 1 means that the two coils are very tightly coupled; (ii) branches are three-wire; (iii) there is one tap setting for each transformer instead of for each phase winding; (iv) the coils impedances are assumed to go to infinity (i.e., very huge values); and (v) losses from coil resistances are negligible (no active power consumed in the windings or the core can be considered) [35], [36].

In power system analysis, especially in 'unbalanced (O)PF', the analysis is carried out based on phaser form instead of waveform and this ignores harmonics at any multiples of the fundamental frequency. The idealized transformer model can be very close to the transformers' operation in transmission networks, as the transmission transformers' efficiency is very close to 100%, which is not the case in distribution transformers. Therefore, the transformer model's prominent accurately represents the voltage drop across and PF within the distribution transformer, including losses. The mentioned idealized transformer assumptions and approximations are hard to justify in distribution systems; thus, a detailed mathematical model is needed. A comprehensive modeling approach of the transformers is detailed in [37], in which an n-windings transformer can be disintegrated into an n of simple idealized two-winding transformers and lossy branches. However, Dugan and McDermott [7] proposed an extended lossy n-winding transformers model, which is compatible with OpenDSS software. The proposed loss model is a good trade-off between the model details and collecting its parameters. An explicit model, which is a mathematical translation of the assumptions in [37], is shown in [36]. Here, a lossy and multi-winding transformer model is proposed, combining multi-conductor π-sections, shunts, and an idealized two-winding transformer. The proposed decomposition transformer model simplifies the examination of lossy, n-winding transformers to the examination of ideal two-winding transformers. The proposed transformer model is represented by both current-voltage (I-V) and power-voltage (P-V) variables, while Dugan [37] represented the transformer based on I-V variables. The proposed model in [36] is used by PowerModelsDistribution [23] to conduct the 'unbalanced OPF'.

The transformers can be categorized into two main types based on their operation: no-load tap changers (NLTCs) and on-load tap changers (OLTCs). The OLTCs can alter the voltage level by changing the number of turns ratio while the transformers are energized in discrete steps. The operation of the OTLC can be gang-operated or not, based on the way the taps are controlled. Either the tap ratio across phases has the same set-point [26], [28] or they are controlled individually [25], [27], [29], [38]. The tap changer is mostly connected to the LV distribution transformer's primary side. Its operation relies on the currents in all the connected MV feeders. It can be either operated jointly (as gang operation), or for each phase separately. It can be assumed that the tap changers are equally valid for each feeder by considering the ratio between each feeder's demands to be approximately constant. However, such an assumption might not be valid for the PV systems connected to one feeder as they may have a variation on the output based on different solar irradiation than those linked to other feeders in the same primary substation. Accordingly, the OLTC aims to maintain the voltage within a specific range, defined as a specified bandwidth. Here, when that bandwidth is surpassed, the voltage is altered by tap steps [39]. The tap's position is calculated using a control circuit. Standard step regulators include a reversing switch allowing a $\pm 10\%$ control range [14].

Two idealized transformer models are described in this subsubsection. The first model shows the per-phase scaling and rotation of the voltage phasor, which permits tap setting optimization. The second model summarizes the configuration transformation from a three-wire to four-wire grid via a delta-wye transformer.

- Idealized tap changing
  The idealized tap changing is modeled based on the work in [21]. The tap variable for each wire can be defined in a polar form with transformation matrix ($\mathbf{T}_t$) as:

$$\mathbf{T}_t = \begin{bmatrix} T_{t,a} \\ T_{t,b} \\ T_{t,c} \end{bmatrix} = \begin{bmatrix} T_{t,a}^{\text{mag}} T_{t,a}^{\angle} \\ T_{t,b}^{\text{mag}} T_{t,b}^{\angle} \\ T_{t,c}^{\text{mag}} T_{t,c}^{\angle} \end{bmatrix}. \tag{31}$$

  Accordingly, the limits for the magnitude and angle for each tap in each wire can be limited as:

$$\underbrace{\begin{bmatrix} T_{t,a}^{\min} \\ T_{t,b}^{\min} \\ T_{t,c}^{\min} \end{bmatrix}}_{\mathbf{T}_t^{\min}} \leqslant \underbrace{\begin{bmatrix} T_{t,a}^{\text{mag}} \\ T_{t,b}^{\text{mag}} \\ T_{t,c}^{\text{mag}} \end{bmatrix}}_{\mathbf{T}_{t,a}^{\text{mag}}} \leqslant \underbrace{\begin{bmatrix} T_{t,a}^{\max} \\ T_{t,b}^{\max} \\ T_{t,c}^{\max} \end{bmatrix}}_{\mathbf{T}_t^{\max}}, \tag{32}$$

$$\begin{bmatrix} -\pi/2 \\ -\pi/2 \\ -\pi/2 \end{bmatrix} \leqslant \underbrace{\begin{bmatrix} T_{t,a}^{\angle min} \\ T_{t,b}^{\angle min} \\ T_{t,c}^{\angle min} \end{bmatrix}}_{\mathbf{T}_t^{\angle min}} \leqslant \underbrace{\begin{bmatrix} T_{t,a}^{\angle} \\ T_{t,b}^{\angle} \\ T_{t,c}^{\angle} \end{bmatrix}}_{\mathbf{T}_{t,a}^{\angle}}$$

$$\leqslant \underbrace{\begin{bmatrix} T_{t,a}^{\angle max} \\ T_{t,b}^{\angle max} \\ T_{t,c}^{\angle max} \end{bmatrix}}_{\mathbf{T}_t^{\angle max}} \leqslant \begin{bmatrix} \pi/2 \\ \pi/2 \\ \pi/2 \end{bmatrix}. \tag{33}$$

A simple idealized transformer, t, can be modeled with $\mathbf{T}_t$ [23]. The voltage transformation at bus i can be represented with respect to the voltage at bus j as:

$$\mathbf{V}_i = \mathbf{T}_t \mathbf{V}_j. \tag{34}$$

While the corresponding current transformation can be given as:

$$(\mathbf{T}_t)^{\mathrm{H}} \mathbf{I}_{lij} + \mathbf{I}_{lji} = 0. \tag{35}$$

- Idealized configuration transformers
The idealized configuration transformers are also modeled based on the work in [21]. Accordingly, the number of wires can be changed across a transformer. Here, the length of the voltages' vector at bus i and bus j ($\mathbf{V}_i$ and $\mathbf{V}_j$) as well as the length of the current flows' vector from bus i to bus j and vice versa ($\mathbf{I}_{lij}$ and $\mathbf{I}_{lji}$) can be defined as:

$$\mathbf{V}_i \in \mathbb{C}^{n\times 1}, \quad \mathbf{I}_{lij} \in \mathbb{C}^{n\times 1}, \tag{36}$$
$$\mathbf{V}_j \in \mathbb{C}^{m\times 1}, \quad \mathbf{I}_{lji} \in \mathbb{C}^{m\times 1}. \tag{37}$$

Here, a matrix transformation ($\mathbf{C}_t$) can be defined to link the voltage and the current. Accordingly, there is no reason to assume the structure of $\mathbf{C}_t \in \mathbb{C}^{n\times m}$ as it need not to be square, diagonal, or full rank (i.e., generally it is not invertible). Therefore,

$$\mathbf{V}_i = \mathbf{C}_t \mathbf{V}_j, \tag{38}$$

and

$$(\mathbf{C}_t)^{\mathrm{H}} \mathbf{I}_{lij} + \mathbf{I}_{lji} = 0. \tag{39}$$

When $\mathbf{C}_t$ is not fully ranked, the $\mathbf{V}_i$ is linearly dependant on $\mathbf{V}_j$, but not the other way around. Similarly, $\mathbf{I}_{lji}$ is also linearly dependant on $\mathbf{I}_{lij}$ and not the other way around. The relationship between $\mathbf{I}_{lji}$ and $\mathbf{I}_{lij}$ can be expressed as:

$$\mathbf{I}_{lji} = -(\mathbf{C}_t)^{\mathrm{H}} \mathbf{I}_{lij}. \tag{40}$$

According to voltage and current linearity dependence, the PF variables at either end of the line l between bus i and bus j are linearly dependant on $\mathbf{V}_j \left(\mathbf{I}_{lij}\right)^{\mathrm{H}}$, which can be expressed as:

$$\mathbf{S}_{lij} = \mathbf{V}_i \left(\mathbf{I}_{lij}\right)^{\mathrm{H}} = \mathbf{C}_t \mathbf{V}_j \left(\mathbf{I}_{lij}\right)^{\mathrm{H}}, \tag{41}$$
$$\mathbf{S}_{lji} = \mathbf{V}_j \left(\mathbf{I}_{lji}\right)^{\mathrm{H}} = -\mathbf{V}_j \left(\mathbf{I}_{lij}\right)^{\mathrm{H}} \mathbf{C}_t. \tag{42}$$

Using the properties as $\mathrm{tr}(A+B) = \mathrm{tr}(A) + \mathrm{tr}(B)$ and $\mathrm{tr}(AB) = \mathrm{tr}(BA)$, the following formula can be obtained:

$$\mathrm{tr}(\mathbf{S}_{lij}) + \mathrm{tr}(\mathbf{S}_{lji}) = \mathrm{tr}(\mathbf{C}_t \mathbf{V}_j \left(\mathbf{I}_{lij}\right)^{\mathrm{H}}) - \mathrm{tr}(\mathbf{V}_j \left(\mathbf{I}_{lij}\right)^{\mathrm{H}} \mathbf{C}_t) = 0, \tag{43}$$

where tr $(\cdot)$ stands for the trace operator.
The above formulas prove that the model is a lossless transformer. Therefore, $\mathbf{C}_t$ can be used to define any transformer. A delta-wye transformer can be described by $\mathbf{C}_t = \mathbf{T}^{\Delta}$ [21].

4) LOADS

A load is a component consuming active power and consuming or injecting reactive power, which is an accumulation of several devices' behaviour at a household level. Loads in LVDNs vary with time. Therefore, a ''steady-state'' load does not exist. An accurate load model should look to the demand for an individual customer instead of a group of customers. The loads on LVDNs can be specified by a complex power and power factor, active power and power factor, or active and reactive powers [14]. The loads' voltage is always the voltage at the LVDNs feeder's LV terminals. The accuracy of modeling the voltages and losses in LVDNs strongly depends on determining the currents that the system must provide to the customers. The current at the customer side is usually characterized using the load models. The accuracy of these models depends on the precision of the demand data used, which is calibrated in some way from measured data. These data can be derived from direct measurements or from scaled synthesized data. The load model allows for the change in the demand over time in respect to the supplied voltage [3]. The variety of demand over time can be modeled according to standard load profiles, e.g., from the smart city, smart grid in [40]. This data give the half-hourly demand within the day for customers from the Newcastle region of New South Wales (NSW), Australia. Load profiles like these can be implemented directly to characterize the demand.

Another approach can be utilized using the Centre for Renewable Energy Systems Technology (CREST) demand model, in which a single customer's demand is statistically formed from the known active building occupancy and data representing typical appliances [41]. In this model, the demand per appliance is calculated to be consistent with a load profile, reflecting regional variations. Therefore, the 'bottom-up' method can be considered a very flexible one that allows the characteristics to be modified; thus, any additional appliances or future DERs connection in the household can be incorporated [42]. The daily behaviour of each customer is different from one customer to another. Therefore, the load model can be characterized by considering the same appliance behaviour for a customer from day to day, but the occupancy patterns are either completely independent, or are the same for each day [43]. Accordingly, the assumption aiming to specify a different correlation between the load profiles for each customer to characterize their behaviour on different days does not make sense. In addition, the assumption that aims to average the load profiles ignores the fact that some buildings may have different occupancy rates. Thus, this assumption also is not accurate as it may under-estimate the worst-case range since low or high demand behaviours are randomised among customers.

The model of loads varies based on the representation of the voltage magnitude, such as a constant real and reactive power, a constant current, a constant impedance, or any combination of the previous representations [14]. Accordingly, the ZIP load representation is a linear combination of these three variations. While exponential models allow higher order

exponents. ZIP and exponential load models can describe the voltage-dependent behaviour. More explanation about the various device classes' sensitivity for voltage changes can be found in the overview in [44]. The loads can be connected to the buses in single-phase, two-phase or three-phase connections. In addition, loads can be modeled in LVDNs as delta-connected or wye-connected configurations. In general, the loads can be assumed to be a single-phase connections as this is the most common type of load connections in LVDNs in Australia and most countries worldwide. Each load $d \in D$ at bus $n \in N$ in the LVDNs can be represented by one or a combination of the above-mentioned load representations based on the work in [14], as:

- Constant real and reactive power load model
  The line currents ($\mathbf{I}_d$) for constant real and reactive power loads ($\mathbf{P}_d\mathbf{Q}_d$ loads) can be represented as:

$$\mathbf{I}_d = \left(\frac{\mathbf{S}_d}{\mathbf{V}_i}\right)^*, \tag{44}$$

  where $\mathbf{S}_d = \mathbf{P}_d + j\mathbf{Q}_d$, and $\mathbf{I}_d$ can be represented in a full matrix form as:

$$\mathbf{I}_d = \begin{bmatrix} \left(\frac{S_{d,a}}{V_{i,a}}\right)^* \\ \left(\frac{S_{d,b}}{V_{i,b}}\right)^* \\ \left(\frac{S_{d,c}}{V_{i,c}}\right)^* \end{bmatrix} = \begin{bmatrix} I_{d,a} \\ I_{d,b} \\ I_{d,c} \end{bmatrix}. \tag{45}$$

- Constant impedance load model
  The constant load impedance ($\mathbf{z}_d$) can be calculated directly based on the specified complex power ($\mathbf{S}_d$) and assumed line-to-neutral voltages ($\mathbf{V}_i$) as:

$$\mathbf{z}_d = \begin{bmatrix} \frac{|V_{i,a}|}{(S_{d,a})^*} \\ \frac{|V_{i,b}|}{(S_{d,b})^*} \\ \frac{|V_{i,c}|}{(S_{d,c})^*} \end{bmatrix} = \begin{bmatrix} z_{d,a} \\ z_{d,b} \\ z_{d,c} \end{bmatrix}. \tag{46}$$

  Therefore, the load currents ($\mathbf{I}_d$) can be estimated as a function of the constant load impedances as:

$$\mathbf{I}_d = \begin{bmatrix} \frac{V_{i,a}}{z_{d,a}} \\ \frac{V_{i,b}}{z_{d,b}} \\ \frac{V_{i,c}}{z_{d,c}} \end{bmatrix} = \begin{bmatrix} I_{d,a} \\ I_{d,b} \\ I_{d,c} \end{bmatrix}. \tag{47}$$

- Constant current load model
  The load currents ($\mathbf{I}_d$) in this model are obtained based on (45). Here, the magnitudes of the load currents are held constant, while the angle of the voltage (Θ_i) changes. Therefore, the angle of the current will be changed, which leads to a constant power factor of the load [14].
- Combination loads model
  A combination loads model can be modeled by assigning a percentage of the total load to every one of the three load models above. The total line current of the combination loads model ($\mathbf{I}_d$) is the sum of the three components, given as:

$$\mathbf{I}_d = \underbrace{\mathbf{I}_d}_{\text{constant } \mathbf{P}_d\mathbf{Q}_d} + \underbrace{\mathbf{I}_d}_{\text{constant } \mathbf{z}_d} + \underbrace{\mathbf{I}_d}_{\text{constant } \mathbf{I}_d}. \tag{48}$$

5) GENERATORS

Generators are devices that aim to generate and inject active and reactive powers into the network. The amount of the power injected is subject to the load consumption, losses occurred by the components, and the injected power from other devices (e.g., PV systems). Besides, the amount of injected power can be dealt with as a part of an optimization problem based on the network constraints. The generators can contain single-phase, two-phase, or three-phase units. The generators can be operated in PV mode or PQ mode. Each generator $g \in G$ is located at bus $n \in N$ and connected to phase $\phi_g \in \Phi$. Similarly to the load model, it is assumed that the nodal voltage has a nominal magnitude and its phase angle is zero for all phases Φ. The operation modes for the generator $g \in G$ can be listed based on the work in [14], as follows:

- Generator operating as a PQ mode
  In this mode, the values of the injected currents ($\mathbf{I}_{gen}$) are known, while the voltages are estimated. The injected currents are obtained based on the nodal voltages, which have a nominal magnitude as:

$$\mathbf{I}_{gen} = \left(\frac{\mathbf{S}_{gen}}{\mathbf{V}_i}\right)^*, \tag{49}$$

  where $\mathbf{S}_{gen} = \mathbf{P}_{gen} + j\mathbf{Q}_{gen}$; where $\mathbf{S}_{gen}$ stands for the generated complex power by generator g, $\mathbf{P}_{gen}$ and $\mathbf{Q}_{gen}$ represent the generated active and reactive powers by generator g, respectively; and $\mathbf{I}_{gen}$ can be represented in a full matrix form as:

$$\mathbf{I}_{gen} = \begin{bmatrix} \left(\frac{S_{gen,a}}{V_{i,a}}\right)^* \\ \left(\frac{S_{gen,b}}{V_{i,b}}\right)^* \\ \left(\frac{S_{gen,c}}{V_{i,c}}\right)^* \end{bmatrix} = \begin{bmatrix} I_{gen,a} \\ I_{gen,a} \\ I_{gen,a} \end{bmatrix}. \tag{50}$$

- Generator operating as a PV mode
  In this mode, the values of the injected active power and the voltage at bus n are known. Therefore, the injected reactive power is estimated to regulate the voltage. Here, the value of the injected currents ($\mathbf{I}_{gen}$) by generator g are

found, based on the active power and voltages as:

$$\mathbf{I}_{gen} = \begin{bmatrix} \frac{P_{gen,a}}{V_{i,a}} \\ \frac{P_{gen,b}}{V_{i,b}} \\ \frac{P_{gen,c}}{V_{i,c}} \end{bmatrix}. \quad (51)$$

6) PHOTOVOLTAIC SYSTEMS

PV systems are a special type of generators. The PV systems contain an inverter which aims to provide an alternating-current (AC) power to the network and PV modules which are considered as the direct-current (DC) source. The output of a PV system is not fixed as the output of the PV modules is a function of solar radiation and ambient temperature. PV systems can be used to mitigate the voltages in LVDNs by using the functionality of the inverters with the concept of ''smart inverter control'', which allows the inverters to curtail the active power and consume or inject the reactive power as a function of the system voltage within the thermal limits of the inverter and the network constraints.

- Inverters

  Inverters are mainly used to convert a DC power produced by DC sources, such as PV modules or storage batteries, to an AC power. In general, a PV system is considered as an active power generator if the power factor is considered as unity. Otherwise, it can also generate or consume reactive power through the inverters. The operation of the inverters is limited based on several boundaries. Therefore, the per-phase power is limited by an upper bound of the thermal power for the inverter (the apparent power magnitude) [27], [38], [45], lower and upper bounds of active and/or reactive power(s) [45], [46], upper and/or lower or constant power factor bound(s) [45], [47], or by limiting the active and reactive powers to an affine [48] or convex set [49]. The total active power can be fixed to the amount of the DC power produced by the PV module(s), or variable by curtailing the DC power from the source [27], such as by using a maximum power point tracking (MPPT) for PV modules.

  Some research works have modeled the inverter as a balanced model with a once-power set-point for all the phases [47]. Two important extensions are mentioned here. First, current balancing exists for three-wire inverters, this cannot inject zero-sequence current because there is no neutral wire [50]. Second, harmonic compensation capabilities can be obtained by applying operational limits to the sum of the fundamental and harmonic components [51]. Therefore, the inverter can be modeled based on the common approach, in which it is considered as a controllable injection source of power at each phase. In general, the model of the inverter can be given by:

$$\mathbf{S}_{pv} = \mathbf{P}_{pv} + j\mathbf{Q}_{pv}, \quad (52)$$

  where $\mathbf{P}_{pv}$ is the AC PV output active power.

Here, the relationship between power, current and voltage is calculated as:

$$\mathbf{S}_{pv} = \mathbf{V}_i \left(\mathbf{I}_{pv}\right)^{\mathrm{H}}, \quad (53)$$

where, this relation can be represented for the magnitudes in full matrix form based on the work in [52], as:

$$\begin{bmatrix} |S_{pv,a}|^2 \\ |S_{pv,b}|^2 \\ |S_{pv,c}|^2 \end{bmatrix} = \begin{bmatrix} |V_{i,a}|^2 \\ |V_{i,b}|^2 \\ |V_{i,c}|^2 \end{bmatrix} \circ \begin{bmatrix} |I_{pv,a}|^2 \\ |I_{pv,b}|^2 \\ |I_{pv,c}|^2 \end{bmatrix}. \quad (54)$$

The basic inverter without any smart controller is provided just active power at unity power factor. In this case, $\mathbf{S}_{pv} = \mathbf{P}_{pv}$. The value of the $\mathbf{P}_{pv}$ can be calculated using two assumptions. The first is by finding the inverter efficiency at each value of the $P^{\mathrm{PV,mpp}}$ ($\eta_{inverter}$) from the inverter's datasheet and multiplying it with the value of $P^{\mathrm{PV,mpp}}$ as:

$$\mathbf{P}_{pv} = \sum_{\phi \in \Phi} P_{pv,\phi} = P^{\mathrm{PV}} \cdot \eta_{inverter}, \quad (55)$$

where P^{PV} is the PV DC output power, which is mostly a function of the $P^{\mathrm{PV,mpp}}$, solar radiation and ambient temperature (e.g., P^{PV} in OpenDSS can modeled as in (89)), and $\eta_{inverter}$ is the efficiency of the inverter.

The above assumption is applied in modeling the PV system by OpenDSS software. The issue with this assumption is that it is hard to list all the efficiency values at all the possible $P^{\mathrm{PV,mpp}}$ based on the inverter's efficiency curve. In OpenDSS, the inverter efficiency curve can be defined by points which are not limited; however, its objects are interpolated linearly between defined points to determine the actual value [53]. In addition, OpenDSS does not consider the standby losses of the inverter in the calculation. The standby losses' value is not included in the inverter's efficiency curve, as it is very close to zero; therefore, it is not defined at low power.

Other inverter models calculate the losses of the inverter and find the value of $\mathbf{P}_{pv}$ accordingly. These losses include the internal and standby losses ($P_{pv}^{\mathrm{internal}}$ and $P_{pv}^{\mathrm{standby}}$). Accordingly, $\mathbf{P}_{pv}$ can be obtained by,

$$\mathbf{P}_{pv} = \sum_{\phi \in \Phi} P_{pv,\phi} = P^{\mathrm{PV}} - P_{pv}^{\mathrm{internal}} - P_{pv}^{\mathrm{standby}}. \quad (56)$$

The value of $P_{pv}^{\mathrm{standby}}$ can be obtained from the inverter's datasheet, while the value of the $P_{pv}^{\mathrm{internal}}$ can be calculated as:

$$P_{pv}^{\mathrm{internal}} = \sum_{\phi \in \Phi} \left(r_{pv,\phi} \cdot |I_{pv,\phi}^{\mathrm{rated}}|^2\right), \quad (57)$$

where $r_{pv,\phi}$ stands for the copper loss in the inverter at phase ϕ.

By substituting (57) in (56), (56) can be rewritten as:

$$\mathbf{P}_{pv} = \sum_{\phi \in \Phi} P_{pv,\phi} = P^{\mathrm{PV}} - \sum_{\phi \in \Phi} \left(r_{pv,\phi} \cdot \mid I_{pv,\phi}^{\mathrm{rated}} \mid^2 \right) - P_{pv}^{\mathrm{standby}}. \quad (58)$$

The inverter loss model in (56-58) can be considered to the extent that it works very well in practice. It includes an additional step to the model in (55) by getting the efficiency curve and then fitting this to the model to increase its accuracy. However, using the actual values of the parameters instead of curve fitting will lead to more accurate results.

The inverters can support the voltage in the LVDNs by consuming or injecting reactive power. To do so, smart inverter control techniques can be applied. These techniques are described below.

- Inverter smart control

Inverters can support the voltage profiles in the LVDNs. Three main kinds of controllers can be used for this purpose. These controllers are either centralized, distributed or decentralized (or local) [54]. A centralized controller has a communication channel with each controllable device (e.g., inverter) to perform computations based on normal operation of the network or a set of settings and sends new commands back. A distributed controller is an algorithm that aims to link each controllable device into communication with its neighbors, but without a centralized controller. It does not need a huge investment. A decentralized controller is a purely local algorithm and does not communicate with the other controllable devices. In general, centralized controllers perform better than decentralized controllers. A comprehensive review has been published in [55] on different control approaches for voltage mitigation in distribution networks.

Centralized controller algorithms aim to balance the voltages for all three-phase nodes simultaneously. This can be carried out by coordinating the injection or absorption of the reactive power by all online inverters at the same time to balance the voltage levels at the critical node approximately. This controller needs extensive data from the distribution system at each node to determine an optimum response. Therefore, it requires communication channels and sensors to monitor the data in the distribution system. The high investment cost, especially for the communication infrastructure, is the main drawback of this controller. Also, communication malfunction may lead to a degraded response of the controllers and upset the imbalance further. Preliminary investigation into strategies to decrease the impact of delays in controllers' response was conducted in [56], but more work is needed. The balancing still cannot be secured perfectly as alterations in reactive power injections can be noted at the critical bus, which will not precisely match the difference value of the reactive power because of the reactive power losses on the lines between the critical node and the PV systems. Here, improving the operation of the centralized controllers within a feedback loop may resolve this problem. Accordingly, Oshiro *et al.* [57] considered centralized information of the distribution system to coordinate the behaviour of the PV inverters and to manage the transformer tap changers.

Distributed controller algorithms have some advantages over centralized controller algorithms. The information that should be shared is limited with a subset of neighboring points and controllable devices. The limited sharing of data is aimed to improve cybersecurity and reduces the extra expenses in improving the communication infrastructure. Also, the privacy level of data, cost functions, measurements, and constraints are higher. Furthermore, there is robustness concerning the failure of individual points or controllable devices to respond. Finally, they are computationally superior compared with the centralized controller algorithms, as they can perform parallel computations in terms of their solution speed and maximum problem size [54]. Here, Jashfar and Esmaeili [58] proposed a distributed controller approach to enhance the voltage profile and reduce the network's losses by coordinating the reactive power from PV inverters, capacitor banks, and transformer tap changers at a subset of neighboring nodes. Besides, Molzahn *et al.* [54] surveyed the application of control algorithms and distributed optimization in power systems.

The decentralized controller algorithms aim to balance the voltages simultaneously for all three-phase nodes by balancing the voltages at a specific bus. The perfect balancing cannot be achieved as the inverter's injected reactive power is limited by the PV phase connections. This approach does not need communications support as it is implemented based on local data from the bus that the PV inverter is connected to. A decentralized controller may cause an over injection if two nodes nearby need a similar amount of reactive power to approximately balance both. Simultaneously, both nodes' responses may lead to overcompensation of the voltage unbalance factor (VUF) and direct oscillations in the process of feedback. A decentralized voltage control approach based on sensitivity analysis was proposed in [59]. In addition, Bajo *et al.* [60] suggested a decentralized controller to mitigate the voltage imbalance using the voltage magnitude measurements. Recently, decentralized control was implemented in [61] to enhance the voltage profile.

Here, OpenDSS software uses the distributed controller algorithm [7], even so, the decentralized controller algorithm is very important as a backup controller algorithm. Here, it is worth mentioning that power system networks were run and controlled, some of them until now, based on the decentralized controller algorithms.

Therefore, distributed and decentralized controller algorithms should be used at the same time. Nevertheless, centralized controller algorithms show better results in terms of balancing the voltages, to the extent that this is technically possible, by coordinating proper control techniques between the controllable devices (e.g., inverter). In the case of any failure, then distribution or decentralized controller algorithms can be used as a backup controller algorithm.

The commercially available PV inverter is usually operated based on an active power property (i.e., watt priority) if not specified otherwise. The PV inverter is installed based on the customers' primary goals, aiming to maximize the exported potential energy to the network. The PV inverter has two main priorities: active power priority and reactive power priority. It is worth mentioning that the current Australian standard (AS/NZS 4777.2:2015) [62] does not explicitly specify the PV system installation's power priority mode. In active power priority, the inverter always prioritizes active power injection. Here, the inverter's injected active power is limited by its capability and the thermal limits of the utilization of the network's assets. If the voltage at the connection point of the inverter exceeds the synchronization voltage limits, the inverter may shut down the PV system as it cannot absorb or inject any reactive power at periods when reactive absorption is most required to reduce voltages. In reactive power priority, the inverter always prioritizes absorbing any reactive power by decreasing the active power injection, mostly during peak generation periods (i.e., midday). Here, the active power injection is lowered to raise the absorption of reactive power to maintain the voltages within their limits, which allows the PV system to keep operating but with fewer benefits for the customer. This priority is better for the customer as the system does not shut down once the voltages exceed the limits, but it reduces the active power injection by decreasing it or injecting reactive power to keep the voltages within limits [63].

Therefore, the PV inverter can mitigate the voltage in the LVDNs using three main control techniques: constant power factor, volt-var and volt-watt techniques. In addition, volt-var and volt-watt techniques can be combined as a fourth technique. The relationship between active power, reactive power and power factor is illustrated in Figure 4.

- Constant power factor technique
  The constant power factor (pf) technique aims to ensure that the pf is constant at all the timesteps. Therefore, the active power injection to the network is proportional to the reactive power to secure that as:

$$\mathbf{pf} = \frac{\mathbf{P}_{pv}}{|\,\mathbf{S}_{pv}\,|} = \frac{\mathbf{P}_{pv}}{|\,\mathbf{P}_{pv} + j\mathbf{Q}_{pv}\,|} = \mathbf{C}, \qquad (59)$$

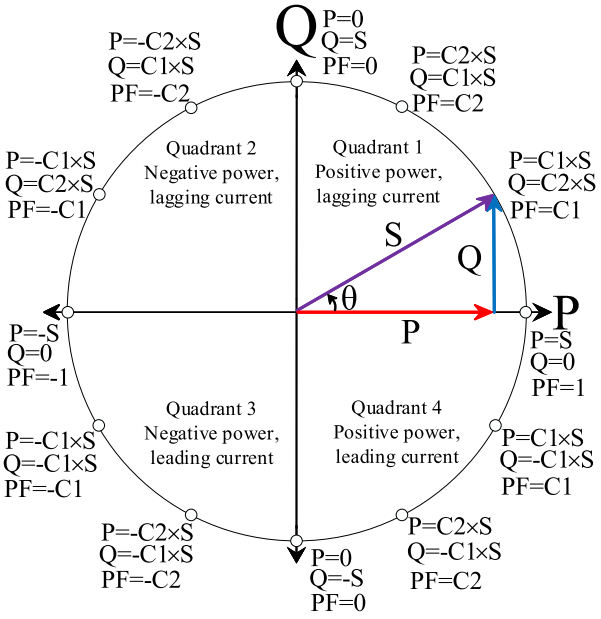

FIGURE 4. Power triangle and the circle of constant apparent power, where C1 and C2 are constants.

where $0 \leqslant \mathbf{C} \leqslant 1$ is a constant, which should be defined as leading or lagging.

In other words, the PF can be represented as a relationship between real and reactive powers as:

$$\tan\left(\cos^{-1}(\mathbf{pf})\right) = \frac{\mathbf{Q}_{pv}}{\mathbf{P}_{pv}}, \qquad (60)$$

where $0 \leqslant (\mathbf{pf} = \mathbf{C}) \leqslant 1$, leading or lagging.

When the reference pf is negative, the inverter absorbs reactive power (inductive characteristic) and, when it is positive, the inverter injects reactive power (capacitive characteristic); Accordingly, if the active power production from the PV modules is low because of the low solar radiation, then the reactive power will also be low [64]. Accordingly, the inverter behaviour in the constant pf technique is shown in Figure 5.

Based on the Figure 5, the absorbed reactive power amount is as low as the active power generation at the low solar radiation period. In contrast, the inverter injects or absorbs the maximum possible reactive power during the 100% active power generation operation to secure a constant pf.

- Volt-var technique
  The volt-var technique is an inverter setting, which aims to maintain the voltage for each PV system at a PV system terminal within predefined voltage limits. The volt-var technique can be set according to (i) the voltage at the point of the PV connection; (ii) the available reactive power capability of the inverter, and (ii) predefined volt-var setpoints, which are set either by the DNSP or the

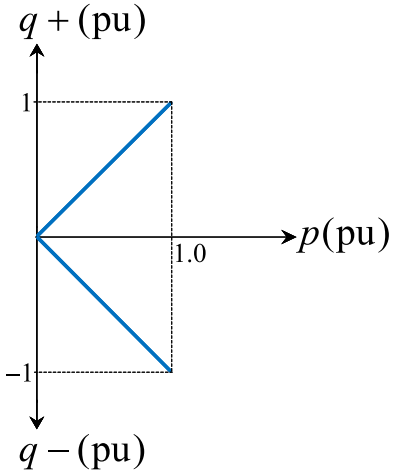

FIGURE 5. Constant power factor inverter control technique.

owner. In this technique, the inverter aims to absorb the reactive power to bring the voltage down if it exceeds the predetermined upper voltage level and injects reactive power to boost the voltage up to the normal predetermined voltage level [63]. Therefore, the volt-var technique aims to ensure that the bus voltage is within its limit by injecting or absorbing reactive power to or from the network. In the decentralized controller, this technique uses local voltage information provided as a consequence of power generation and consumption. Therefore, this technique is a voltage-dependent reactive power technique. The compensated reactive power depending on the monitored voltages according to a volt-var curve [65]. The volt-var curve shows the relationship between reactive power and voltage using a piecewise linear curve as illustrated in Figure 6.

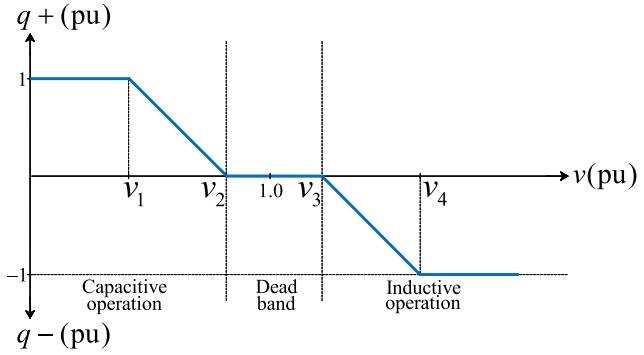

FIGURE 6. Volt-var inverter control technique.

The standards (e.g., AS/NZS 4777.2:2015) define the maximum and minimum voltage bounders and the dead zone. If the bus voltage exceeds the predefined limits, the inverter injects or absorbs the rated reactive power [66]. Accordingly, the inverter reactive power behaviour at phase ϕ ($Q_{pv,\phi}(v)$) based on the parameters used in Figure 6 can be determined using the following algorithm:

$$Q_{pv,\phi}(v) = \begin{cases} Q^{\max}_{pv,\phi} & \text{if } V_{i,\phi} < v_1 \\ \dfrac{V_{i,\phi} - v_1}{v_1 - v_2} Q^{\max}_{pv,\phi} & \text{if } v_1 < V_{i,\phi} < v_2 \\ 0 & \text{if } v_2 < V_{i,\phi} < v_3 \\ -\dfrac{V_{i,\phi} - v_3}{v_4 - v_3} Q^{\max}_{pv,\phi} & \text{if } v_3 < V_{i,\phi} < v_4 \\ -Q^{\max}_{pv,\phi} & \text{if } V_{i,\phi} > v_4, \end{cases} \quad (61)$$

where $Q^{\max}_{pv,\phi} = \sqrt{\left(S^{\max}_{pv,\phi}\right)^2 - \left(P^{\text{PV}}\right)^2}$.

This technique works well in normal operating conditions because the inverter's active power generation is normally less than its rating. Therefore, the inverter can inject reactive power by increasing its losses [67].

– Volt-watt technique

The volt-watt technique is an inverter setting that aims to manage the PV system's AC output active power subject to predefined voltage limits. These limits can affect each PV system's active power capability, which can be limited according to (i) the voltage at the point of the PV connection; and (ii) based on volt-watt set-points predefined either by the DNSP or the owner [63]. Accordingly, the volt-watt technique curtails the amount of the active power injected by the inverter to the connected point based on voltage-rise conditions. This method is also known as the active power curtailment strategy. This technique can operate under three main conditions. The first condition is that the bus voltage is within the voltage limits; therefore, the inverter aims to inject all the generated active power from the PV system to the bus. The second is that the bus voltage is located between a reference voltage and the maximum voltage limit. In this case, the active power is curtailed using the MPPT by the power curtailment ratio. The third is that the bus voltage exceeds its maximum limit. In this case, the injected active power is zero [68]. These conditions can be defined as a relationship between active power and voltage using a piecewise linear curve, which is known as a volt-watt curve as shown in Figure 7.

Based on Figure 7, the inverter active power and the power curtailment ratio can be expressed based on the following algorithm:

$$P_{pv,\phi}(v) = \begin{cases} P^{\text{PV}} & \text{if } V_{i,\phi} < v_1 \\ \dfrac{V_{i,\phi} - v_1}{v_1 - v_2} \cdot P^{\text{PV}} & \text{if } v_1 < V_{i,\phi} < v_2 \\ 0 & \text{if } V_{i,\phi} \leqslant v_2. \end{cases} \quad (62)$$

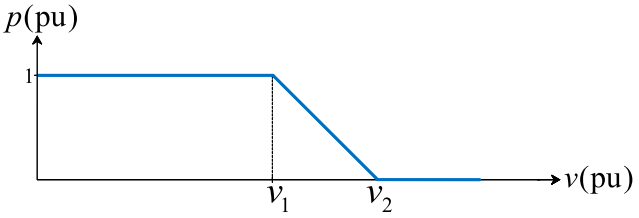

FIGURE 7. Volt-watt inverter control technique.

In general, this technique is effective if the PV output is high and demand is low (i.e., midday), which aims to bring the voltages within the statutory limits. Also, it helps manage thermal limits simultaneously occurring by the over-voltages and overload. It is also helpful if the existing control algorithms (e.g., voltage control through OLTC transformer) are failed to handle these issues [63]. The PV systems at the end of the feeder have more active power loss than the other PV systems; thus, the amount of the active power curtailment will be more, which is unfair [69]. Several studies have been conducted to ensure the same value of active power curtailment for all the PV systems in the LVDNs, which causes less energy yield in the whole feeder, such as the study in [70]. The volt-watt technique can operate effectively using only local measurements without communication coordination between the PV systems and a central controller [71], [72].

In general, the volt-var technique improves the voltage profile and the PF, but it has inherent drawbacks. First, it increases the thermal utilization of assets, especially in low-capacity LV transformers, as they became overloaded even when the PV penetration levels are relatively low. This can be resolved by network augmentation. Second, the volt-var technique significantly increases the reactive power exported by the head of the MV feeder, which may let the power factor at the transmission-distribution network beach permissible limits. This issue can be dealt with by installing power factor correction units to compensate the power factor. Therefore, avoiding the volt-var disadvantages needs extra investment [63]. To ensure the customers' greatest benefits by allowing the inverter to inject the maximum generated energy into the network with the reactive power priority, the inverter can be selected as oversized (e.g., 120% of the PV module capacity). Therefore, the inverter can inject or absorb reactive power in peak generation periods without the sacrifice of active power to meet the inverter's thermal capability. This solution needs extra investment and might be a cost-effective solution. However, to confirm this claim a cost/benefit analysis is needed. Such an analysis is not part of this paper, and can be constructed in future research work.

On the other hand, the volt-watt technique is more effective than the volt-var technique for suppressing the voltage violation, but it reduces the financial benefits for the end-users [73]. Therefore, the combination of volt-var and volt-watt techniques can be considered a highly effective solution to mitigate the voltage issues regardless of the type of feeder, PV penetration, and/or solution adopted (i.e., off-load taps transformer, OLTC transformer, and/or augmentation). The combination of both techniques can keep the voltages in the network within the voltage limits due to reactive power being significantly absorbed from multiple PV systems. Therefore, enabling both techniques gives the customers and the DNSPs satisfaction by reducing the curtailment and solving the voltage rise issues. On the other hand, disabling the volt-var technique has significant effects on the customer by increasing the active power curtailment, which reduces the customers' financial benefits. However, enabling the volt-var and volt-watt techniques without considering other solutions (i.e., off-load taps transformer, OLTC transformer, and/or augmentation) increases asset congestion risk (i.e., transformers and lines) and may cause a poor power factor issue as PV penetration levels continue to rise. In this paper, the effectiveness of other solutions (i.e., off-load taps transformer, OLTC transformer, and/or augmentation) with the volt-var and volt-watt techniques is not considered [63]. This can also be considered in future work.

Here, it is worth mentioning that the PV inverter's active and reactive power control influences both voltage and frequency [74]. Accordingly, the frequency has a direct influence on the voltage angle. This influence's amount and direction are different based on the line impedance ratio as shown in Figure 8.

If the R/X ratio is 0, the active power affects the frequency only, while the reactive power affects the voltage only, as shown in Figure 8.a. This assumption is considered in transmission networks. However, some researchers consider that the R/X ratio in the distribution networks is ∞. Therefore, it is clear that changing the active power influences the voltage level only, while changing the reactive power influences the frequency only, as illustrated in Figure 8.b. This assumption is not true in distribution networks. While the more realistic approach is that the R/X ratio is 1 or approximately 1 in the distribution networks. Accordingly, changing either the active or reactive powers, or both, influences both the voltage level and the frequency, as shown in Figure 8.c.

- PV modules

  PV modules are considered the DC source of PV systems by generating DC power. This DC power is generated by converting solar radiation based on the semiconductor properties, including the temperature effects. The PV modules are connected to inverters in order to achieve AC power. Therefore, the PV system (i.e., PV modules and inverter) can be modeled directly as an injection

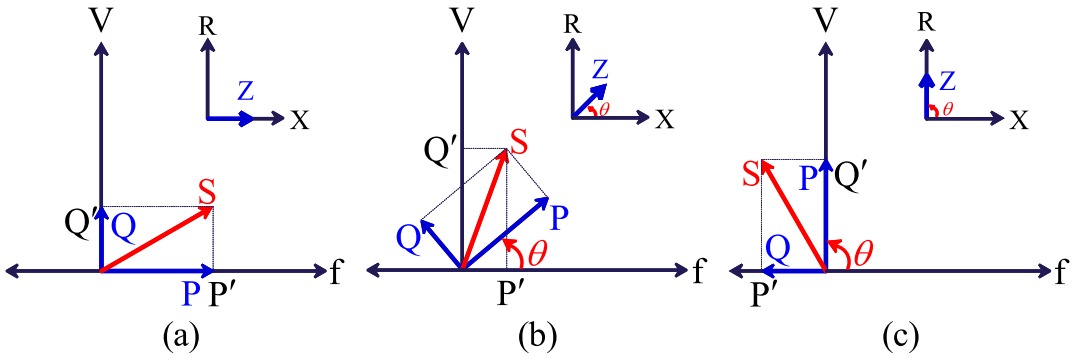

FIGURE 8. Influence of active and reactive power on voltage and frequency for different line impedance ratios: (a) R/X=0, (b) R/X=1, and (c) R/X=∞.

of active power with a unity power factor [75], or a source of active and reactive powers source with an explicit inverter model [27]. Accordingly, the PV system's output power can be a fixed value or curtailable to some lower bound [27]. For example, the PV system's output power can be reduced when net demand surpasses some controllable proportion of the installed PV system's capacity [75]. The fairness of these strategies concerning individual PV installations is examined and listed in [70].

For PV hosting capacity in LVDNs studies, it is mostly assumed that the solar radiation is the same across the covered area [76]. This assumption is required in case of leakage of the meteorological data for different locations within the coordinates of the LVDNs. Here, the short-term solar radiation data may vary across the coordinates of the LVDNs, where all the components are subject to the same voltage set point. Therefore, the PV model should allow for the uncertainty of the meteorological data, such as the solar radiation and ambient temperature, to ensure an accurate reflection of the PV system's performance. To do so, the short-term meteorological data should be considered, including the solar radiation and temperature effects on the PV model. Based on the literature, several models are proposed to model the characteristics of the PV modules. These models are based on the PV output power, PV output current and Chenlo's PV model. Here, these models are reviewed in three main variations as below.

- Variation I
  The first variation aims to characterize the performance of PV modules based on the output power. Several models are used in the literature for modeling the PV output power. Here, some authors applied the same models for PV output energy, as the energy for a timestep equals the power at the same timestep. Therefore, two approaches are included in the first variation. In the first approach, the PV output power is obtained based on two main aspects. The first uses the PV power density function, while the second uses a linear regression model (i.e., single or multiple) in terms of the PV power output at the maximum power point (MPP). In the second approach, PV output power is modeled based on the area of the PV module(s).
  According to the first aspect, the average PV output power ($P^{\mathrm{PV,avg}}$) can be characterized based on the PV power density function ($f\left(P^{\mathrm{PV}}\right)$), which is applied in [77], as:

$$P_t^{\mathrm{PV,avg}} = \int_{P^{\mathrm{PV,min}}}^{P^{\mathrm{PV,max}}} P_t^{\mathrm{PV}} \cdot f\left(P^{\mathrm{PV}}\right) \cdot \mathrm{d}P^{\mathrm{PV}}. \quad (63)$$

The main drawback for the model in (63) is that it neglects the temperature effects and the efficiency of the PV module. Therefore, Lee *et al.* [78] used a single linear regression model to characterize the PV output power as a relationship between the PV power output at the maximum power point (MPP) ($P^{\mathrm{PV,mpp}}$) and solar radiation (G_t) as:

$$P_t^{\mathrm{PV}} = P^{\mathrm{PV,mpp}} \cdot \left(\frac{G_t}{1000}\right). \quad (64)$$

The main drawback for the model in (64) is that the temperature effect is neglected. Accordingly, a multiple linear regression model was discussed in [79], which includes the temperature effects to characterize the PV output power as:

$$P_t^{\mathrm{PV}} = P^{\mathrm{PV,mpp}} \cdot \left(\frac{G_t}{1000}\right) \cdot \left(1 + \left(\frac{\gamma^{\mathrm{PV}}}{100}\right) \cdot \left[T_t^{\mathrm{c}} - 25\right]\right), \quad (65)$$

where $(G_t/1000)$ can also be labeled as PSH, γ^{PV} stands for the temperature coefficient of $P^{\mathrm{PV,mpp}}$ (%/C°), and T_t^{c} stands for the PV cell temperature, which can be obtained as:

$$T_t^{\mathrm{c}} = T_t^{\mathrm{a}} + \left(\frac{\mathrm{NOCT} - 20}{800}\right) G_t, \quad (66)$$

where T_t^{a} represents the ambient temperature, and NOCT stands for the nominal operating cell temperature of a PV module, which can be obtained from the datasheet.

In second approach, a multiple linear regression model is formulated to estimate the PV output power based on the area of the PV module (A^{PV}) and its efficiency (η^{PV}) as in (67). The efficiency of the PV module (η_t^{PV}) is estimated at each timestep as a function of the PV cell temperature and its effects on the power at MPP. This model is used in [80]–[82], which can be represented as:

$$P_t^{\mathrm{PV}} = A^{\mathrm{PV}} \cdot G_t \cdot \eta_t^{\mathrm{PV}}, \tag{67}$$

where η_t^{PV} can be calculated as:

$$\eta_t^{\mathrm{PV}} = \eta^{\mathrm{PV,man}} \cdot \left(1 - \gamma^{\mathrm{PV}} \cdot \left[T_t^{\mathrm{c}} - 25\right]\right), \tag{68}$$

where $\eta^{\mathrm{PV,man}}$ stands for the nominal PV efficiency, which is given by the manufacturer.

The main drawbacks of this variation are that the density function model cannot be considered quantitatively accurate across significant ranges of segregation strength and density fields as all models present nonphysical characteristics under in-commensurate circumstances. In addition, the linear regression models have several disadvantages, such as proneness to under-fitting and sensitivity to outliers. Accordingly, this variation cannot model the uncertainty accurately. As well, the exact values of the PV current and voltage cannot be estimated directly and accurately. Therefore, the results from these models can be used for rough calculations, such as the rough size of the capacity of the PV systems.

– Variation II

The second variation models the performance of PV modules based on the PV output current. In this variation, the PV output current can be obtained based on two main aspects. The first uses a linear regression model (i.e., single or multiple) as a relation between the PV current at MPP or the PV short-circuit current, and solar radiation and ambient temperature. The second is based on the physical parameters of the PV cell itself. Here, the PV output voltage is assumed to be known, which is not true in all the cases.

In general, regression models are used to model the PV output current based on the PV short-circuit current or the PV current at MPP. For example, the model presented in [83] used a single linear regression model as a relationship between PV short-circuit current and solar radiation. This model can be mathematically formulated as:

$$I_t^{\mathrm{PV}} = I^{\mathrm{PV,sc}} \cdot \left(\frac{G_t}{1000}\right), \tag{69}$$

where $I^{\mathrm{PV,sc}}$ is the PV short-circuit current.

The model in (69) does not include the temperature effects. Therefore, Dufo-Lopez *et al.* [83] used a multiple linear regression model by including the temperature effects as:

$$I_t^{\mathrm{PV}} = I^{\mathrm{PV,sc}} \cdot \left(\frac{G_t}{1000}\right) \cdot \left(1 + \left(\frac{\alpha^{\mathrm{PV}}}{100}\right) \cdot \left[T_t^{\mathrm{c}} - 25\right]\right), \tag{70}$$

where α^{PV} represents the temperature coefficient of short-circuit current (%/C°).

Another regression model was developed using a multiple linear regression model based on the relationship between the PV current at MPP ($I_t^{\mathrm{PV,mpp}}$) and the PSH with respect to the temperature factor (f_{temp}^{PV}) and a dirty factor (f_{dirt}^{PV}) as well as the efficiency of the PV module. This model was used in [84], as:

$$I_t^{\mathrm{PV}} = I_t^{\mathrm{PV,mpp}} \cdot \mathrm{PSH} \cdot f_{temp}^{PV} \cdot f_{dirt}^{PV} \cdot \eta^{\mathrm{PV}}, \tag{71}$$

where f_{temp}^{PV} is a function of temperature and can be calculated as:

$$f_{temp}^{PV} = 1 + \left(\frac{\alpha^{\mathrm{PV}}}{100}\right) \cdot \left(T_t^{\mathrm{a}} - 25\right). \tag{72}$$

A similar model was used based on the $I_t^{\mathrm{PV,mpp}}$ and including the temperature effects but without using the efficiency of the PV module. This model was used in [85], as:

$$I_t^{\mathrm{PV}} = N_{pc}^{PV} \cdot I_t^{\mathrm{PV,mpp}} \cdot \left(\frac{G_t}{1000}\right) + \left(1 + \alpha^{\mathrm{PV}} \cdot \left[T_t^{\mathrm{c}} - 25\right]\right), \tag{73}$$

where N_{pc}^{PV} is the number of PV cells connected in parallel per a PV module.

A more accurate model was used to characterize the PV output current in [86]. This model is close to the single-diode PV cell model but developed based on the $I^{\mathrm{PV,sc}}$. This model can be represented as:

$$I_t^{\mathrm{PV}} = I^{\mathrm{PV,sc}} \cdot \left[1 - \exp\left(\frac{V_t^{\mathrm{PV}} - V^{\mathrm{PV,oc}} + R^{\mathrm{PV,s}} \cdot I_t^{\mathrm{PV}}}{\left(N_{sc}^{PV} \cdot a^{\mathrm{PV}} \cdot b \cdot T_t^{\mathrm{c}}\right)/q}\right)\right], \tag{74}$$

where V_t^{PV} stands for the PV output voltage, N_{sc}^{PV} is the number of PV cells connected in series per a PV module, a^{PV} is the diode ideality factor, b stands for the Boltzmann's constant, and q represents the charge of the electron.

The main drawbacks for the above mentioned models are that the PV voltage is unknown, which means it should be initialized or assumed, in order to find the value of the PV current. In addition, these models are carried out based on regression formulas,

which cannot handle high uncertainty in the data, such as solar radiation. Finally, they neglect the physical components inside the PV cell.

To overcome the above mentioned limitations, several models have been developed to characterize the PV output current based on the physical components of the PV cells in the PV modules. These models are known as single-diode PV cell, double-diode PV cell and triple-diode PV cell models. These models are used widely in the literature as they can model the performance of PV modules based on actual measured data.

Accordingly, a single-diode PV cell model is used to describe the non-linear behaviour of the PV module, due to its simplicity and sufficient accuracy. The non-linear behaviour of the single-diode PV cell model can be represented based on the work in [87], as:

$$I_t^{\mathrm{PV}} = I^{\mathrm{PV,ph}} - I^{\mathrm{PV},0} \cdot \left[\exp\left(\frac{V_t^{\mathrm{PV}} + I_t^{\mathrm{PV}} \cdot R^{\mathrm{PV,s}}}{V_t^{\mathrm{PV,t}}} \right) - 1 \right] - \frac{V_t^{\mathrm{PV}} + I_t^{\mathrm{PV}} \cdot R^{\mathrm{PV,s}}}{R^{\mathrm{PV,sh}}}, \tag{75}$$

where $I^{\mathrm{PV,ph}}$ is the generated photocurrent, $I^{\mathrm{PV},0}$ stands for the diode reverse saturation current, $R^{\mathrm{PV,s}}$ and $R^{\mathrm{PV,sh}}$ are the series and shunt resistances, which represent the losses in a PV cell, and $V_t^{\mathrm{PV,t}}$ stands for the thermal voltage, which can be estimated as:

$$V_t^{\mathrm{PV,t}} = \frac{a^{\mathrm{PV}} \cdot b \cdot T_t^{\mathrm{c}}}{q}. \tag{76}$$

The value of I_t^{PV} is recursive by the inclusion of a series resistance in the PV cell model, which makes the solution complex. Thus, the Newton-Raphson method is used for a solution with fast convergence [88]. The Newton-Raphson method can be represented as:

$$x_{m+1} = x_m - \frac{f(x_m)}{f'(x_m)}, \tag{77}$$

where $f'(x_m)$ stands for the derivative of $f(x_m)$, $f(x) = 0$, x_m represents the present value of the estimated quantity at the current iteration and x_{m+1} is the value of the estimated quantity at the next iteration. Here, $I_k^{PV,e}$ is estimated iteratively. Usually, the $I_k^{PV,e}$ converges within three or no more than four iterations.

The single-diode PV cell model results in acceptable under normal operating conditions but frequently demonstrates degraded behaviour under low solar radiation. Therefore, an additional diode is considered to include the effect of charge carrier recombination losses on the depletion region. Accordingly, the non-linear behaviour of the double-diode PV cell model can be represented based on the work in [89], as:

$$I_t^{\mathrm{PV}} = I^{\mathrm{PV,ph}} - I^{\mathrm{PV},01} \cdot \left[\exp\left(\frac{V_t^{\mathrm{PV}} + I_t^{\mathrm{PV}} \cdot R^{\mathrm{PV,s}}}{V_t^{\mathrm{PV,t1}}} \right) - 1 \right] - I^{\mathrm{PV},02} \cdot \left[\exp\left(\frac{V_t^{\mathrm{PV}} + I_t^{\mathrm{PV}} \cdot R^{\mathrm{PV,s}}}{V_t^{\mathrm{PV,t2}}} \right) - 1 \right] - \frac{V_t^{\mathrm{PV}} + I_t^{\mathrm{PV}} \cdot R^{\mathrm{PV,s}}}{R^{\mathrm{PV,sh}}}, \tag{78}$$

where $I^{\mathrm{PV},01}$ and $I^{\mathrm{PV},02}$ stand for the first and second diode reverse saturation currents, respectively, where $I^{\mathrm{PV},01}$ equals $I^{\mathrm{PV},0}$ in (75), and $V_t^{\mathrm{PV,t1}}$ and $V_t^{\mathrm{PV,t2}}$ are the thermal voltages in the first and second diode, respectively. Here, $V_t^{\mathrm{PV,t1}}$ equals $V_t^{\mathrm{PV,t}}$ in (75) and can be obtained by (76). While $V_t^{\mathrm{PV,t2}}$ can be obtained as:

$$V_t^{\mathrm{PV,t2}} = \frac{a^{\mathrm{PV},2} \cdot b \cdot T_t^{\mathrm{c}}}{q}, \tag{79}$$

where $a^{\mathrm{PV},2}$ represents the ideality factor of the second diode.

The Newton-Raphson method in (77) can also be used to estimate the value of I_t^{PV} in (79). The triple-diode PV cell model is considered more accurate than the ideal, single and double-diode PV cell models by dealing with the PV cell's fairly complex non-linear behaviour, but it is more complicated than previously mentioned PV cell models. The triple-diode PV cell model can be considered useful for describing small PV cells' behaviour, which suits some applications where a non-negligible leakage current occurs through peripheries. The non-linear behaviour of the triple-diode PV cell model can be represented based on the work in [90], as:

$$I_t^{\mathrm{PV}} = I^{\mathrm{PV,ph}} - I^{\mathrm{PV},01} \cdot \left[\exp\left(\frac{V_t^{\mathrm{PV}} + I_t^{\mathrm{PV}} \cdot R^{\mathrm{PV,s}}}{V_t^{\mathrm{PV,t1}}} \right) - 1 \right] - I^{\mathrm{PV},02} \cdot \left[\exp\left(\frac{V_t^{\mathrm{PV}} + I_t^{\mathrm{PV}} \cdot R^{\mathrm{PV,s}}}{V_t^{\mathrm{PV,t2}}} \right) - 1 \right] - I^{\mathrm{PV},03} \cdot \left[\exp\left(\frac{V_t^{\mathrm{PV}} + I_t^{\mathrm{PV}} \cdot R^{\mathrm{PV,s}}}{V_t^{\mathrm{PV,t3}}} \right) - 1 \right] - \frac{V_t^{\mathrm{PV}} + I_t^{\mathrm{PV}} \cdot R^{\mathrm{PV,s}}}{R^{\mathrm{PV,sh}}}, \tag{80}$$

where $I^{\mathrm{PV},03}$ stands for the third diode reverse saturation current, and $V_t^{\mathrm{PV,t3}}$ is the thermal voltage in the third diode, which can be calculated as:

$$V_t^{\mathrm{PV,t3}} = \frac{a^{\mathrm{PV},3} \cdot b \cdot T_t^{\mathrm{c}}}{q}, \tag{81}$$

where $a^{PV,3}$ represents the ideality factor of the third diode.

As in single- and double-diode PV cell models, the value of I_t^{PV} in (81) can be estimated using Newton-Raphson method in (77) can be used.

The main drawback of this variation is that the PV output voltage is required to find the PV output current. In some of the models it is considered that the PV output voltage is available, while others need initial assumed values for the PV output voltage, which could impact the results' accuracy. However, the single-, double- and triple-diode PV cell models are considered more precise than the linear regression models, but they need actual data to estimate their parameters. The estimation of the parameters need extraction methods, which is more complicated than the regression models. In addition, the values of the PV output voltage should be previously known to calculate the PV output current. Even so, the Newton-Raphson method should be applied to find the PV output current. Therefore, the accuracy of such models strongly depends on the accuracy of the measurements as well as the capability of the extraction method. Here, these models are mostly specified on a certain PV module brand; therefore, in most cases, they could not be generalized for all PV modules.

- Variation III

The third variation aims to model the PV output current and voltage based on the I-V curve of a PV module. This variation can be carried out based on the information from the PV module's datasheet. Selecting the proper PV model involves a trade-off between simplicity and accuracy. Chenlo's model [91], which is presented in [92] has an accuracy of 97.8% as reported by Ibrahim *et al.* [87]. It extrapolates the I-V pairs for any PV module at any solar radiation (G_t) and ambient temperature (T_t^a) based on measured I-V pairs or taken from the datasheet at STC. The principle of work for this model can be summarized as illustrated in Figure 9. The model starts by obtaining the reference PV module short-circuit current ($I^{PV,sc,ref}$) and the reference PV module open-circuit voltage ($V^{PV,oc,ref}$) at the STC or measured values of G^{ref} and T^{ref} as:

$$I_t^{PV,sc}(G_t, T_t^a) = I^{PV,sc,ref}(G^{ref}, T^{ref}) \cdot \frac{G_t}{G^{ref}} + \alpha^{PV} \cdot (T_t^a - T^{ref}), \quad (82)$$

$$V_t^{PV,oc}(G_t, T_t^a) = V^{PV,oc,ref}(G^{ref}, T^{ref}) + V_t^{PV,t} \cdot \ln\left(\frac{G_t}{G^{ref}}\right) + \beta^{PV} \cdot (T_t^a - T^{ref}), \quad (83)$$

where G^{ref} and T^{ref} are the reference solar radiation and ambient temperature at a reference point, respectively; G_t and T_t^a are solar radiation and ambient temperature at time t for the new point, respectively; $I_t^{PV,sc}$ is the unknown short-circuit current; $I^{PV,sc,ref}$ is the short-circuit current for the reference I-V curve; α^{PV} is the temperature coefficient of $I^{PV,sc}$ at STC; $V_t^{PV,oc}$ represents the unknown open-circuit voltage; $V^{PV,oc,ref}$ is the open-circuit voltage for the reference I-V curve; and β^{PV} is the temperature coefficient of $V^{PV,oc}$.

Therefore, the unknown I-V pairs at MPP ($I_t^{PV,mpp}$, $V_t^{PV,mpp}$) at G_t and T_t^a can be calculated based on the known I-V pairs at the reference I-V curve ($I^{PV,ref}$, $V^{PV,ref}$) at G^{ref} and T^{ref} as follows:

$$I_t^{PV,mpp}(G_t, T_t^a) = I^{PV,mpp,ref}(G^{ref}, T^{ref}) + \Delta I_t^{PV,sc}, \quad (84)$$

$$V_t^{PV,mpp}(G_t, T_t^a) = V^{PV,mpp,ref}(G^{ref}, T^{ref}) + \Delta V_t^{PV,oc}, \quad (85)$$

where,

$$\Delta I_t^{PV,sc} = I_t^{PV,sc}(G_t, T_t^a) - I^{PV,sc,ref}(G^{ref}, T^{ref}), \quad (86)$$

$$\Delta V_t^{PV,oc} = V_t^{PV,oc}(G_t, T_t^a) - V^{PV,oc,ref}(G^{ref}, T^{ref}). \quad (87)$$

Accordingly, the PV output DC power (P^{PV}) is equal to the PV output power at MPP ($P^{PV,mpp}$) at time t. Here, $P^{PV,mpp}$ is calculated as a multiplication of current at MPP ($I^{PV,mpp}$) and voltage at MPP ($V^{PV,mpp}$) considering the solar radiation and ambient temperature effects as:

$$P_t^{PV} = P_t^{PV,mpp}(G_t, T_t^a) = I_t^{PV,mpp}(G_t, T_t^a) \cdot V_t^{PV,mpp}(G_t, T_t^a). \quad (88)$$

In OpenDSS software, the PV module is characterized using a regression model, which is close to Variation II [53]. The PV output DC power (P^{PV}) is function of ($P^{PV,mpp}$) and a per unit variation of the $P^{PV,mpp}$ and temperature factor at $G = 1$ kW/m^2 (Factor(T_t^c)) as:

$$P_t^{PV} = P^{PV,mpp} \cdot G_t \cdot \text{Factor}(T_t^a). \quad (89)$$

The disadvantages of the above model are (i) it does not provide enough information to calculate the Factor(T_t^a), which is the temperature coefficient of the power at MPP with respect to the T^a; and (ii) to simplify the model, it considers the relation between the changes in solar radiation and the power output from the PV as linear, where in reality this is not constant for the entire range of solar radiation values. Therefore, it is necessary to model the relation between the power and the solar radiation at each timestep to express the real behaviour of the PV module. Accordingly, this model does not reflect uncertainty accurately.

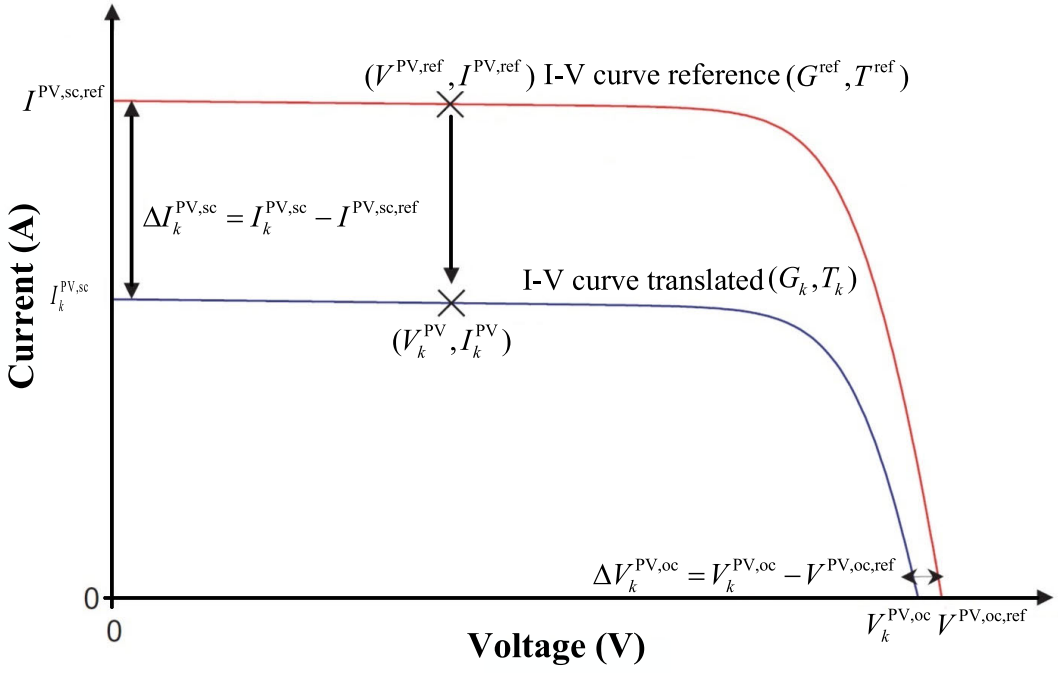

FIGURE 9. The Chenlo's model to obtain the PV I-V pairs at any G_t and T_t^{a}.

To sum up, the PV module should be selected, bearing in mind the trade-off between simplicity and accuracy. In addition, the PV module should be able to be generalized, so that it can be used to characterize the performance for any PV module based on the available information. Here, the available information represents the characteristics in the datasheet provided by the manufacturers. Therefore, Variation III can be implemented to generalize the modeling of the PV modules using the information from the datasheet directly within an acceptable range of accuracy. This is because the other variations need more information or have limitations in characterizing the uncertainty of the meteorological data accurately.

7) SHUNTS

A bus shunt, which is indexed by h, has an admittance of $\mathbf{y}_h = \mathbf{g}_h + j\mathbf{b}_h$. Tuples of shunts and their connected bus are defined as $hi \in \mathcal{T}^{\mathrm{shunt}}$. The current relates to the voltage of a shunt h at bus i, with $hi \in \mathcal{T}^{\mathrm{shunt}}$ can be represented based on Ohm's law according to the work in [20], as:

$$\mathbf{I}_h = \mathbf{y}_h \mathbf{V}_i. \tag{90}$$

Here, the current flows from the bus to the shunts can be defined in full matrix form as:

$$\mathbf{I}_h = \begin{bmatrix} I_{h,a} \\ I_{h,b} \\ I_{h,c} \end{bmatrix}. \tag{91}$$

Accordingly, the shunt complex power matrix ($\mathbf{S}_h$) can be defined as:

$$\mathbf{S}_h = \mathbf{P}_h + j\mathbf{Q}_h = \mathbf{V}_i \left(\mathbf{I}_h\right)^{\mathrm{H}}. \tag{92}$$

The shunt power can also be represented as a function of shunt admittance based on the nodal voltage only by substituting (91) in (92) according to the work in [20], as:

$$\mathbf{S}_h = \mathbf{V}_i \left(\mathbf{V}_i\right)^{\mathrm{H}} \left(\mathbf{y}_h\right)^{\mathrm{H}}. \tag{93}$$

8) CONNECTION CONFIGURATIONS OF LOADS, GENERATORS, AND PV SYSTEMS

The loads, generators and PV systems can be connected to the network either in wye connection or in delta connection as below:

- Wye connection
  The wye loads, generators and PV systems are connected between a phase and ground. Therefore, the phase-to-ground voltage differences for wye units are defined as $\mathbf{V}_i$. Here, the loads, generators and PV systems models, which are described above, are modeled based on phase-to-ground voltages. Therefore, they are considered as wye-connected models.
- Delta connection
  The delta loads, generators and PV systems are connected between two phases. Therefore, the phase-to-phase voltage differences for delta loads, generators and PV systems ($\mathbf{V}_i^{\Delta}$) can be defined in terms of phase-to-ground voltages ($\mathbf{V}_i$) based on

the work in [93], as:

$$\mathbf{V}_i^{\Delta} = \begin{bmatrix} \mathbf{V}_{i,ab}^{\Delta} \\ \mathbf{V}_{i,bc}^{\Delta} \\ \mathbf{V}_{i,ca}^{\Delta} \end{bmatrix} = \underbrace{\begin{bmatrix} 1 & -1 & 0 \\ 0 & 1 & -1 \\ -1 & 0 & 1 \end{bmatrix}}_{\mathbf{T}^{\Delta}} \underbrace{\begin{bmatrix} V_{i,a} \\ V_{i,b} \\ V_{i,c} \end{bmatrix}}_{\mathbf{V}_i} = \begin{bmatrix} V_{i,a} - V_{i,b} \\ V_{i,b} - V_{i,c} \\ V_{i,c} - V_{i,a} \end{bmatrix}, \quad (94)$$

where $\mathbf{T}^{\Delta}$ represents a linear transformation.
Here, Claeys *et al.* [93] defined the load phase current ($\mathbf{I}_d$) as a relation between $\mathbf{I}_d^{\Delta}$ and $\left(\mathbf{T}^{\Delta}\right)^{\mathrm{T}}$, as:

$$\mathbf{I}_d = \begin{bmatrix} I_{d,a} \\ I_{d,b} \\ I_{d,c} \end{bmatrix} = \underbrace{\begin{bmatrix} 1 & 0 & -1 \\ -1 & 1 & 0 \\ 0 & -1 & 1 \end{bmatrix}}_{\left(\mathbf{T}^{\Delta}\right)^{\mathrm{T}}} \underbrace{\begin{bmatrix} I_{d,ab}^{\Delta} \\ I_{d,bc}^{\Delta} \\ I_{d,ca}^{\Delta} \end{bmatrix}}_{\mathbf{I}_d^{\Delta}}. \quad (95)$$

Similarly, $\left(\mathbf{T}^{\Delta}\right)^{\mathrm{T}}$ can be used to define the generator phase current ($\mathbf{I}_{gen}$) and the PV system phase current ($\mathbf{I}_{pv}$), respectively, as:

$$\mathbf{I}_{gen} = \begin{bmatrix} I_{gen,a} \\ I_{gen,a} \\ I_{gen,a} \end{bmatrix} = \underbrace{\begin{bmatrix} 1 & 0 & -1 \\ -1 & 1 & 0 \\ 0 & -1 & 1 \end{bmatrix}}_{\left(\mathbf{T}^{\Delta}\right)^{\mathrm{T}}} \underbrace{\begin{bmatrix} I_{gen,ab}^{\Delta} \\ I_{gen,bc}^{\Delta} \\ I_{gen,ca}^{\Delta} \end{bmatrix}}_{\mathbf{I}_{gen}^{\Delta}}, \quad (96)$$

and

$$\mathbf{I}_{pv} = \begin{bmatrix} I_{pv,a} \\ I_{pv,b} \\ I_{pv,c} \end{bmatrix} = \underbrace{\begin{bmatrix} 1 & 0 & -1 \\ -1 & 1 & 0 \\ 0 & -1 & 1 \end{bmatrix}}_{\left(\mathbf{T}^{\Delta}\right)^{\mathrm{T}}} \underbrace{\begin{bmatrix} I_{pv,ab}^{\Delta} \\ I_{pv,bc}^{\Delta} \\ I_{pv,ca}^{\Delta} \end{bmatrix}}_{\mathbf{I}_{pv}^{\Delta}}. \quad (97)$$

Accordingly, the complex power consumed in a delta-connected load ($\mathbf{S}_d^{\Delta}$), a delta-connected generator ($\mathbf{S}_{gen}^{\Delta}$) and a delta-connected PV system ($\mathbf{S}_{pv}^{\Delta}$) can be formulated, respectively, as:

$$\mathbf{S}_d^{\Delta} = \mathbf{V}_i^{\Delta} \circ \left(\mathbf{I}_d^{\Delta}\right)^* = \mathbf{T}^{\Delta}\mathbf{V}_i \circ \left(\mathbf{I}_d^{\Delta}\right)^*, \quad (98)$$

$$\mathbf{S}_{gen}^{\Delta} = \mathbf{V}_i^{\Delta} \circ \left(\mathbf{I}_{gen}^{\Delta}\right)^* = \mathbf{T}^{\Delta}\mathbf{V}_i \circ \left(\mathbf{I}_{gen}^{\Delta}\right)^*, \quad (99)$$

and

$$\mathbf{S}_{pv}^{\Delta} = \mathbf{V}_i^{\Delta} \circ \left(\mathbf{I}_{pv}^{\Delta}\right)^* = \mathbf{T}^{\Delta}\mathbf{V}_i \circ \left(\mathbf{I}_{pv}^{\Delta}\right)^*. \quad (100)$$

F. KIRCHHOFF'S CURRENT LAW

The current summation at bus i can be obtained based on Kirchhoff's current law (KCL) in rectangular current coordinates as:

$$\sum_{lij \in \mathcal{T}} \mathbf{I}_{lij} + \sum_{di \in \mathcal{T}^{\text{loads}}} \mathbf{I}_d + \sum_{gi \in \mathcal{T}^{\text{generators}}} \mathbf{I}_{gen} + \sum_{pvi \in \mathcal{T}^{\text{photovoltaics}}} \mathbf{I}_{pv} + \sum_{shi \in \mathcal{T}^{\text{shunt}}} \mathbf{I}_h = 0. \quad (101)$$

Here, the currents of line shunts, bus shunts, loads, generators and PV systems with a fixed set point can be directly substituted into the equation given above.

In addition, KCL can be represented in complex power variables based on the work in [20] by taking the conjugate transpose of (101) and element-wise multiplying with $\mathbf{V}_i \neq 0$ on the left side of (101) as:

$$\sum_{lij \in \mathcal{T}} \text{diag}(\mathbf{S}_{lij}) + \sum_{di \in \mathcal{T}^{\text{loads}}} \text{diag}(\mathbf{S}_d) + \sum_{gi \in \mathcal{T}^{\text{generators}}} \text{diag}(\mathbf{S}_{gen}) + \sum_{pvi \in \mathcal{T}^{\text{photovoltaics}}} \text{diag}(\mathbf{S}_{pv}) + \sum_{shi \in \mathcal{T}^{\text{shunt}}} \text{diag}(\mathbf{S}_h) = 0, \quad (102)$$

which means the diagonal element of the apparent power matrices of the connected branch flows, loads, generators, PV systems and shunts need to sum to zero for each bus.

Similarly, the KCL can be represented in real and reactive power equivalent forms as:

$$\sum_{lij \in \mathcal{T}} \text{diag}(\mathbf{P}_{lij}) + \sum_{di \in \mathcal{T}^{\text{loads}}} \text{diag}(\mathbf{P}_d) + \sum_{gi \in \mathcal{T}^{\text{generators}}} \text{diag}(\mathbf{P}_{gen}) + \sum_{pvi \in \mathcal{T}^{\text{photovoltaics}}} \text{diag}(\mathbf{P}_{pv}) + \sum_{shi \in \mathcal{T}^{\text{shunt}}} \text{diag}(\mathbf{P}_h) = 0, \quad (103)$$

$$\sum_{lij \in \mathcal{T}} \text{diag}(\mathbf{Q}_{lij}) + \sum_{di \in \mathcal{T}^{\text{loads}}} \text{diag}(\mathbf{Q}_d) + \sum_{gi \in \mathcal{T}^{\text{generators}}} \text{diag}(\mathbf{Q}_{gen}) + \sum_{pvi \in \mathcal{T}^{\text{photovoltaics}}} \text{diag}(\mathbf{Q}_{pv}) + \sum_{shi \in \mathcal{T}^{\text{shunt}}} \text{diag}(\mathbf{Q}_h) = 0. \quad (104)$$

G. DISCUSSION OF ACCURACY

The network can be balanced if the voltages' magnitudes and the currents' magnitudes are equivalent through all the phases, but the angles between the phases are 120°, in which phase "a" leads phase "b" and phase "b" leads phase "c". In this case, the network can be modeled as a single-phase equivalent model. The representation of a single-phase equivalent model can be a positive sequence or balanced model, which removes redundant equations under this symmetry. This assumption can be used in the transmission networks [14].

On the other hand, using the balanced model in modeling the distribution networks is not recommended as it is insufficient for modeling and analysing the distribution networks [14]. The entire distribution networks are affected by the phase unbalance. Therefore, modeling the phase unbalance effects can significantly increase the analysis's accuracy and complexity, which requires the derivation of unbalanced multi-phase component models. Accordingly, modeling the distribution networks is more challenging and complex than modeling the transmission networks [94]. For example, the balanced models' impedance model can be represented with a single complex scalar, while its representation in the entire unbalanced model is a complex 3×3 matrix for the same component. Moreover, a neutral conductor may be required to model the LV networks next to the phase conductors, resulting in a 4×4 impedance matrix. Obtaining precise parameters for these models can be a challenge. As the analysis is carried out using the computer, it is more accurate to model the phase unbalance effects to avoid any under- or over-estimation of the network behaviour.

In multi-period problems, the forecasting of the future demand and renewable generation must be considered. Forecasting the uncertainty is essential in a rolling horizon approach [95]. Uncertainty forecasting can be considered using the probability-based approaches [47], or merely solving the problem by updating the forecasts. These multi-period optimization models are able to be implemented in real applications, such as in modeling predictive controls.

III. POWER FLOW

The power flow (PF) equations aim to represent the relationship between the voltage phasors and the power injected to a node by units and shunts in an electrical power system. The PF equations can be considered the fundamental equations to conduct the analysis and express an electrical power system's operation. They are considered as the key constraints of many optimization and control problems in an electrical power system. Some surveys and tutorials are published to explain a specific problem and/or a solution algorithm in PF [96], [97], different OPF representations [98]–[111], distributed optimization and control techniques [54], [112]–[114], voltage stability analysis [115]–[118], unit commitment (UC) [119]–[122], state estimation [123]–[126], transient-stability constraints [127], [128], security constraints [129]–[132], cascading failure [133], transmission switching [134], complex theory [135], and more general power stability concepts [136]. Besides, a recent survey in [8] has covered some of the PF relevant topics. The reference implementations for several of the PF equations in this section are provided in software packages, such as MATPOWER [137], PowerModels.jl [138] and PowerModelsDistribution [23].

The power equations are non-linear. Therefore, some of the PF equations that are related to some optimization problems (i.e., OPF) are NP-Hard [139], even for radial typologies [140], and may have multiple local solutions [141]. Several non-linear programming techniques can be used to solve power system optimization problems. Most of these techniques typically seek local optima for power system optimization problems. Starting from specified initializations, these are achievable points with objective conditions superior to all nearby points; however, they are potentially inferior to the global optimum. A summary of traditional non-linear programming techniques for solving the PF is presented in Subsection III-B. For more details, the reader can refer to the reviews in [101]–[106] about the traditional local solution techniques.

The development of novel representations of PF equations is an active research topic. Some recent research works included a variety of new PF representations. An elliptical PF representation to compute multiple PF solutions is proposed in [142]. Besides, Wu *et al.* [143] also used an elliptical PF representation to compute multiple local solutions for OPF problems. The work in [144] and its extension in [145] used the power divider formulation to transfer the bus power injections to the PFs on each line to investigate network allocation, loss allocation, and active PF satisfaction problems. The authors in [146] and [147] identified the Lagrange multipliers' patterns of power system optimization problems using a PF formulation based on Laplacian structural characteristics. Accordingly, Subsection III-A provides a variety of representations of the unbalanced PF equations. This includes the branch flow model (BFM) and the bus injection model (BIM) for several coordinate networks.

A. MODELS

Two main models are used to represent the unbalanced PF equations. These two models are BFM and BIM. Here, BFM keeps the current variables through the series impedance, which is represented in impedance form [14]. Thus, the edge case of zero impedance remains representable. However, the BIM excludes all current variables, which leads to reactive and active PFs being represented merely as a function of the voltage differences between connected buses. The series impedance is consequently used in admittance form, which makes it improbable to represent zero-impedance branches. The BFM and BIM equations are extracted from the works in [20] and [14].

Figure 10 shows the harmonized matrix variables representation of a single-wire equivalent unbalanced π-model branch in both natural variable spaces to express the basic relationships. However, Figure 3 can be used for actual implementation in modeling software as it illustrates the scalar representation of all variables and parameters.

1) BRANCH FLOW MODEL

Branch flow model (BFM) is focused on the electrical quantities flowing on the lines, which is also referred to as the ''DistFlow'' equations [148], [149]. The derivation of unbalanced BFM is explained in this subsubsection. Here, a variable complex PF in the series element in π-section

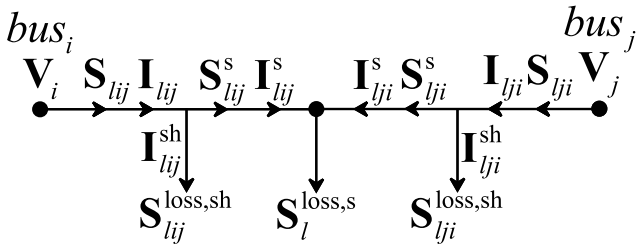

FIGURE 10. Power flow and losses matrix variables representation for an unbalanced π-model branch.

model ($\mathbf{S}^{s}_{lij}$) is defined as:

$$\mathbf{S}^{s}_{lij} = \mathbf{P}^{s}_{lij} + j\mathbf{Q}^{s}_{lij} = \mathbf{V}_i \left(\mathbf{I}^{s}_{lij}\right)^{H}, \tag{105}$$

where $\mathbf{P}^{s}_{lij}$ and $\mathbf{Q}^{s}_{lij}$ represent the active and reactive PF in the series element in π-section model.

The power losses in the electrical circuits are caused by passive components. Therefore, these losses should be modeled to conduct the PF accurately. In the π-section model, the losses happen due to the series impedance ($\mathbf{S}^{loss,s}_{l}$), the shunt admittances at the beginning of the branch ($\mathbf{S}^{loss,sh}_{lij}$), and the shunt admittances at the end of the branch ($\mathbf{S}^{loss,sh}_{lji}$). The series impedance losses depend on the voltage drop over the series impedance, and the series current flows in it [20]. Accordingly, $\mathbf{S}^{loss,s}_{l}$ can be represented as:

$$\mathbf{S}^{loss,s}_{l} = \left(\mathbf{V}_i - \mathbf{V}_j\right) \left(\mathbf{I}^{s}_{lij}\right)^{H}. \tag{106}$$

The voltage drop over the series impedance from bus i to bus j can be represented as a relationship between $\mathbf{z}^{s}_{l}$, and $\mathbf{I}^{s}_{lij}$ as:

$$\left(\mathbf{V}_i - \mathbf{V}_j\right) = \mathbf{z}^{s}_{l}\mathbf{I}^{s}_{lij}. \tag{107}$$

Therefore, substituting (107) in (106), (106) can be written as:

$$\mathbf{S}^{loss,s}_{l} = \mathbf{z}^{s}_{l}\mathbf{I}^{s}_{lij} \left(\mathbf{I}^{s}_{lij}\right)^{H} = \mathbf{z}^{s}_{l}\mathbf{I}^{s}_{lji} \left(\mathbf{I}^{s}_{lji}\right)^{H}, \tag{108}$$

which is symmetrical for the series current flows from either end due to (29). However, the $\mathbf{S}^{loss,sh}_{lij}$ is a function of the $\mathbf{I}^{sh}_{lij}$ and the $\mathbf{V}_i$ as:

$$\mathbf{S}^{loss,sh}_{lij} = \mathbf{V}_i \left(\mathbf{I}^{sh}_{lij}\right)^{H}. \tag{109}$$

Similarly, the $\mathbf{S}^{loss,sh}_{lji}$ can be represented as:

$$\mathbf{S}^{loss,sh}_{lji} = \mathbf{V}_j \left(\mathbf{I}^{sh}_{lji}\right)^{H}. \tag{110}$$

Here, $\mathbf{I}^{sh}_{lij}$ and $\mathbf{I}^{sh}_{lji}$ can be represented through Ohm's law over the shunt admittance at the beginning and end of the line, respectively, as:

$$\mathbf{I}^{sh}_{lij} = \mathbf{y}^{sh}_{lij}\mathbf{V}_i, \tag{111}$$

$$\mathbf{I}^{sh}_{lji} = \mathbf{y}^{sh}_{lji}\mathbf{V}_j. \tag{112}$$

Accordingly, substituting (111) in (109), (109) can be written as:

$$\mathbf{S}^{loss,sh}_{lij} = \mathbf{V}_i \left(\mathbf{V}_i\right)^{H} \left(\mathbf{y}^{sh}_{lij}\right)^{H}. \tag{113}$$

Similarly, substituting (112) in (110), (110) can be written as:

$$\mathbf{S}^{loss,sh}_{lji} = \mathbf{V}_j \left(\mathbf{V}_j\right)^{H} \left(\mathbf{y}^{sh}_{lji}\right)^{H}. \tag{114}$$

The sum of the PFs in the π-section branch model from both ends should equal the branch losses; therefore, the power balance model for the branch losses based on the work in [20], using different loss components (108), (113) and (114), can be represented as:

$$\begin{aligned}\mathbf{S}_{lij} + \mathbf{S}_{lji} &= \mathbf{S}^{loss,sh}_{lij} + \mathbf{S}^{loss,s}_{l} + \mathbf{S}^{loss,sh}_{lji} \\ &= \mathbf{V}_i \left(\mathbf{V}_i\right)^{H} \left(\mathbf{y}^{sh}_{lij}\right)^{H} + \mathbf{z}^{s}_{l}\mathbf{I}^{s}_{lij} \left(\mathbf{I}^{s}_{lij}\right)^{H} \\ &\quad + \mathbf{V}_j \left(\mathbf{V}_j\right)^{H} \left(\mathbf{y}^{sh}_{lji}\right)^{H}. \end{aligned} \tag{115}$$

2) BUS INJECTION MODEL

Bus injection model (BIM) represents the electrical quantities at each and every bus. The bus injection model can be represented by I–V formulations and voltage-based formulations. I-V PF formulation relates the voltages, current injections, and power injection variables [20]. Voltage-based formulation relates to the voltage phasors and complex power injections [14]. The derivation of unbalanced BIM in terms of I–V formulations and voltage-based formulations is expressed in this subsubsection.

- The I–V formulation
  The I–V formulation is structured according to two main fundamental characteristics of AC power systems. First, the linear relationship between the voltage phasors and current injection phasors between two buses; second, the definition of complex power [14]. The mathematical representation of the above two characteristics yields the I–V PF formulation below. Here, the current flows from bus i to bus j ($\mathbf{I}_{lij}$) can be represented as:

$$\mathbf{I}_{lij} = \mathbf{I}^{s}_{lij} + \mathbf{I}^{sh}_{lij}, \tag{116}$$

where $\mathbf{I}^{sh}_{lij}$ is defined in (111), and $\mathbf{I}^{s}_{lij}$ can be defined as:

$$\mathbf{I}^{s}_{lij} = \mathbf{y}^{s}_{l}\left(\mathbf{V}_i - \mathbf{V}_j\right), \tag{117}$$

therefore, (116) can be rewritten as:

$$\mathbf{I}_{lij} = \mathbf{y}^{s}_{l}\left(\mathbf{V}_i - \mathbf{V}_j\right) + \left(\mathbf{V}_i - \mathbf{V}_j\right)^{H} \left(\mathbf{y}^{s}_{l}\right)^{H}. \tag{118}$$

Similarly, the current flows from bus j to bus i ($\mathbf{I}_{lji}$) can be given as:

$$\mathbf{I}_{lji} = \mathbf{I}^{s}_{lji} + \mathbf{I}^{sh}_{lji}, \tag{119}$$

where $\mathbf{I}^{sh}_{lji}$ is defined in (112), and $\mathbf{I}^{s}_{lji}$ can be defined as:

$$\mathbf{I}^{s}_{lji} = \mathbf{y}^{s}_{l}\left(\mathbf{V}_j - \mathbf{V}_i\right), \tag{120}$$

as a result, (119) can be given as:

$$\mathbf{I}_{lij} = \mathbf{y}_l^{\mathrm{s}} \left(\mathbf{V}_i - \mathbf{V}_j\right) + \left(\mathbf{V}_i - \mathbf{V}_j\right)^{\mathrm{H}} \left(\mathbf{y}_l^{\mathrm{s}}\right)^{\mathrm{H}}. \quad (121)$$

Accordingly, the complex power between bus i and bus j ($\mathbf{S}_{lij}$) and vice versa ($\mathbf{S}_{lji}$) can be represented as:

$$\mathbf{S}_{lij} = \mathbf{P}_{lij} + j\mathbf{Q}_{lij} = \mathbf{V}_i \left(\mathbf{I}_{lij}\right)^{\mathrm{H}}, \quad (122)$$

$$\mathbf{S}_{lji} = \mathbf{P}_{lji} + j\mathbf{Q}_{lji} = \mathbf{V}_j \left(\mathbf{I}_{lji}\right)^{\mathrm{H}}. \quad (123)$$

The characteristics of the I–V formulation of the PF equations provide some advantages in various contexts [14]. For example, the I–V formulation's non-linearities are isolated from the bilinear outcomes in (122 and (123. Here, each bilinear term has singularly quantities correlated with a single bus, which is contrasted with other PF representations that have non-linearities that couple variables associated with different buses. Besides, the I–V formulation simplifies the straightforward representations for the components whose current flows cannot be represented individually as functions of their terminal voltages, like ideal transformers and ideal circuit breakers [150]. Such components are more complex for explicit modeling in other PF representations. In contrast, the representation of voltage and current variables might have more variables than other PF representations, leading to computational implications. Here, several researchers employed the I–V formulation characteristics, such as [150]–[157].

- Voltage-based formulations

  The voltage-based formulations can be represented by substituting the current injection equation (118) into the power injection equation (122), which yields a system of polynomial equations in terms of the complex voltage phasors and their conjugates as:

$$\mathbf{S}_{lij} = \mathbf{V}_i \left(\mathbf{V}_i\right)^{\mathrm{H}} \left(\mathbf{y}_{lij}^{\mathrm{sh}}\right)^{\mathrm{H}} + \mathbf{V}_i \left(\mathbf{V}_i - \mathbf{V}_j\right)^{\mathrm{H}} \left(\mathbf{y}_l^{\mathrm{s}}\right)^{\mathrm{H}}. \quad (124)$$

  Similarly for $\mathbf{S}_{lij}$, substituting (121) in (123), (123) can be written as:

$$\mathbf{S}_{lji} = \mathbf{V}_j \left(\mathbf{V}_j\right)^{\mathrm{H}} \left(\mathbf{y}_{lji}^{\mathrm{sh}}\right)^{\mathrm{H}} + \mathbf{V}_j \left(\mathbf{V}_j - \mathbf{V}_i\right)^{\mathrm{H}} \left(\mathbf{y}_l^{\mathrm{s}}\right)^{\mathrm{H}}. \quad (125)$$

  Here, (124) and (125) are non-linear complex matrices form of the BIM for $\mathbf{S}_{lij}$ and $\mathbf{S}_{lji}$, respectively. The complex variables format of the PF equations has some benefits for several analysis forms, such as holomorphic embedding methods [158] and in computing the bounds on the number of PF solutions [159]. The real values for quantities can be obtained by converting (124) and/or (125) using different representations of the complex-valued admittance matrix, voltage phasors, and power injections. Accordingly, these quantities can result in a variety of PF formulations.

Note that using the rectangular coordinates for both the voltage phasors and the admittance matrix results in a system of quadratic polynomials [14]. However, using polar coordinates for the voltage phasors leads to a system of coupled trigonometric functions. The properties of the quadratic equations and their power system applications are derived in [160]. Also, note that more general line models can be represented using both PF models (i.e., BFM and BIM). An example of this line mode is utilized in MATPOWER [137], which allows for shunt susceptances, non-unity transformer voltage ratios, and non-zero transformer phase shifts. More details about the BFM representation of this line model can be found in [161].

B. ALGORITHMS

The unbalanced PF representation can be considered as the basis of distribution network analysis. The main idea of solving the unbalanced PF equations is to determine the values of the three-phase voltages at the buses and the connection points, and the three-phase currents and PFs through all the conducting components, which results in a non-linear system of equations. The solution of the non-linear unbalanced PF equations should be obtained by considering the topology and components of the network and the set points of connected loads and generators. As shown previously, the variables used to represent the unbalanced PF equations can be either in the voltage phasors form, as in BIM or the squared voltage magnitudes at the buses and the active power, reactive power, and squared magnitudes of the current flows on the lines, as in BFM.

Mostly, the systems of non-linear equations may have multiple PF solutions. These solutions can be ''HV/small-angle-difference'' or ''LV/ large-angle-difference''. Typically, the first solution corresponds to a desired operating point; therefore, it is of interest to achieve this solution. However, the other solution is of interest for some applications (i.e., stability analysis). The system's size affects the number of PF solutions [159], [162], [163]. The upper bounds of the number of solutions are obtainable asymptotically with expanding network size as shown in [164]. In contrast, the number of PF solutions for normal operating conditions is significantly smaller than these bounds [142], [165]–[167].

The buses' types can be classified based on PQ, PV, or slack buses. Therefore, selecting the right bus type reflects the typical equipment behaviour. PQ buses are mainly used for representing the buses connected to the loads, which treat the active and reactive powers as specific quantities. This will enforce the active and reactive power equations. PV buses are typically used for representing the buses connected to the generators. This will enforce the active power and squared voltage magnitude equations with particular and specific values for the active power and the voltage magnitude. Finally, a single slack bus is chosen with a specified voltage magnitude and angle. The active and reactive powers at the slack bus are obtained from the active and reactive power equations, respectively; this thus satisfies network-wide conservation of complex power [9].

A couple or more of the constant parameter values can be defined per bus and phase to solve the unbalance PF equations. These parameter values can be specified based on the type of the bus. Commonly, the values of the active

and reactive power injections should be specified at the PQ bus, while the active power injections and voltage magnitudes should be defined at the PV buses. Finally, the voltage angle and magnitude should be set at a slack bus. Therefore, specifying the constant parameter values based on the bus type will result in a square system of equalities. Accordingly, solving the PF equations aims to obtain the values for the associated variables consistent with the parameter values mentioned above, without considering inequality limits (i.e., constraints on voltage magnitudes and line flows, etc.). Several non-linear PF solution algorithms have been proposed in [96] and recently in [97]. Accordingly, Balamurugan and Srinivasan [168] explained the two different frames (i.e., phase frame and sequence frame) that can be considered to perform the unbalanced three-phase PF analysis. Several methods can be incorporated in the context of the phase frame, namely (Kirchhoff) compensation, forward/backward sweep, modified Newton/Newton-like and implicit Zbus Gauss methods. Such methods consider the unbalanced quantities directly. However, decoupled negative, positive, and zero sequence networks represent and solve the unbalanced three-phase system in the context of the sequence frame. Accordingly, this subsection summarizes some of the most used algorithms to solve the PF equations, such as meta algorithms (i.e., Newton-based and fixed-point iteration methods) and concrete algorithms (backward/forward sweep, continuation (predictor-corrector Euler homotopy), current injection and holomorphic embedding algorithms). These algorithms have been widely used in several applications in power systems analyses.

1) META ALGORITHMS

The meta algorithms can be categorized based on their variants into two main methods. These are Newton-based methods and fixed-point iteration method. Newton-iteration variants are more reliably convergent in situations with non-linear network components. However, the fixed-point iteration implementation variants need no derivative information and are quick as they are represented by linear algebra equations [169].

- Newton-based methods
  Newton-based iterative methods solve the PF equations by leveraging some linear approximations developed around a specified operating point. Historically, in the late 1950s, Newton-based methods were deployed to solve the PF equations for modest-size power systems [170]. Later, they were refined for solving linear systems of equations based on sparsity-exploiting numerical techniques for more significant problems [171], [172].
  Newton-based methods for PF applications can be implemented to solve a linear system of equations by alternating between calculating the power/current injection mismatches and updating the voltage phasors' values. The mismatches stand for the difference between the power/current injections obtained based on the voltage phasors' values at the current iteration and the specified power injections. Ideally, the obtained voltage phasors should drive the mismatches toward zero. Thus, the linear system is solved to compute the updated voltage phasors by computing the power/current injection mismatches at each iteration. Here, the Newton-based methods will keep repeating the procedure mentioned above until all of the power/current injection mismatches are under a particular tolerance, which indicates that the obtained solution has acceptable accuracy. Newton-based methods could converge quadratically to a PF solution if the solution's initialization were sufficiently close. The regions of sufficiently close initialization, which will converge to a PF solution, are fractal. In contrast, if the initialization is not near a PF solution, Newton-based methods exemplify the complicated behaviour exhibited [173]–[175]. Also, note that step-size control via ''optimal multipliers'' precludes Newton-based methods' divergence [176]. The algorithms based on Newton-Raphson method show several difficulties at distribution levels, which are well documented in [177].
  Some of the variables are fixed to their corresponding values. These variables vary based on the type of bus. The voltage magnitudes are fixed at PV buses, while the angle and voltage magnitude values are fixed at the slack bus. However, some of the quantities, which do not have specified values, can be eliminated from the calculation procedure at the beginning, such as the reactive power injections at PV buses, and the active and reactive power injections at the slack bus. The values for these quantities can be explicitly calculated after solving for the angles and voltage magnitudes.
  The Newton-based methods can be implemented using any of the Taylor expansion linearizations. The computational characteristics are different from PF linearization to another [178]. For example, the computational speed can significantly improve for many PF problems using the fast-decoupled PF linearization [179]. Here, detailed analytical and empirical analyses of the fast-decoupled PF's convergence behaviour are provided in [180] and [181]. Some of the power system software packages, such as MATPOWER [137], apply Newton methods based on various PF representations.
- Fixed-point iteration method
  The fixed-point iteration method can solve non-linear PF equations [7]. The method starts by representing all of the circuit elements in the primitive admittance matrices in a system nodal admittance matrix format for the principal solution. Every element in a primitive admittance matrix sums directly into one particular location in the system admittance matrix. Accordingly, it is very straightforward to build the system admittance matrix. The current vector can be formed as through the decomposition of currents from the power conversion elements (e.g., loads, generators, etc.). Thus, the decomposition

of current can be formed as the difference between the current drawn by the linear portion of the element embedded in the system admittance matrix and the non-linear power conversion element.

The fixed-point iteration method is fast. Therefore, it is suitable for sequential time solutions. Nevertheless, it can be slightly sensitive in some circuit models. To ensure a good convergence in distribution systems, two main aspects should be considered: (i) the voltages' initial values must be near to the final solution; and (ii) the power delivery elements' series impedance needs to be less than the load devices' equivalent shunt impedance [7].

The first consideration (i.e., (i) above) can be achieved easily, even for rather complex multi-phase circuits. The initial solution can be found based on a non-iterative direct solution of the system admittance matrix. Here, the admittance matrix is performed without the decomposition of currents apart from current and voltage sources. This initial solution is used to find the sequential-time PF solutions, which is fairly close to the new voltage solution. There is no guarantee that the second consideration (i.e., (ii) above) can be achieved. Therefore, the convergence failures should be avoided, especially in the middle of a long yearly simulation. This can be avoided by making the power conversion models revert to a linear one if the voltage deviates from within a prescribed band (i.e., $\pm 5\%$ or $\pm 10\%$ of rated voltage) [7].

2) CONCRETE ALGORITHMS

Concrete algorithms are developed to solve the PF equations. The most well-known and used algorithms are summarized here. The summarized algorithms are backward/forward sweep algorithm, continuation (predictor-corrector Euler homotopy) algorithm, current injection algorithm and holomorphic embedding algorithm. These algorithms are implemented based on meta algorithms (i.e., Newton-based methods and/or fixed-point iteration method), except holomorphic embedding algorithm. Accordingly, backward/forward sweep algorithm is implemented based on the fixed-point iteration method [14]. In comparison, predictor-corrector Euler homotopy algorithm implies only a standard Newton-based method to solve its $2n + 1$ equations in $2n + 1$ unknowns [9]. While a current injection algorithm can be implemented based on either Newton-based methods or fixed-point iteration methods, which are also called ''Newton variants of a current injection method'' or ''fixed-point iteration variants of a current injection method,'' respectively [7]. However, a holomorphic embedding algorithm is implemented based on a method for embedding the original algebraic equations in a holomorphic functional extension of the original equations and a direct (non-iterative) method to calculate the holomorphic functions' power series. The solution based on the direct method does not depend on the variables from the previous iteration, which aims to avoid convergence to a non-desired solution where multiple solutions exist and indicating voltage collapse when there is no solution [182].

- Backward-forward sweep algorithm

  Newton's method can solve the PF equations. However, these equations' recursive structure advances itself to a more intuitive backward/forward sweep algorithm [14], [183]–[185]. To do so, number the source bus (e.g., substation) as bus 0. Here, the voltage at bus 0 can be represented as the set-point voltage. For simplification, it can be assumed that there are no other voltage-regulated buses in the network. The algorithm can be expressed in several steps as follows:
  - **Step I**: Initialize the squared voltage magnitude at the end buses of the feeder by setting its value to be 1.0 p.u.
  - **Step II**: The complex power is defined as 0 at the end buses, and the squared voltage magnitude at the end buses is given, either by Step I or Step V.
  - **Step III**: Go backward from the ends of the feeder to the source bus to compute the active power, reactive power, current flows, and the squared voltage magnitude at each bus (i.e., previous bus in the path from the end bus to the source bus).
  - **Step IV**: Calculate the voltage mismatch at the source bus, where the reference value for the squared voltage magnitude at the source bus is computed in Step III.
  - **Step V**: Set the squared voltage magnitude at the source bus to be equal to the squared set-point voltage magnitude. Here, using the values which are computed in Step III (e.g., active power and reactive power), go forwards from the source bus to calculate the summation of active power and reactive power in the network together with the current flows and the squared voltage magnitude at each bus (i.e., next bus in the path from the source bus to the end bus), using the values of the active power, reactive power, current flows and the squared voltage magnitude for the previous bus. In the case where multiple lines are emanating from a bus, then distribute these new values for the summation of active power and reactive power to the lines in proportion to the flows computed at Step III.
  - **Step VI**: Calculate the power mismatches at all of the end buses.
  - **Step VII**: Check the convergence criteria, which satisfy the condition of the power mismatch being less or equal to the tolerance parameters for power for all of the end buses, and the voltage mismatch being less or equal to the tolerance parameters for voltage mismatch. If these criteria are satisfied, stop the algorithm and print out the results. Otherwise, go back to Step II.

  The backward/forward sweep algorithm can be extended to solve the radial unbalanced three-phase

networks [14]. Here, González-Morán *et al.* [186] improved the backward/forward sweep algorithm, which applies the matrix formulation in an orthogonal-stationary reference frame to solve unbalanced PF equations. The orthogonal-stationary reference frame can generalize the arbitrary connections and device locations and the definition of radially distribution systems. In addition, Mahmoud and Yorino [187] proposed a robust quadratic-based backward/forward sweep (QBBFS) method to solve multi-phase PF problems in distribution systems. The QBBFS method can accommodate different load types, capacitors, distribution transformers, and distributed generation. The QBBFS provides accurate PF results, and it can converge with lower iteration numbers than the existing PF-based backward/forward sweep algorithm methods. Also, it has robust convergence characteristics, especially at heavy loading and high R/X ratios. Furthermore, Hameed *et al.* [188] modified the backward/forward sweep algorithm for islanded radial microgrids. Moreover, Fortenbacher *et al.* [189] proposed a related forward-backward sweep technique for solving optimization problems. The technique proposed in [189] includes several applications, such as solving multi-period OPF problems and optimizing energy storage devices' placement. The formulations of the backward/forward sweep algorithm applied to radial distribution systems with distributed generation are well simplified in [190].

- Continuation (predictor-corrector Euler homotopy) algorithm

  The numerical continuation is often referred to as the process that aims to find a new solution corresponding to different parameter values moving from a known feasible point [191]. Typically, this process can be suitable to find a new solution of the PF that corresponds to different parameter values (e.g., a much higher loading level) than that used in the current solution. Continuation problems have been extensively investigated in power systems in [192]–[195]. Several algorithms have been exploited to solve the PF equations. The ablest continuation algorithm is a predictor-corrector Euler homotopy algorithm [191], [192].

  The continuation PF problem can be solved using predictor-corrector Euler homotopy algorithm as summarized in [9] in the following steps:

  – **Step I**: Define the 1-manifold (or curve) based on the general PF equations as a function of the voltage variables (e.g., angles and magnitudes) for each bus and the parameters. This curve stands for the path between a PF solution and different parameter values. The general PF equations and the equation representing the path solutions corresponding to the parameter values are mentioned in [9].
  – **Step II**: Predict the next point on the curve. This is done by finding the vector tangent to the curve at a point (assume that this point satisfies the predictor-corrector algorithm and is known) and moves along that vector for a predefined distance. This distance is a (scalar) control parameter that effectively establishes the distance between successive points on the curve. The next point on the curve can be predicted as the summation of the known point with the multiplication of the distance and tangent to the curve at the known point.
  – **Step III**: This step is to correct to a reference point, which is defined as a vector of the voltage variables (i.e., angles and magnitudes at every bus) and the curve's parameter values. This is done by solving the intersection of the curve and a hyperplane which both pass through the next point predicted in the previous phase and the orthogonal to the curve's tangent at the known point.
  – **Step IV**: By fixing the values of the first point, the tangent to the curve at the first point, and the distance between successive points along the curve, the reference point is considered to be the only unknown. Here, the resultant equations, which are discussed in detail in [9], are able to be solved with a standard Newton-based method.
  – **Step V**: After the second point on the curve has been established, an approximate tangent vector can usually be adopted to obtain successive points. The approximate tangent vector at the k-th point is taken to calculate the $(k+1)$-th point.
  – **Step VI**: Check the iteration number. If the iteration number equals or exceeds the maximum number of iterations, then terminate the algorithm and print out the results. Otherwise, go to Step II.

  The exact tangent vector needs more computation than the approximate tangent vector. Nevertheless, the approximation vector, which is incorporated into the procedure above, may decrease the accuracy of the results in regions of high curvature.

- Current injection algorithm

  Current injections with state variables are presented in [196] to solve the PF formulations. This representation is expressed in a combination of rectangular and polar coordinates. In this work, a PQ bus is represented by two equations consisting of the imaginary and real components of the current injection mismatches, which are expressed by means of the rectangular voltage coordinates. However, a PV bus is represented by a single active power mismatch equation associated with angle deviation. While Tinney [197] described the current injection algorithm in terms of a constant nodal admittance matrix. This researcher concluded that this algorithm cannot be generalized for all the PF applications as the satisfactory modeling of PV nodes is still undeveloped. Accordingly, da Costa *et al.* [198] developed a generalized current injection algorithm, which used $2n$ current injection equations in rectangular coordinates

for both PV and PQ buses for balanced distribution networks. However, Garcia *et al.* [169] extended the work in [198] to solve the PF equations for unbalanced three-phase networks.

Current injection formulation has an interesting property, in which the structure of the Jacobian matrix is the same as the bus admittance matrix; therefore, it has sparsity properties. Also, the number of elements that need to be recalculated in the iteration process is minimal. Accordingly, the Jacobian matrix will be constant in strictly radial distribution systems with no cogeneration plants. Therefore, the current injection algorithm is robust and converges in fewer iterations than the backward/forward sweep algorithm, especially for heavily loaded systems [169].

The implementation of the algorithm to solve the unbalanced PF equations can be summarized in several steps based on the work in [169], as follows:

- **Step I**: Assemble the nodal admittance matrix, set voltages to initial values and begin the iteration count.
- **Step II**: Determine the three-phase current injections for all of the buses. Then, obtain the power mismatches at all of the end buses. The power mismatch can be obtained by subtracting the obtained active and reactive power injections in this step from specified active and reactive powers at a given bus, respectively. Here, the specified active and reactive powers at a given bus can be computed by subtracting the active and reactive powers of loads from the active and reactive powers of generators for the given bus, respectively.
- **Step III**: Test for convergence by ensuring that the active and reactive power mismatches are less or equal the tolerance parameters. If the convergence criteria is satisfied, go to Step VIII. Otherwise, go to the next step.
- **Step IV**: Compute the Jacobian matrix, which contains identical partitions to the bus admittance matrix.
- **Step V**: Solve for the voltage increments at each iteration. The voltage increments can be solved by using the sparse matrix techniques, which applies the well-known Tinney-2 ordering scheme to solve the linear system of equations that resulted from applying Newton's method to the real and imaginary parts of the three-phase current mismatches for all of the buses.
- **Step VI**: Update the voltages in the final sparse matrix of the system, then go to Step II.
- **Step VII**: Check the iteration number. If the iteration number equals or is more than the maximum number of iterations, then go to Step VIII. Otherwise, go to Step II.
- **Step VIII**: Terminate the algorithm and print out the results.

In this context, Sunderland *et al.* [199] presented an improved current injection method for a PF analysis of unbalanced multiple-grounded 4-wire distribution networks. Here, all the network elements are represented using suitable admittances to ensure that they result in a system's admittance matrix considering all network phases. The same approach is implemented in OpenDSS software [7], which utilizes a phase frame of reference to solve the PF problem in generic n-phase networks.

- Holomorphic embedding algorithm

The holomorphic embedding algorithm was introduced in [182], in 2012. Trias [182] utilized a holomorphic power balanced equation in order to transform the complex node voltage to a function of the node voltage power series with analytic continuation techniques [200], [201]. Later, Subramanian *et al.* [202] extended the holomorphic power balanced equation for PV nodes with active power constraints. Here, the extension equation can be represented as the summation of two conjugate complex power and voltage magnitude constraints determined by two conjugate complex voltage multiplications.

The holomorphic embedding algorithm can converge a PF solution under heavy power transmission. It considers non-divergence, which assures its robustness under heavy load scenarios [182], and it is not sensitive to the initial points like the Newton–Raphson method [203]. Systematic description of a holomorphic embedding algorithm and comparisons with the Newton-Raphson algorithm are covered in [204]. Besides, compared to the homotopic continuation PF algorithm [205], the holomorphic embedding algorithm can fully use complex analyticity and analytic continuation, and it is considered a global method [206]. In contrast, the homotopic continuation PF algorithm only utilizes single differentiability and continuity, and it is considered a local method [207].

Embedding the ZIP load model in an ACPF with a more accurate feature description is derived in [208] and [209]. DC PF and non-linear DC circuits [206], flexible AC transmission system, and transformer taps [210] can also be modeled using holomorphic power balanced equations. Accordingly, Sun *et al.* [203] improved the holomorphic embedding algorithm to handle the three-phase active distribution networks, delta connection load, ZIP load, and distributed generators (DGs) by introducing three-phase network constraints of the complex node voltage power series. Here, phase-to-phase complex voltage variables and additional linear constraints are added to the algorithm. Besides, conventional non-linear zero-power injection-network constraints are converted to a linear zero-current injection network to improve the algorithm's efficiency. Later, Keihan Asl *et al.* [211] developed linear and non-iterative characteristics of the holomorphic embedding algorithm to solve the unbalanced PF problems in radial

distribution networks. The developments include using a suitable and straightforward approach in calculating the admittance matrix, which converts the admittance matrix of an unbalanced network to a symmetric matrix (i.e., like a balanced network). All the network elements (e.g., lines, loads, DG units, shunt admittance, capacitors and transformers) can be modeled in the admittance matrix (or transformed into the equivalent current vector).

The steps for implementing the holomorphic embedding algorithm to solve the unbalanced PF equations based on research in [211] are as follows:

- **Step I**: Import the lines and loads data considering the mutual relationship between sections. Also, import the PV elements data and define their locations in the unbalanced distribution network.
- **Step II**: Calculate the admittance matrix as a relationship between the bus current injection vector and the bus voltage vector. The admittance matrix can be represented as the interface of bus voltages and line parameters, containing shunt elements, series elements and mutual coupling impedances.
- **Step III**: Model the tap-changer, doubly-fed induction generator, and DG units. Accordingly, modify the current vector or admittance matrix.
- **Step IV**: Formulate equations for each bus type as shown in [211].
- **Step V**: Compute the germ solution of bus voltages by taking into account the 120° phase between them, and set the parameter n at a suitable value, where n should satisfy the convergence.
- **Step VI**: Solve a linear system of equations and evaluate the power series coefficients for all buses' voltage and reactive power for the PV buses.
- **Step VII**: Check the reactive power of PV buses within the permissible range. If not within, the bus type should be altered to a PQ bus and return to Step IV. Otherwise, go to Step VIII.
- **Step VIII**: Terminate the algorithm and print out the results.

The holomorphic embedding algorithm has been applied in voltage stability analysis [212], [213] and nonlinear network reduction [214]. Compared with the Newton–Raphson method, the holomorphic embedding algorithm can calculate the PF solution under different load scales concurrently [215], [216], rather than by a step-by-step process, which speeds up voltage stability. Moreover, the holomorphic embedding algorithm is applicable to large-scale transmission networks [207]. Other interesting work is proposed in [217], who modified the holomorphic embedding algorithm to solve the hybrid AC-DC microgrid PF problems.

C. TOOLS

The electrical networks' PFs are simulated using PF solvers (i.e., implementation of an algorithm), which are considered the essential technology for the simulation. Several tools (i.e., software and packages) are in use for this purpose. These tools can be categorized based on the access to commercial and open access. Some of the most used commercial tools are Digsilent PowerFactory, Siemens' Power System Simulator (PSS)/Sincal, and CYMDIST. At the same time, the most used open-access tools for unbalanced PF simulation are Open Distribution System Simulator (OpenDSS) [218], GridLab-D [219], [220], and Open Platform for Energy Networks (OPEN) [221]. In contrast, pandapower [222], and PowerWorld Simulator are transmission level tools operated with the assumption that the system is a balanced three-phase system. Besides, PowerWorld Simulator was developed to simulate high voltage systems, and is mostly utilized for transmission planning, management of power markets, and studying large-scale renewable energy generators. However, other open-access tools are used in power distribution modeling, but they do not support the unbalanced PF. Examples are Hybrid Optimization of Multiple Energy Resources (HOMER), Calliope, Open Source energy MOdelling SYStem (OSeMOSYS), PLEXOS, TIMES, and Power Grid and Market Analysis (PowerGAMA). These tools use active-power only/power balance approaches. The reader can refer to [221], [223], [224] for a detailed comparison of tools with distribution modeling support.

In Australia, the available commercial tools that are in use by most of the DNSPs are Digsilent PowerFactory and PSS/Sincal. In comparison, open-access tools, such as OpenDSS, are used in some industrial projects (e.g., Advanced Planning of PV-Rich Distribution Networks [225]. Simultaneously, pandapower [222] is the most used tool in the energy market (e.g., Ausnet). Even so, pandapower does not support distribution network contexts in its current version. Digsilent PowerFactory supports both balanced and unbalanced PF, PSS/Sincal supports balanced power and unbalanced PF (3-wire and 3-phase), OpenDSS supports balanced and unbalanced PF and pandapower supports only balanced PF.

1) DISTRIBUTION UNBALANCED PF TOOLS

Each tool has been developed with different objectives and resource levels. In this subsubsection, the aim is to review the commercial (e.g., Digsilent PowerFactory, PSS/Sincal, CYMDIST, etc.), and open-access (e.g., OpenDSS, GridLAB-D, OPEN, etc.) tools that are designed for unbalanced distribution system analysis.

- DIgSILENT PowerFactory
  DIgSILENT PowerFactory is considered to be a leading commercial power system analysis software and was developed by DIgSILENT GmbH [226]. The software offers several applications for analyzing generation, transmission, distribution, and industrial systems. It has features for advanced applications, including distributed generation, wind power, real-time simulation and performance monitoring for system supervision and testing [227]. It is considered user-friendly with its

flexibility for interfacing and scripting. It suits integrated and highly automated solutions and has reliable, flexible system modeling capabilities, powerful algorithms and its own database concept.

The DIgSILENT PowerFactory is compatible with Windows. The software can import and convert network model data from several other modeling applications. Besides, bi-direction data exchange is possible using a DGS interface tool that supports various data formats. It deals with ''.ascii'', ''.xml'', ''.csv'', and ''.odbc'' files. It supports supervisory control and data acquisition (SCADA) and geographic information system (GIS) interfacing. Also, the software can import the data from several platforms, such as PSS/E, PSS/U, PSS/Sincal, UCTE, common information model (CIM) data exchange tools (e.g., ENTSO-E Profiles 2009, CGMES 2.4.15 certified and CGMES 3.0), Neplan, Integral 7, Elektra, ISU, Reticmaster, and PRAO1. Furthermore, the software can export the data for some other platforms, namely CIM1 (e.g., ENTSO-E Profiles: 2009, CGMES 2.4.15 certified and CGMES 3.0), UCTE, PSS/E1, and Integral 71 [228].

DIgSILENT PowerFactory offers several basic features such as PF analysis, short-circuit analysis, sensitivities/distribution factors, and basic MV/LV network analysis. Also, it offers a list of advanced features, such as quasi-dynamic simulation, contingency analysis, network reduction, protection functions, distance protection, cable analysis, power quality, and harmonic analysis, arc-flash analysis, connection request assessment, transmission network tools, distribution network tools (e.g., tie open point optimization, voltage profile optimization, phase balance optimization, optimal equipment placement, optimal capacitor placement, hosting capacity analysis and outage planning), probabilistic analysis, outage planning, reliability analysis functions, linear optimization problems in a power system, UC, and dispatch optimization, state estimation, economic analysis tools, small-signal stability, electromagnetic transients, stability analysis functions, motor starting functions, system parameter identification, scripting, automation, and interfaces [229].

Moreover, DIgSILENT PowerFactory offers several power equipment models, network representation, network diagrams, network model management, and graphic features. The software has a large and comprehensive components modeling library, fully version-controlled with regular model updates, selectable complexity (classical, standard), synchronous machines (e.g., motor/generator), asynchronous machines (e.g., motor/generator, standard (single- or double-cage IM), saturable (single-cage IM and doubly-fed IM), asynchronous starting, and machine parameter identification. It can be adapted for a static generator (e.g., wind- and PV-generators, micro-turbines, fuel cells, general storage devices, batteries etc.). It has an external grid model for simple representation of the external supply system, a dedicated PV system model, and load models. Special LV and MV load models with input based on annual energy values and load profiles, DC or AC overhead lines, DC or AC cable systems are also supported. In addition, DIgSILENT PowerFactory has busbar trunking systems, booster transformer, and 2-, 3- and 4-winding transformer/auto transformer. It also offers modelling of high-voltage direct current (HVDC) systems. Moreover, it supports HVDC-MMC models, representation of various power electronics based equipment, and electromagnetic transients modelling of any user-defined power electronics topology. It includes containment of electromagnetic transients user-defined power electronics (PE) equipment models within sub-models, allowing simple and unified single line diagrams with all other calculation functions, thyristor controlled series compensation (TCSC), static var compensation (SVC), shunt/filter models, and harmonic filters (single- and double-tuned, high pass). Furthermore, it supports series reactor, step-voltage regulator, series capacitor, circuit breakers, common impedance, signal analysis models (e.g., fast Fourier transform (FFT) analysis), protection devices, controller models (e.g., station and secondary controller) including various control methods (e.g., transformer tap controller, virtual power plants and PF capability curves for generators), and parameter characteristics (e.g., scaling factor, vector, matrix, files) for modelling of load profiles. DIgSILENT PowerFactory offers wind/PV infeed, temperature dependencies, composite models for node and branch models, and grid organisation and element grouping (e.g., zones, areas, boundaries, circuits, routes, feeders, operators, owners, etc.) [230].

DIgSILENT PowerFactory offers two main PF solvers: the AC Newton-Raphson algorithm for unbalanced and balanced PF problems and a linear DC method. The Newton-Raphson algorithm is an enhanced non-decoupled Newton-Raphson technique with power or current mismatch iterations placed into the current injection algorithm (i.e., the Newton variant of the current injection method) [231]. Besides, the DC load flow, solving for active PFs and voltage angles is robust and rapid as it linearizes the system equations with no iterations required. Several factors affect the DC PF's accuracy. First, the voltage profile must be as flat as possible, which means the voltage deviations should be as small as possible. Otherwise, the active power estimation error may be high. Second, the R/X ratio should be sufficiently high. Otherwise, this violates the assumption of negligible resistance [232], [233].

DIgSILENT PowerFactory can model single- and three-phase PV systems considering voltage-dependent reactive power capability constraints and PV plant controllers with set-point characteristics by applying an external dynamic model and capability curve. Also,

it offers voltage profile optimization for bi-directional PF in systems with high distributed PV generation, including optimal distribution transformer tap positions and capability limits of PV inverters. Thus, DIgSILENT PowerFactory offers active and reactive power local and remote (i.e., decentralized, distribution and centralized) control strategies, droop characteristics for PV systems, and other voltage regulation options, such as SVC, shunt, and tap controllers using quasi-dynamic simulation language (QDSL) models [229], [234].

- PSS/Sincal

  PSS/Sincal is a power system analysis software developed by Siemens AG [235]. It has several capabilities in dealing with generation, distribution network planning and analysis, transmission network planning and analysis, and industrial power systems, including maintaining high reliability of supply, protection, and efficiently integrating renewables and DERs. It is an object-oriented data model that allows the development of user-defined applications and handles complex multi-user projects. It can conduct several analyses, namely, PF analysis, short-circuit analysis, harmonics contingency analysis, stability analysis, and electromagnetic transients analysis [236].

  PSS/Sincal is fully compatible with Windows. The software can handle the data provided by the GIS, SCADA, distribution management systems (DMS), and meter data management system (MDMS). Moreover, it can import and export the data from access, oracle, SQL-server, and SQLite. PSS/Sincal can interface with other platforms, such as PSS/E, PSS/ODMS, DIgSILENT PowerFactory, UCTE, DVG, CYMDIST, DINIS, CIM (e.g., v10, v12, v14, and v 16), PSS/SincalSmartLF, and PSS/Adept. Also, the software offers the ability for scripting using VBA, VBS, C++,.Net, Python, and Java to improve the models or the results representation using Windows component object model (COM) interface [236].

  The software supports several component models from a simple bus-branch to a full substation model, including single-phase, two-phase, bi-phase and three-phase topology to model any network type (e.g., complex load modeling, overhead lines and cables, phase shifters and asymmetrical transformers), supports any network structure, predefined work element groups (e.g., areas, zones, owners, etc.), defined and automatically detected restoration schemes, co-simulation options between applications (including DC and AC or real-time usage), substation models or any user-specific configuration, node-branch/bus-breaker, enhanced protection modeling, equipment such as (remote) circuit breaker, disconnector, voltage and current transformers, fault observations, trench model for automatic network design and cost model layer for OPEX and CAPEX simulations, extensive localized equipment libraries, libraries for protection devices and with dynamic models (e.g., wind generators, FACTs, batteries, PV and others), libraries with simulation characteristics (e.g., harmonic distortions, motor start-up/torques curves and operation), load profiles and reliability patterns, a built-in calculator for line drop compensation, automatic motor identification, and cable and transformer design tools. Besides, the software allows user-defined models [236], [237].

  PSS/Sincal implemented the Newton variants of the current injection method to solve the balanced and unbalanced PF problems in electrical networks and 4-wire systems, considering a high modeling depth for elements and controlled elements. Accordingly, the software supports several applications in PF analysis: (i) planning of new networks and network areas as well as the analysis and restructuring of existing networks; (ii) determination of the voltages at all nodes in a symmetrical or asymmetrical network; (iii) compliance with regulatory requirements of the permissible minimum and maximum operating voltages; (iv) determination of the equipment utilization (loading) in a symmetrical or asymmetrical network; (v) checking and planning of switching operations and switching configurations; (vi) optimization of the settings of controllable and adjustable equipment (e.g., tap position for transformers and capacitors); (vii) validated network model based on measurement results, and (viii) loss observations [236], [237].

  The software can model and simulate controlled elements with regulators such as transformers, capacitors, and reactors or the individual control of network elements depending on any variables (e.g., voltage, current and power) in the entire network model. PSS/Sincal offers a central volt/var optimization (VVO) module to control the voltage and the power factor in LV and MV radial feeders, which aims to keep the voltages at all consumer nodes within the defined voltage range and transfer the reactive power as little as possible. Therefore, the volt/var optimization can determine the location, number, and size of the capacitors and the transformer's settings at the beginning of the feeder. This will ensure that the voltage ranges of all the feeder's consumer nodes are within the permissible range under high load and under low load. However, the software does not support the smart inverter control strategies to mitigate the voltage issues [236], [237].

- CYMDIST

  Eaton Corporation developed a distribution system analysis base package of the CYME software, which is called CYMDIST [238]. The package is not open-license software, but a trial version is available. It performs several types of simulations in electric distribution system planning by bundling all the required modeling and analysis tools. The package supports balanced or unbalanced distribution models and can handle PF problems and carry out the voltage drop analysis in radial,

meshed or looped configurations. Here, the package performs several analyses, such as PF, load allocation and estimation, fault analysis (e.g., fault location, short-circuit/fault flow, series and simultaneous fault and voltage sag), optimal capacitor placement, load balancing, sizing motor starting, and batch analysis.

CYMDIST can deal with ''.csv'' files and import AutoCAD drawing files. Results can be exported results to Excel or a browser to pre- or post-process data [223]. CYMDIST is compatible with MATLAB and Python, which allows customizing the package's capabilities for specific user needs. It can also interface with Windows COM.

CYMDIST can represent a distribution network from sub-transmission to the customer meter, including the LV secondary system (e.g., meshed or radial), the MV primary system, and the sub-transmission system in detail [239]. Accordingly, it can support modeling of the LV distribution system, including single- and three-phase center-tap transformers, service drop cables (e.g., triplex and quadruplex), LV spot load linked to the center-tap, center-tap connected sources, meters and single-phase center tap connected generators, shunt capacitors, motors, and reactors. Moreover, detailed modeling of the substations is possible using the equipment library (e.g., buses, cables, switches, transformers, protection devices, circuit breakers, etc.). CYMDIST allows the users to create new components based on the available templates of the library and the nameplate data of particular equipment [240]. Several DG models are available in CYMDIS, including for wind energy conversion systems, PV generators, and micro-turbines. Some PV generators can be modeled as electronically coupled generators [241]. The package also contains a user interface with some flexibility and a customizable work space, to which users can drag and drop graphical representations of elements to construct the model of a power system. Furthermore, users can also access online maps and include other visualization.

CYMDIST performs steady-state and time-series analysis of a power system under different operating conditions, and simulations with time-series and fixed data. Also, it can simulate the dynamic behaviour of distribution systems in diverse transient event conditions through an add-on optional module. CYMDIST applies an unbalanced Newton-Raphson algorithm for solving the unbalanced PF equations. The solver considers underground secondary networks (e.g., spot networks or urban grids), LV installations, and sub-transmission systems tied to the distribution systems. The analysis output can be obtained for the entire system, or individual locations including current, voltage, power factor, abnormal conditions, losses, and unbalanced factors.

CYMDIST can model single- and three-phase DERs (e.g., PV cells, fuel cells, wind energy conversion systems, and micro-turbines). Here, the impacts of the DER can be evaluated within minutes in CYMDIST. Also, the package applies the DRIVE module, designed by the Electric Power Research Institute (EPRI), to return hosting capacity calculation results. Moreover, the package offers a volt/var optimization module, aiming to find the optimal settings and configuration of the installed capacitors and load tap changers transformers in a distribution network, based on remote or local control of voltage and reactive PF. The volt/var optimization is conducted based on objectives, such as improving voltage profile, reducing the losses in the system, and peak shaving [242]. Even so, CYMDIST does not support the smart inverter control strategies.

- OpenDSS

  Distribution System Simulator (DSS) was devised by Electrotek Concepts in 1997 for distribution networks. In 2004, EPRI made the package open-access. Accordingly, the package is called Open Distribution System Simulator (OpenDSS) in 2008 [7], [218], [243], [244]. It was initially developed to analyze the North American unbalanced and n-phase distribution system and model the m-winding transformers. OpenDSS can handle the European-style distribution systems (e.g., comparatively MV networks and extensive LV networks) [218]. The software also supports modeling DER for grid modernization and integration to the distribution system. Transmission system studies combined with DER are covered by the software, which provides a holistic assessment of power system response. It can capture both location-specific and time-specific DG benefits and model the variable DG that do not follow typical load shapes (e.g., renewable generators, EVs, and storage) based on sequential-time simulations [218].

  The software is programmed in Delphi and Pascal. However, some scripting is done based on MATLAB interfaces to improve its performance. It is Windows (e.g., Win32 and Win64) based tool. It can interface with Windows COM, which permits the inclusion of external communication simulation programs (e.g., ns2 and OpNet). OpenDSS is compatible with some other platforms, such as MATLAB, Excel, Python and Julia. Furthermore, it supports ''.csv'', ''.xlsx'' (i.e., Excel), ''.txt'', and ''.mat'' (i.e., MATLAB) files. The outputs of the software can result in several file types, such as ''.csv'', ''.xlsx'' and ''.mat'' files. The software is well documented, and has several examples and IEEE Test Feeders [245].

  OpenDSS has several simulation capabilities, such as PF analysis (i.e., the results include the voltages, losses, flows, and other information available for the total system, certain defined areas and each component), short-circuit fault studies (i.e., a conventional fault study for all buses, a single snapshot fault and applying faults randomly), harmonic flow analysis (i.e., by defining harmonic spectra connected to generator, load, voltage and current source objects and some other power

conversion elements), dynamics (e.g., basic electromechanical transients for inverter modeling, governor and/or exciter model and induction machine model), load parametric variation (e.g., load growth), and geomagnetically induced current (GIC) analysis (i.e., quasi-DC models limited for three-phase systems) [245]. OpenDSS has several solution modes that express the resolution of the results to enhance distribution planning studies and interconnection studies with large capacities of variable generation. The solution modes cover snapshot PF as well as the time period of 1-second to 5 seconds (i.e., duty cycle mode), 1-hour to 24 hours increments (i.e., daily mode), and 1-hour to 8,760 hours increments (i.e., yearly mode). It also offers some flexibility to users for customizing solutions [245].

OpenDSS has four main categories: power delivery, power conversion, control, and meter elements, that the users can use. Some of the variables of these elements can be redefined by the user (i.e., user-written model). Firstly, the power delivery elements include capacitor model (e.g., basic, grounded wye-connection, delta-connection, and ungrounded wye-connection), multi-phase and two-port lines or cables π-model with shunt capacitance, reactor model (e.g., basic, grounded wye-connection, delta-connection, and ungrounded wye-connection), multi-phases and multi-windings (e.g., two or more) transformer model (e.g., wye-delta connections), GICTransformer model (i.e., used as a combination with GICLine model), and autotransformer model. Secondly, the power conversion elements include GICLine model (i.e., is used in the calculation of GIC), load model as kW and pf, kvar and pf or kW and kvar (e.g., a dutycycle load shape, daily load shape and yearly load shape), generator model as kW and pf or its kW and kvar, which automatically converts into a form of Thevenin equivalent model when the program switches to dynamics mode (e.g., a dutycycle load shape, daily load shape and yearly load shape), induction machine (e.g., asynchronous machine) model, and storage model. Thirdly, the control elements include CapControl (i.e., capacitor control) model, RegControl (i.e., voltage regulator or load tap changer (LTC) control) model, and InvControl (i.e., inverter control strategies) model. Finally, the meter elements include EnergyMeter model and Monitor model [245].

The non-linear elements (e.g., loads and distributed generators) are considered as injection sources to be used in the iterative PF algorithms. However, in the direct PF solution, the non-linear element can be modeled as admittances in the system admittance matrix. The user can select the representation of the non-linear elements by allocating the global LoadModel property to primitive ''Admittance'' or ''Powerflow'' (i.e., A or P). The default option is ''P''. Accordingly, the PF problem can be solved based on two main algorithms: (i) fixed-point iteration variant of current injection method (i.e., ''Normal'' current injection mode), which is the default mode; and (ii) Newton variant of current injection method (i.e., ''Newton'' mode). The fixed-point iteration variant of current injection method (i.e., ''Normal'' mode) is faster than the ''Newton'' mode. Besides, it is a fairly straightforward fixed-point iterative method, now almost as robust as the Newton mode for hard to solve circuits. Accordingly, PF calculations use an iterative algorithm (i.e., Normal or Newton) with non-linear load models, while fault studies employ a direct solution method with linear load models. Furthermore, dynamics mode simulations can implement linear load models or a mixture of linear and non-linear models [245].

OpenDSS provides separate models of the controllers (e.g., fuses and relays) and controllable devices (e.g., tap changers and capacitors) with small-time increments with the users' flexibility to customize the controller models. The software also models several types of generators and PV systems (i.e., PVSystem objects) and storage batteries. PV systems can be modeled as single-phase and three-phase systems. The PV systems can be controlled by several inverter control modes (i.e., the InvControl object) to achieve fixed power factor, volt-watt, volt-var, combined mode (i.e., volt-watt/volt-var), and other advanced inverter control features [245]–[247].

OpenDSS is developed with an object-oriented structure, which enables the addition of new models of power-carrying equipment and controls with less concern for breaking, and facilities for collaborating on Smart Grid Research [7]. OpenDSS is considered a separate, stand-alone output post-processing program that can produce a model's circuit plots. OpenDSS-G [248] is a developed version of OpenDSS for an on-screen design and editing interface. OpenDSS-G supports online editing, zooming, or dragging and dropping shapes. OpenDSS-G has several features, such as full compatibility with OpenDSS, harmonics and frequency sweep simulation, improved graphical environment, time mode, dynamics mode, export utilities, and parallel processing. For more details about the use of OpenDSS-G and it is additional features, the reader can refer to the OpenDSS-G youtube channel in [249].

- GridLAB-D

  GridLAB-D was developed by the U.S. Department of Energy Office of Electricity Delivery and Energy Reliability at Pacific Northwest National Laboratory (PNNL) in 2008 [219]. GridLAB-D is a power distribution system simulation and analysis tool combined with distribution automation models and software integration tools for power system analysis [220]. It can carry out energy-efficiency impact analysis and renewable energy integration. The software supports a residential model including a series of residences and appliances (e.g., dishwasher, refrigerator, cooker, heater, dryer and electric vehicle charger) that can be modeled and

integrated into the distribution network. Besides, it examines the detailed interplay between all elements of a distribution system, from substation to end-use load (e.g., line, transformer, regulator, capacitor, fuse, generator, solar PV and wind power generators, and unbalanced loads). It also combines the market (i.e., auction) simulation and appliance controllers under the ''market model''. GridLAB-D supports the modeling and simulation of smart grids as it offers a set of essential modules (e.g., market, real-time, and communications network modules). Moreover, it supports demand-side management and its reliability metrics calculations (i.e., system average interruption duration index and system average interruption frequency index).

The software is written in C/C++. However, some scripting is done based on MATLAB interfaces to improve its performance. It is compatible with Windows (e.g., Win32 and Win64) and 32/64 bit for Linux/Unix and Mac OSX. The different network elements need a text-based format (i.e., ''.glm'' format) to describe them. However, the simulation parameters need to be defined within the command window. It is compatible with some other tools, such as MATLAB, web services, and MySQL. Furthermore, it supports ''.csv'' (i.e., Excel), and ''.mat'' (i.e., MATLAB) files to pre-process or post-process data. The outputs of the software can be produced as results in several file types, such as ''.csv'' and ''.mat'' files. The software has several examples and IEEE Test Feeders.

The software can conduct PF analysis, time-series calculation, and power loss calculation. It can handle single and three-phase unbalanced radial or meshed networks. The ''powerflow'' module performs distribution level solver methods to obtain the steady-state node voltage and line current values in a system given the system model, electrical loads connected at each node, and voltage at the substation [250]. A three-phase unbalanced PF solver is implemented in the software. Two main algorithms are used based on the network topology. These methods are fixed-point iteration variant of forward-back sweep method (i.e., default algorithm) and three-phase unbalanced Newton variant of current injection method (i.e., Gauss-Seidel or Newton-Raphson algorithms) [251]. The fixed-point iteration variant of forward-back sweep method is used if the network topology is strictly radial. The specific methodology and equations of the fixed-point iteration variant of the forward-back sweep method are described in [14]. However, the three-phase unbalanced Newton variant of the current injection method (i.e., Gauss-Seidel or Newton-Raphson algorithms) is used if the network topology is non-radial. The implementation of Gauss-Seidel or Newton-Raphson algorithms is described in [169], [252], respectively.

A ''solver_method'' switch has to be passed in the ''.glm'' file to change the solver method in GridLAB-D. Accordingly, ''FBS'' stands for the forward-back sweep algorithm (i.e., default solver), ''GS'' for the Gauss-Seidel algorithm, and ''NR'' for the Newton-Raphson algorithm. Most components' models in the ''powerflow'' library are available for use. Some of the components still need to be implemented based on the PF solver. For example, switches, relays, fuses, split-phase transformers, and regulators still need to be implemented in the Gauss-Seidel solver. Also, some specific regulator models still need to be implemented in the Newton-Raphson solver. In default mode, the ''powerflow'' module cannot model the shunt admittance of overhead or underground lines. This feature can be enabled by setting ''line_capacitance'' to ''true'' [251]. The method for modeling components in the ''powerflow'' module is consistent with that in [14], with some minor adjustments needed for Gauss-Seidel implementation.

The GridLab-D can model many PV generators using the ''solar'' object [253]. The inverter can be modeled using the ''inverter_dyn'' object, which is a reworked ''inverter'' object. The ''inverter_dyn'' object was created to focus on dynamic responses of the inverter [254]. The inverter model could be either three-phase or single-phase. The ''inverter_dyn'' object aims to model the dynamic behaviour of a grid-forming/grid-following inverter and better support the dynamic simulations of GridLAB-D. Two main inverter modeling modes are used in the software: grid-following and grid-forming. The grid-following mode applies constant PQ control, frequency-watt control, and volt/var control. The grid-forming mode uses droop controls, overload mitigation control, and isochronous control [253], [254]. The software also supports a coordinated volt-var control (CVVC) strategy to coordinate regulators and capacitors on a distribution feeder, or a feeder group. Accordingly, a predefined voltage level and reactive power compensation for a feeder group is controlled by one centralised entity based on the control logic proposed in [255]. In addition, level control and remote control (i.e., control for a remote node) for the capacitor banks (e.g., voltage, current, kVAR, and volt/var) are available in GridLab-D [250].

GridLab-D has some limitations [223]: (i) it cannot perform the short-circuit analysis for complex networks (i.e., it is only able to accommodate simple radial networks); (ii) it has no inbuilt conversion tool to import models from other programs; (iii) it suffers from a lack of documentation for beginner users; and (iv) it does not support a user interface for on-screen design and editing; therefore, the users should execute the model using the command line. To overcome the on-screen design and editing issue, Al Faruque and Ahourai [256] developed the GridMat tool, which offers a visual interface within MATLAB for modelling the elements for power and control algorithms via Simulink.

- OPEN
  Open Platform for Energy Networks (OPEN) [257] was developed by Oxford University's Energy and Power Group's Open Platform for Energy Networks in 2020. OPEN offers four main base classes, including asset, energy system, market, and network. It contains two energy management system (EMS) methods for controllable ''Asset'' objects. These methods are (i) multi-period optimization with a basic 'copper plate' network model; and (ii) multi-period optimization with a linear multi-phase distribution network model including voltage and current flow constraints. OPEN has two main simulation methods: (i) for open-loop optimization and (ii) for model predictive control (MPC). In the open-loop optimization method, the EMS method aims to find the controllable asset's references over the EMS time series; therefore, the EMS method is run prior to the operation. In contrast in the MPC, the EMS method aims to update the flexible asset's references at each step in the EMS time series; therefore, the EMS method is utilized with a receding horizon.
  OPEN is programmed in Python. It uses a pandapower package internally as the main toolbox. It also uses other Python toolboxes, such as pandas, scipy, cvxopt, scikit-learn, Numpy, Picos = 1.1.2, Matplotlib, numba, and requests. This toolbox is an object-orientated, which provides code reuse, modularity, and extensibility. The toolbox can read ''.csv'', ''.xlsx'' (i.e., Excel), and ''.txt''. The toolbox illustrates two examples [221]: (i) EVs smart charging; and (ii) flexible heating ventilation and air conditioning (HVAC) demand-side response.
  OPEN has several electrical components, such as constant power loads/sources in wye and delta connection configurations, capacitor banks, and constant impedance loads. Also, the π-equivalent circuit is used to model the lines. Moreover, transformers can also be modeled with any combination of delta primary and secondary connections, or wye and wye-grounded connections. However, constant current loads, switches, voltage regulators, over-current devices, and motors are not supported in the current version [221].
  The loads and DERs are defined using the ''Asset'' object. It has several attributes that allow the users to define phase connection, network location, and real and reactive output power profiles over the simulation time series. The output power profiles and state variables of the flexible ''Asset'' classes can be updated using an update control method called ''EnergySystem'' simulation methods with control references. The update control method also implements constraints that limit the implementation of references. OPEN includes the following ''Asset'' subclasses: ''NondispatchableAsset'' for uncontrollable loads and generation sources, ''StorageAsset'' for storage systems, and ''BuildingAsset'' for buildings with flexible HVAC [221]. The ''EnergySystem'' class has two types of methods (i) EMS methods to calculate ''Asset'' control references; and (ii) simulation methods to obtain control references for ''Asset'' objects, update the state of ''Asset'' objects, and update the state of the network. The ''EnergySystem'' class has two different time series, one for the EMS and the other for simulation. Moreover, a ''Market'' class defines an upstream market to which the ''EnergySystem'' is connected. A ''Market'' class has several attributes, such as the network's location, prices of exports and imports over the simulation time series, export and import power limits, and the demand charge paid on the maximum demand over the simulation time series.
  OPEN offers two options for solving PF problems in distribution network modeling: (i) balanced PF analysis using PandapowerNet'' class, which is carried out using the open-source Python package pandapower; and (ii) unbalanced PF analysis using ''Network_3ph'' class [221]. The balanced PF problems can be solved based on a Newton-Raphson solution method and DC approximation. While the unbalanced PF problems can be solved based on the fixed-point variants of the continuation method [258] (i.e., a linearization model of multi-phase Z-Bus method [259]. Finally, OPEN does not support coordination, distribution, or local voltage control strategies, especially for inverters.

2) SUMMARY AND COMPARISON

All the tools reviewed in Subsubsection III-C1 can perform unbalanced PF analysis. DIgSILENT PowerFactory, PSS/Sincal, and CYMDIST are commercial software that simulate the distribution networks based on fixed and time-series data to study variations on network designs and controls. OpenDSS, GridLAB-D, and OPEN are open-source and freely available tools, capable of simulating networks with fluctuating data values to model and simulate distribution networks efficiently and they are open for collaboration. DIgSILENT PowerFactory, PSS/Sincal, and CYMDIST feature easy-to-use graphical user interfaces (GUIs). On the other hand, OpenDSS, GridLAB-D, and OPEN are based on command-line programs, which means that more time is required to gain familiarity with the proper codes to model and simulate the distribution networks. Here, it is worth mentioning that OpenDSS-G offers GUI for the OpenDSS, but it is still under development.

Each tool has one or multiple methods and/or algorithms to solve the unbalanced PF equations. Here, DIgSILENT PowerFactory uses a Newton variant of the current injection method, and DC load flow for solving active PFs. PSS/Sincal only implements Newton variants of the current injection method. CYMDIST uses the Newton-Raphson algorithm. However, OpenDSS has two main methods to solve unbalanced PF equations: a Newton variant of a current injection method, and a fixed-point iteration variant of a current injection method. In comparison, GridLAB-D offers two

unbalanced PF solver options: a fixed-point iteration variant of a forward-back sweep method (i.e., default algorithm) and a three-phase unbalanced Newton variant of a current injection method (i.e., Gauss-Seidel algorithm or Newton-Raphson algorithm). Moreover, OPEN uses fixed-point variants of the continuation method as an unbalanced PF solver.

All of the reviewed tools can model single- and three-phase PV systems. Several control strategies are implemented by each tool to manage the voltage levels and reactive PFs in the distribution networks. DIgSILENT PowerFactory can control the active and reactive power to mitigate the voltage issues in the distribution networks using local, distribution and centralized control strategies, droop characteristics for PV systems, SVC, shunt, and tap controllers via QDSL models. Although, PSS/Sincal offers a central VVO module to control the voltage and the power factor in LV and MV radial feeders for the capacitors and the transformers (this does not include the smart inverter control strategies to mitigate the voltage issues). Similarly, CYMDIST offers a volt/var optimization option for peak shaving, improving the voltage level and reducing the losses in the network. However, it does not support smart inverter control strategies. OpenDSS supports a distribution control strategy to coordinate controllable devices, especially inverters. In contrast, GridLAB-D offers a centralized coordination strategy (i.e., CVVC) to regulate the voltage levels in the network, which also includes controlling inverters. However, OPEN does not support voltage regulation strategies. More differences between the tools in terms of basic features and a model library for most of the power components are summarized in Table 5.

OpenDSS and GridLab-D can be used to conduct detailed modeling for the distribution networks, and they support unbalanced PF. However, these tools either rarely support or do not support mathematical optimization, although they support many power system components (including exotic transformer configurations). Therefore, these tools can be usefully used to validate optimization-focused tools' performance in terms of the generated PF results.

Other tools can be fashioned by combining several tools to achieve more advanced features, such as better visualization and advanced studies in testing grid designs and control strategies. For example, OpenDSS can be combined with other tools. Accordingly, Montenegro *et al.* [260] proposed GridTeractions, which uses OpenDSS-G in a co-simulation with a laboratory virtual instrument engineering workbench (LabVIEW) (i.e., a system-design platform and graphical development environment) [261] to develop a hardware-software architecture framework for teaching and testing grid designs. Moreover, Sun *et al.* [262] developed a tool comprised of OpenDSS and OPNET (i.e., communication and network simulators used to help users define and work with different topologies and technologies) [263] to investigate the reliability of control strategies by increasing the DERs penetration levels in smart grids. Furthermore, de Souza *et al.* [264] proposed smart grid co-simulation platform, a combination of a network simulator version 3 (ns-3) (i.e., a discrete-event network simulator platform) [265], [266], OpenDSS, and Mosaik (i.e., a modular simulation of active components in smart grids) [267], for a voltage regulation case study in smart grid. GridLab-D can be combined with other tools. Accordingly, Bytschkow *et al.* [268] combined GridLAB-D, CIM, and AKKA (Java-based co-simulation engine) [269] to model a SCADA system. Also, Hansen *et al.* [270] developed a Bus.py package based on GridLAB-D to simulate the communication between a set of customers and an aggregator in a distribution network. This package is a co-simulation for energy management systems (EMS) and the simulation of integrated transmission and distribution (ITD) systems. Besides, Ciraci *et al.* [271] combined GridLAB-D with ns-3 for co-simulating telecommunication and power distribution. The proposed tool is called the framework for network co-simulation (FNCS), aiming to synchronize simulation engines to coordinate time passage and interaction [272]. In 2017, the FNCS was replaced with a multi-federated method named the hierarchical engine for large-scale infrastructure co-simulation (HELICS) [273] by the same research group. HELICS is a high-performance transmission-distribution-communication-market co-simulation framework to support very large scale (100,000+ federates) with off the shelf power-system, communication, market, and end-use tools. Furthermore, the authors in [274] and [275] developed a transactive energy simulation platform (TESP) by aggregating GridLAB-D and ns-3 based on the framework for FNCS and HELICS, and EnergyPlus (i.e., it is a comprehensive building simulator addressing thermodynamics analysis) [276]. TESP provides several features, such as modeling the wholesale market, transactive energy (TE) market, transmission system, distribution system, residential and commercial buildings, and their TE controllers. TESP gives a sizeable list of examples and IEEE test feeders.

Here, it is noted that the individual tools offer stronger simulation engines. GridLAB-D, OpenDSS, or EnergyPlus are stable and mature tools. Combining the tools can offer integration features, but this novel solution does not have the same endurance and stability. In addition, an absence of cross-platform validation means it is not possible to ensure that the simulations yield relevant results for deeper inspections. Moreover, some meta-heuristic-based optimization algorithms are developed and some are still in development to solve the PF problems, mainly requiring iterative evaluation of the PF equations, but no explicit network models exist as yet [277]. These algorithms can easily be applied in addition to the existing PF solvers.

IV. OPTIMAL POWER FLOW

Optimal power flow (OPF) forms the basis for many applications in power systems, a specific power system optimization problem. In general, any mathematical optimization problem comprises (i) parameters (knowns) and variables (unknowns); (ii) constraints which connect

TABLE 5. Basic features and available equipment models in several PF tools.

	Feature	DIgSILENT PowerFactory	PSS/Sincal	CYMDIST	OpenDSS	GridLAB-D	OPEN
Basic Features	PF analysis for radial network	✓	✓	✓	✓	✓	✓
	PF analysis for loop/mesh network	✓	✓	✓	✓	✓	×
	PF analysis for systems with unbalanced loads	✓	✓	✓	✓	✓	✓
	Source unbalance for slack bus	✓	✓	×	✓	✓	✓
	Multiple generation sources	✓	✓	✓	✓	✓	✓
	Three-phase PF analysis	✓	✓	✓	✓	✓	✓
	Single-phase PF analysis	✓	✓	✓	✓	✓	✓
	Choosing the type of PF technique	✓	×	×	✓	✓	✓
	Voltage regulation	✓	✓	✓	✓	✓	×
	PV voltage regulation support in PF	✓	✓	×	✓	✓	×
Available Equipment Models	Distribution lines or cables (π-equivalent)	✓	✓	✓	✓	✓	✓
	Generators	✓	✓	✓	✓	✓	✓
	Three-phase transformers	✓	✓	✓	✓	✓	✓
	Models of PV generators	✓	✓	✓	✓	✓	✓
	Smart inverter control	✓	×	×	✓	✓	×
	Capacitors	✓	✓	✓	✓	✓	✓
	Switches	✓	✓	✓	✓	✓	×
	Over-current devices	✓	×	✓	✓	✓	×
	Motors	✓	✓	✓	✓	✓	×
	Preloaded geographical PV insolation data	✓	×	×	×	✓	×
	Residential end-user models	×	×	×	×	✓	×

variables and parameters through mathematical expressions; and (iii) an objective function, or multiple ones in the case of multi-objective variants. Accordingly, the OPF solver aims to minimize or maximize one or more objective function(s) subject to both the PF equations and network constraints [278]. OPF may combine various PF representations to balance accuracy and computational tractability. In other words, OPF may have a "base case" that is solved based on an explicit model of the PF physics by integrating several "scenarios" which are structured based on simplified PF representations to balance the computational tractability [98]–[111], [129]–[132]. A comprehensive review has been published in [279] on different applications of optimization models for LVDNs.

Typically, the OPF problem's aim is minimizing an objective function, mostly related to the generators. Therefore, each generator *gen* at bus i which has a cost function for active power generation, let it $f_{Ci}\left(\mathbf{P}_{geni}\right)$, where $\mathbf{P}_{geni} = \mathbf{P}_i + \mathbf{P}_{di}$, and $\mathbf{Q}_{geni} = \mathbf{Q}_i + \mathbf{Q}_{di}$. The active and reactive power are limited by $\mathbf{P}_{gen}^{\min}$ and $\mathbf{P}_{gen}^{\max}$, and $\mathbf{Q}_{gen}^{\min}$ and $\mathbf{Q}_{gen}^{\max}$, respectively, which all equal zero at the buses without generators. Moreover, the voltage magnitudes and phase angle differences are also limited by $\mathbf{V}_i^{\min}$ and $\mathbf{V}_i^{\max}$, and $\Theta_{ij}^{\min}$ and $\Theta_{ij}^{\max}$, respectively [9]. Accordingly, the typical three-phase OPF problem can be mathematically expressed as follows:

$$\min \sum_{i\in\mathcal{G}} f_{Ci}\left(\mathbf{P}_{geni}\right), \tag{126}$$

subject to

$$\mathbf{P}_{gen}^{\min} \leqslant \mathbf{P}_{geni} \leqslant \mathbf{P}_{gen}^{\max}, \tag{126a}$$
$$\mathbf{Q}_{gen}^{\min} \leqslant \mathbf{Q}_{geni} \leqslant \mathbf{Q}_{gen}^{\max}, \tag{126b}$$
$$\left(\mathbf{V}_i^{\min}\right)^2 \leqslant |\,\mathbf{V}_i\,|^2 \leqslant \left(\mathbf{V}_i^{\max}\right)^2, \tag{126c}$$
$$\Theta_{ij}^{\min} \leqslant \angle\mathbf{V}_i - \angle\mathbf{V}_j \leqslant \Theta_{ij}^{\max}, \tag{126d}$$
$$\angle\mathbf{V}_0 = 0, \tag{126e}$$
$$\text{a representation of the PF equations,} \tag{126f}$$
$$\text{and limits on line flows.} \tag{126g}$$

Accordingly, the active and reactive power generated by generator *gen* at bus i are constrained by the maximum and minimum bounder limits, as in (126a) and (126b, respectively. Besides, the voltage magnitude and the angle difference across each line at bus i are limited by the upper and lower bounders, as in (126c) and (126d), respectively. The constraint in (126d) for the angle difference across each line at bus i is imposed as a proxy constraint for transient stability requirements. As bus 0 is the reference bus; therefore, constraint in (126e) sets the reference bus angle at zero. The PF equations in (126f) may define in various forms, as described in the previous section. Finally, the limits on line flows in (126g) are typically defined either in terms of apparent power or current flows [9].

The power injections and voltage magnitude set-points can often be varied to optimize some objective function satisfying the engineering constraints. The constraints are often

equalities, such as for a specified demand (e.g., $\mathbf{P}_i = -\mathbf{P}_{di}$), or box constraints for specified upper and lower bounds $\mathbf{P}_i^{\max}$ and $\mathbf{P}_i^{\min}$ (e.g., $\mathbf{P}_i^{\max} \leqslant \mathbf{P}_i \leqslant \mathbf{P}_i^{\min}$). Moreover, some complicated constraints may be used, such as representing the generator capability curves and voltage-dependent loads (e.g., $\mathbf{P}_i$, $\mathbf{Q}_i$, and $\mid \mathbf{V}_i \mid$) [280], [281]. Furthermore, some discrete constraints can be imposed, such as that representing a switched capacitor with shunt susceptance ($\mathbf{b}_i^{\text{sh}}$) and associated binary variable (s_{geni}), where $s_{geni} \in \{0, 1\}$ stands for the generator's on/off status, (e.g., $\mathbf{Q}_i = s_{geni} \cdot \mathbf{b}_i^{\text{sh}} \mid \mathbf{V}_i \mid^2$) or by modeling the ability to shut down a generator in a UC problem (e.g., $s_{geni} \cdot \mathbf{P}_i^{\max} \leqslant \mathbf{P}_i \leqslant s_{geni} \cdot \mathbf{P}_i^{\min}$). Therefore, the line flow expressions for the apparent power and current flow constraints vary based on the PF model [9]. Several line flow expressions are provided in [282] and [283]. Other types of constraints can also be included to solve the OPF problems, such as contingency constraints, stability constraints, and generator capability characteristics. These constraints are described in [108], [129]–[131], [137], and [284]. For more detailed descriptions about OPF and other optimization problems in power systems, the reader can refer to [109], [285]–[287].

A. OBJECTIVES

The OPF aims to solve a set of PF equations subject to an objective function or a group of objective functions. In the case of applying several objective functions, these functions can be combined in a single objective function by assigning a weight to each one to mark its relative importance. Three main objective functions are generally used to solve OPF problems; yet, canonical objectives are often encountered [279]. The solver aims to minimize these functions in most cases, which can be summarized as follows:

- Network losses
  The losses in the lines and the conductive components are indicated by the Joule losses when the currents flow through them. In general, the load behaviour and its type mainly drive the network losses. At a system level, the conservation of power means that 'generation = load + losses'. Accordingly, minimizing the losses if the load is fixed is equivalent to minimizing the total generation. Here, the generation is often referred to as active power generation (i.e., a sum of variables) [27], [51]. Simultaneously, the total generation is minimized as a combination of loss reduction and CVR, which is beneficial in voltage-dependent loads [28]. However, the losses can be directly included in the objective as in [25]. Interestingly, the losses are minimized as a proxy for the unbalance in [28]. Here, it is concluded that the unbalanced operation will increase the losses.
- Generation cost
  The generation cost can be minimized directly by controlling the amount of generation and/or import at the substation to the network load. Here, the active power generation from each generator is formulated a function of a cost. Therefore, the import cost is in proportion to the total imported active power [25], [46]. Several cost functions are used, such as second-order polynomials [26], [45], non-linear polynomials, and piecewise linear [48]. However, the generation cost's expected value is utilised in a probabilistic context as in [47].
- Cost of consumption
  The consumption cost can be minimized in multi-period problems. Here, the minimization is carried out by controlling the loads as a function of a time-varying consumption cost [25], [95].

Furthermore, some other situation-specific objectives have also been also used in OPF problems [279], such as:

- minimizing the voltage unbalance in the network. The voltage unbalance can be represented as the sum of squares of the negative sequence voltage magnitude at each bus [51], [288];
- minimizing the harmonics in the network. The harmonics can be represented as the sum of squares of harmonic voltage magnitudes [51];
- minimizing the amount of PV curtailment [27], [70], [75];
- minimizing the number of curtailed loads [289];
- maximizing the EV charging. The EV charging can inversely be weighted by the individual EV's charge level [290]; and
- maximizing welfare in markets with distribution marginal locational pricing [291], [292].

B. ALGORITHMS

OPF algorithms aim to obtain a point in the feasible space which has the least cost according to a specified objective function. In general, the feasible space can be defined as the set of points that satisfy a system of equations. The feasible space for the PF equations in power system optimization problems can (i) consist of a finite set of isolated points corresponding to the PF solutions, as for specified power injection and voltage magnitude set-point parameter values; or (ii) generally give rise to higher-dimensional power injection, and voltage set-point parameters are allowed to vary. The feasible spaces defined by the PF equations are generically non-convex. Some OPF problems may have multiple local optima [141] and are generally NP-Hard [139], [140]. For more detailed descriptions about the characteristics of the feasible spaces of (O)PF and solving the non-convex (O)PF problems, the reader can refer to [141], [195], [283], [293]–[305].

Several local solution techniques have been devised to solve OPF problems [98]–[107], [129]–[132]. Two main successful classes of traditional techniques are reviewed in this subsection, namely interior point algorithms and sequential quadratic programming (SQP) algorithms. Other local solution techniques are described in detail in [306], [307]. Some unbalanced OPF tools, such as Open-DSOPF [308] and PowerModelsDistribution [23], have solvers that implement

these algorithms and other optimization algorithms to solve the OPF problems.

Several OPF solvers can benefit from dealing with solid duality in the constraint qualification conditions (i.e., zero gaps between the optimal objective values of the primal and dual problems) [9]. Accordingly, Cao *et al.* [309] derived several sufficient conditions to ensure the satisfaction of Slater's constraint qualification condition [310] for an interior point in the feasible spaces of OPF problems in radial network topologies. Furthermore, Hauswirth *et al.* [311] implemented several OPF tools from differential topology to prove that the OPF problems in various contexts can satisfy the linear independence constraint quantification (LICQ) condition [312]. Therefore, an existing set of the unique multipliers satisfy the Karush–Kuhn–Tucker (KKT) conditions for all local optimizers to OPF problems. Besides, Almeida and Galiana [313] investigated the effects of small parameter changes in OPF solutions, which lead to sharp discontinuities in the solution. In numerical algorithms, the constraints are only satisfied by reaching or exceeding a predefined relative or absolute tolerance value because the finite precision of computer calculation becomes a limiting factor. In the context of OPF, the predefined relative or absolute tolerance is typically in the range of 10^{-6} to 10^{-8}.

The OPF problem can be generalized for notational convenience by rewriting the OPF problem in (126) as:

$$\min f\,(x)\,, \tag{127}$$

subject to

$$g_i(x) \leqslant 0, \quad i = 1, \ldots, m_{inequality}, \tag{127a}$$
$$h_j(x) = 0, \quad j = 1, \ldots, m_{equality}, \tag{127b}$$

where $f\,(x)$ is the objective function, which aims to optimize a specified quantity of interest, such as minimization of generation cost, x is a vector representing the optimization variables consisting of the voltage phasors, $g_i(x) \leqslant 0$ are inequality constraints stand for the limits on line flows, power injections, phase angle differences, and voltage magnitudes, $h_j(x) = 0$ are equality constraints, and $m_{inequality}$ and $m_{equality}$ are the number of inequality and equality constraints, respectively.

1) INTERIOR POINT ALGORITHMS

Interior point algorithms (i.e., also referred to as barrier algorithms) have been very appealing approaches to solve OPF problems since the early 90's because of three main merits over other algorithms: (i) they can easily handle inequality constraints by logarithmic barrier functions; (ii) their convergence speed is high, which makes them competitive with simplex algorithms; and (iii) they do not require a strictly feasible initial point [314]–[317]. The first implementation of interior point algorithms was in state estimation [318] and hydro scheduling problems [319]. Consequent work proved that interior point algorithms could locally solve large-scale OPF problems [130], [320]–[322]. Accordingly, it is worth mentioning that leverage information from a nearby solution is generally challenging. Here, interior point algorithms are typically tricky to "warm start" due to the requirement for a sufficiently interior starting point [323].

In general, interior point algorithms are formulated by defining the non-negative slack variables ($s_i \geqslant 0, \forall i = 1, \ldots, m_{inequality}$), which should be introduced firstly, to be able to set the inequality constraints ($g_i(x) \leqslant 0$) with the equivalent formulation ($g_i(x) + s_i = 0$). Then, the inequality constraints are replaced with a barrier term in the objective function. This term tends towards infinity as the inequality becomes binding. Also, this term is weighted by a positive barrier parameter (μ). As the algorithm converges, μ is iteratively decreased towards zero. Interior point algorithms are formulated using a log-barrier (i.e., the sum of the logarithms of the slack variables (s_i)) [9]. The log-barrier formulation can be represented as:

$$\min f\,(x) - \mu \sum_{i=1}^{m_{inequality}} \log\,(s_i), \tag{128}$$

subject to

$$g_i(x) + s_i = 0, \quad i = 1, \ldots, m_{inequality}, \tag{128a}$$
$$h_j(x) = 0, \quad j = 1, \ldots, m_{equality}. \tag{128b}$$

The solution of (128) approaches the solution of (127) as μ tends to zero under mild conditions [324]. The KKT conditions for (127) are:

$$\frac{\partial f\,(x)}{\partial x} + \gamma^T \left(\frac{\partial g\,(x)}{\partial x}\right) + \lambda^T \left(\frac{\partial h\,(x)}{\partial x}\right) = 0, \tag{129a}$$
$$g\,(x) + s = 0, \tag{129b}$$
$$h\,(x) + s = 0, \tag{129c}$$
$$\mathrm{diag}(s)\gamma - \mu\,\mathbb{1}_{m_{inequality}} = 0, \tag{129d}$$

where γ and λ are vectors representing the Lagrange multipliers for (128a) and (128b), respectively; and $\mathbb{1}$ denotes the vector of ones with length given by the associated subscript.

A Newton update step for the KKT conditions in (129) is computed at each iteration. Besides, the variables x, γ, λ and s are updated in steps to ensure that the non-negative variables and s do not reach zero too quickly. Also, μ is updated at each iteration towards zero.

The interior point algorithms aim to guarantee convergence by using line search methods, trust region constraints, techniques to handle non-convexity via merit functions, and other modifications [9]. Here, several interior point algorithms are used in the literature to solve OPF problems, such as the pure primal-dual (PD), predictor-corrector (PC), and multiple centrality corrections (MCC) [325]. For more details about interior point algorithms and various extensions, we recommend to check [130], [307], [324], [326]. Several packages implement interior point algorithms, such as LOQO [327], Knitro [328], and interior point optimizer (Ipopt) [329].

Ipopt is considered more efficient than LOQO and Knitro in terms of performance and iteration counts [329]. Therefore, it is the most used solver in available unbalanced

non-linear OPF tools, such as Open-DSOPF [330] and PowerModelsDistribution [23], and in balanced OPF tools, such as MATPOWER [137] and PYPOWER [331] tools. Ipopt solver was developed by COIN-OR Foundation [332], and is an open-access package. It was written in C++ by Andreas Wächter and Carl Laird. It implements an interior point line search filter method to locate a local solution in non-linear programming. The algorithm's mathematical details are presented in [329], [333]–[336]. It can be used to solve general non-linear programming problems of the form:

$$\min f\,(x)\,, \tag{130}$$

subject to

$$g^L(x) \leqslant g(x) \leqslant g^U, \tag{130a}$$
$$x^L \leqslant x \leqslant x^U, \tag{130b}$$

where $x \in \mathbb{R}^n$ are the optimization variables, $x^L \in \left(\mathbb{R}\bigcup\{-\infty\}\right)^n$ are the lower bounders of x, $x^U \in \left(\mathbb{R}\bigcup\{+\infty\}\right)^n$ represent the upper bounders of $x, f : \mathbb{R}^n \to \mathbb{R}$ stands for the objective function, $g : \mathbb{R}^n \to \mathbb{R}$ represent the general non-linear constraints, $g^L \in \left(\mathbb{R}\bigcup\{-\infty\}\right)^m$ represent the lower bounders for the constraint g, and $g^U \in \left(\mathbb{R}\bigcup\{+\infty\}\right)^m$ stand for the upper bounders for the constraint g. Note that $f(x)$ and $g(x)$ can be linear or non-linear and convex or non-convex, but should be twice continuously differentiable. In addition, the equality constraints of the form $g_i(x) = \overline{g}_i$ can be specified by setting $g_i^L = g_i^U = \overline{g}_i$.

2) SEQUENTIAL QUADRATIC PROGRAMMING ALGORITHMS

Sequential quadratic programming (SQP) algorithms were firstly applied in the mid-80's to solve OPF problems [337], where a sparse implementation demonstrated scalability to systems with thousands of buses. Later, SQP algorithms were modified to work on OPF problems with more flexibility and efficiency [105], [106]. SQP algorithms repeatedly solve specially constructed quadratic programs to obtain the local solutions of non-linear optimization problems. The SQP algorithm can solve the generic OPF problem in (127) at each iteration k to determine a search direction $d^{(k)}$:

$$d^{(k)} = \arg\min_d f\left(x^{(k)}\right) + \left(\nabla f\left(x^{(k)}\right)\right)^T \cdot d + \frac{1}{2} d^T \left(\nabla^2_{xx}\mathcal{L}\left(x^{(k)}, \gamma^{(k)}, \lambda^{(k)}\right)\right) \cdot d, \tag{131}$$

subject to

$$gi(x^{(k)}) + \left(\nabla gi(x^{(k)})\right)^T \cdot d \leqslant 0,, \tag{131a}$$
$$hj(x^{(k)}) + \left(\nabla hj(x^{(k)})\right)^T \cdot d = 0,. \tag{131b}$$

where $i = 1, \ldots, m_{inequality}$, $j = 1, \ldots, m_{equality}$, γ and λ are vectors representing the Lagrange multipliers for (131a) and (131b), respectively; $x^{(k)}$ stands for the value of the decision variables at the current iterate; $\mathcal{L} = f(x) + \gamma^T g(x) + \lambda^T h(x)$ represents the Lagrangian of (131); ∇ and ∇^2_{xx} are the gradient and Hessian, respectively, with respect to x.

The primal decision variables are updated at each iteration by adding the step $d^{(k)}$ obtained by solving (131) (i.e., $x^{(k)} = x^{(k+1)} + d^{(k)}$). The dual variables give the values for the Lagrange multipliers at the next iteration $(k+1)$ ($\gamma^{(k)}$ and $\lambda^{(k)}$) for the constraints (131a) and (131b), respectively, calculated at the current iteration.

The optimization problem in (131) is a non-convex quadratic program, which can be solved using several algorithms. SQP algorithms aim to compute ∇^2_{xx}. When it is difficult to be computed, SQP algorithms can implement "quasi-Newton" techniques, which aim to construct modified matrices used in place of $\nabla^2_{xx}\mathcal{L}\left(x^{(k)}, \gamma^{(k)}, \lambda^{(k)}\right)$. SQP algorithms can use various methods and techniques, such as various line search techniques, trust region methods, merit functions, etc. [306], [307].

The SQP algorithms iterate the convergence superlinearly or quadratically towards the solution by finding the set of inequality constraints binding at the solution to (127) (i.e., active set). Therefore, initializing the SQP algorithms near the solutions is helpful here. More applications of quadratic programming (QP) and linear programming (LP) techniques to OPF problems can be found in [101]–[103]. Besides, more details about the variation of SQP algorithms from a general optimization perspective can be found in [306], [307]. SQP algorithms are used by several solvers, such as Knitro [328], SNOPT [338], and FilterSQP [339].

C. RELAXATION AND APPROXIMATION

The solution of the OPF problems can be non-convex, which may have multiple local optima [141] and is generally NP-Hard [139], [140]. A variety of relaxations and approximations have been developed which employ tools from convex optimization. This subsection focuses on semidefinite programming (SDP), a convex optimization tool relevant to relaxations and approximations. For more details about the other convex optimization tools, such as LP, QP, and second-order cone programming (SOCP), the reader can refer to [9], [340].

SDP can generalize SOCP. The decision variables of SDP can be represented as a symmetric matrix X, instead of organizing them as a vector x as in LP and SOCP [9]. The mathematical formulation of the canonical form of SDP can be represented as:

$$\min_X \ \mathrm{tr}\,(CX)\,, \tag{132}$$

subject to

$$\mathrm{tr}\,(A_i X) = b_i, \quad i = 1, \ldots, r, \tag{132a}$$
$$X \succeq 0, \tag{132b}$$

where $X \succeq 0$ stands for the positive semidefiniteness of the matrix X, C and A_i represent the specified square symmetric matrices, b_i stand for specified scalars and r is the number of SOCP constraints. Note that the constraint in (132a) is linear in the entries of the matrix variable $\mathbf{X}$, as $\mathrm{tr}\,(AB) = \sum_i \sum_j A_{ij} B_{ji}$.

In SDP, the scalar inequality constraints can be reformulated by expanding the positive semidefinite matrix X with a 1×1 diagonal block to represent a non-negative slack variable (conceding that the positive semidefiniteness of a matrix infers non-negativity of all its diagonal values [341]. Accordingly, the constraints $\mathrm{tr}\left(\tilde{A}_i X\right) \geqslant \tilde{b}$, and $X \succeq 0$ can be written as $\mathrm{tr}\left(\tilde{A}_i X\right) + x_s = \tilde{b}$, and $\begin{bmatrix} X & 0 \\ 0 & x_s \end{bmatrix} \succeq 0$, where x_s stands for a scalar slack variable, which proves that SDP can generalize SOCP. Also, it implies that SDP can generalize SOCP by reformulating the SOCP constraint (i.e., $\| E_i x_s + b_i \|_2 \leqslant g_i^T x_s + d_i$, where $i = 1, \ldots, r$) to an SDP constraint as:

$$\begin{bmatrix} \left(g_i^T x_s + d_i\right) I & \left(E_i x_s + b_i\right) \\ \left(E_i x_s + b_i\right)^T & \left(g_i^T x_s + d_i\right) \end{bmatrix} \succeq 0, \tag{133}$$

where I represents an appropriately sized identity matrix, in which its dimension equals the number of rows of $\mathbf{E}$ [342].

In general, SDP solvers mix LP, SOCP, and SDP constraints. As the performance of LP and SOCP constraints is superior to SDP constraints, it is recommended to simplify SDP constraints by reformulating them in the form of LP constraints or a mix of LP and SOCP constraints. Otherwise, formulate a constraint as an SDP constraint [9].

Complex variables are particularly relevant to the PF equations to find feasible points for PF and OPF problems because of the phasor representations of voltages. All the available SDP solvers utilize real-valued operations in their internal computations. However, there are several theoretical and practical advantages in complex-valued SDP formulations. For more details on SDP constraints in complex variables, the reader can refer to [343], [344]. Besides, the works in [345]–[347] provided alternative presentations.

The complex analogue of (132) can be mathematically represented as:

$$\min_{Z} \ \mathrm{tr}\left(\check{C} Z\right), \tag{134}$$

subject to

$$\mathrm{tr}\left(\check{A}_i Z\right) = \check{b}_i, \quad i = 1, \ldots, r, \tag{134a}$$

$$Z \succeq 0, \tag{134b}$$

where $Z \succeq 0$ is a positive semidefinite Hermitian matrix, $\check{C}$ and $\check{A}_i$ represent Hermitian matrices (i.e., matrices resulting in $\mathrm{tr}\left(\check{A}_i Z\right)$ and $\mathrm{tr}\left(\check{C} Z\right)$ are real-valued quantities), and $\check{b}_i$ stands for a real scalar.

To be able to convert (134) to real-valued canonical form as in (132), the Hermitian matrix $Z \in \mathbb{C}^{n \times n}$ should be positive semidefinite, which is satisfied if and only if the matrix $\begin{bmatrix} \mathrm{Re}\,(Z) & -\mathrm{Im}\,(Z) \\ \mathrm{Im}\,(Z) & \mathrm{Re}\,(Z) \end{bmatrix} \in \mathbb{R}^{2n \times 2n}$ is positive semidefinite [340], [348]. The representation of the real and imaginary parts of Z is by real-valued matrix variables and based on the equivalence of the positive semidefinite constraint (134b). This representation allows the conversion form (134) in terms of a $n \times n$ Hermitian matrix variable to the form of (132) with a $2n \times 2n$ real-valued symmetric matrix variable. This conversion is automatically carried out in modeling languages, such as YALMIP [349] and CVX [350].

In general, SDP solvers are considered less mature than LP and SOCP solvers. Several commercial solvers are available, such as MOSEK (free for academia) [348], PENSDP (free for academia) [351], etc. Besides, many solvers are freely available, including SDPA [352], SDPT3 [353], CSDP [354], SeDuMi [355], and others. However, only a few of the solvers are capable of handling mixed-integer SDP problems, such as SCIP-SDP [356], Pajarito [357], and YALMIP [349]. Here, a list of the open-access and commercial convex optimization solvers for LP, mixed-integer LP, QP, mixed-integer QP, SOCP, mixed-integer SOCP, SDP, general non-linear programming and others can be found on a web page in [358]. Furthermore, several applications of SOCP are described in [342] and [348]. In addition, [348] described several applications of SDP.

D. TOOLS

This subsection summarizes the most commonly used tools for handling the optimization problems in unbalanced distribution networks. Several commercial and open-access tools are available which can solve the OPF directly or as components of a greater toolchain. These tools, especially the open-access ones, can help develop and validate any new or existing tool by improving the results' reproducibility [5], [6]. Most of the mature tools are documented, which extends their state-of-the-art status with novel contributions. Furthermore, the used codes of most open-access tools are available for the public, which helps the developers to reproduce the results to review the performance of the tools. Note that when the open-access tools provide unit tests and validation are compared with the other well-known tools, this increases their reliability and the users' trust to implement and/or compare their works with them.

It is more accessible to the user to carry out some other process on the data and/or the results, and formatting the objective functions of the OPF if the algebraic modeling language is developed using a high-level programming language. Some of the used high-level programming languages are JuMP in Julia [359], Pyomo in Python [360], and YALMIP in MATLAB [349]. Furthermore, some open-access tools, such as YALMIP or JuMP with Juniper [361], allow the users to re-use mathematical models for components (i.e., LVDNs components) to solve mixed-integer problems with continuous solvers without mixed-integer support.

1) DISTRIBUTION (UN)BALANCED OPF TOOLS

Based on the literature, the available commercial tools cannot solve non-linear optimization problems in unbalanced distribution networks. In contrast, two open-access tools can handle such non-linear optimization problems, Open-DSOPF [330] and PowerModelsDistribution [23].

Therefore, Open-DSOPF, and PowerModelsDistribution are reviewed in this subsubsection. In addition, MATPOWER [137]/PYPOWER [331] tools do not support unbalanced (O)PF but they are included in this subsubsection as they, especially MATPOWER, are well-known and widely used among industry and academia.

- MATPOWER/PYPOWER
  MATPOWER [362] is an open-source tool for electric power system simulation and optimization, which was first developed in 2010 by Power Systems Engineering Research Center (PSERC) and other individual contributors. It is used widely among industry and academia [137]. This tool supports several types of analysis, such as PF, continuation PF (CPF), extensible AC and DC OPF (e.g., dispatchable loads, piecewise linear cost functions, branch angle difference limits and generator capability curves), UC, and stochastic, secure multi-interval OPF/UC problems [362]. A Python package is developed based on MATPOWER, whereas oct2pypower [363] functions as a bridge from Python to MATPOWER. This package is called PYPOWER [331]; however, it is no longer actively maintained, and the currently available version (PYPOWER version 5.1.15) supports an old MATPOWER version (i.e., version 4.1) [331].
  MATPOWER is written in a MATLAB environment. It is compatible with Windows, Linux/Unix, and Mac OSX. While PYPOWER is written in Python, which is also compatible with Windows, Linux/Unix and Mac OSX. PAYPOWER does not have specific documentation for the models, network representation, solvers, etc. However, it uses the MATPOWER user's manual for version 4.1 as a reference [364]. Essential documentation of the get start functions is available on the package website [331]. In contrast, MATPOWER is well documented, and each M file has its documentation [365]. In addition, MATPOWER has a web based application [366], where the simulations are run on GNU Octave in WebAssembly. However this MATPOWER web based application is very basic and limited without any documentation for beginners. The data structure is normally defined in a case file, either as a function ''.m'' file or a ''.mat'' file.
  MATPOWER utilizes the standard steady-state models of the distribution network's components. The magnitudes of all values are expressed in p.u., while radians express the angles of complex quantities. MATPOWER models the components in a balanced representation. These models are (i) branches, transformers, and phase shifters, which are modeled based on a standard π-section model with series impedance and considering identical admittance shunt on both ends; (ii) slandered balanced generators, which can be used to model a dispatchable load in a negative injection mode; and (iii) constant power loads models (constant current loads and constant impedance are not directly implemented); and (iv) shunt elements, including inductor or capacitor, are modeled as an impedance fixed to the ground. In addition, constant impedance portions can be modeled as a shunt element [365]. MATPOWER/PYPOWER tools neither support the modeling for PV systems nor the inverter smart control strategies.
  As mentioned above, MATPOWER/PYPOWER tools do not support unbalanced (O)PF. Balanced OPF is explicitly devised as an extensible OPF structure [367], which allows the users to define additional costs, variables and linear constraints. For DC OPF, MATPOWER utilizes a MEX build [368] of the high performance BPMPD solver [369] and BPMPD_MEX solver for LP/QP problems. For AC OPF, the tool uses MINOS solver [370] from the MINOPF package [371], and primal-dual interior-point method and a trust region-based augmented Lagrangian method (described in [321] from the TSPOPF package [372]. MATPOWER version 4 also includes Ipopt solver interfaced with MEX to solve both DC and AC OPF problems and its own developed solver called MATPOWER Interior Point Solver (MIPS) [372]. MATPOWER version 4.1 added the Knitro solver [328] and Gurobi Optimizer [373] for AC and DC OPF, respectively. MATPOWER version 5 added a GNU linear programming kit (GLPK) [374], while MATPOWER version 5.1 includes the COIN-OR linear programming (CLP) solver [375]. In the current version (MATPOWER version 7.1) relies on MP-Opt-Model [376] and above-mentioned solvers. To simplify the addition of costs, variables and constraints to the OPF problems, MATPOWER utilizes an object-oriented approach (i.e., ''OPF-model'' (OM)) to devise and modify the problem formulation [367]. PYPOWER uses BPMPD_MEX solver, MIPS and Gurobi Optimizer for DC OPF problems. Besides, it uses several solvers based on MATPOWER version 4.1, such as MINOS solver, Ipopt solver, MIPS solver, and Knitro solver for AC OPF problems.
- Open-DSOPF
  Open-DSOPF [308] is an open-source Python-based package integrating an unbalanced three-phase OPF with OpenDSS software. Open-DSOPF was developed in 2020 by Valentin Rigoni and Andrew Keane at University College Dublin, Ireland [330]. The main idea of this package is to develop a platform to be able to quantify and benchmark different active network management strategies (i.e., smart inverter controls) to avoid the violation of network operational limits by increasing the penetration levels of DERs in distribution networks. Hence, the Open-DSOPF was developed to translate any network model available in OpenDSS automatically to a three-phase OPF problem, which aims to retrieve OPF solutions, run PF simulations, and combine external algorithms/tools (from volt-var curves to forecasting

techniques) into the same platform [330]. The utilized OPF formulation is flexible, which allows the user to modify the objective function and constraints, and it can incorporate any DER model. Therefore, many simulation opportunities can be implemented and evaluated in this package. The developers used a real British LV network with domestic-scale PVs as a test case.

The unbalanced three-phase OPF is written using Pyomo in Python [360], which is automatically created by extracting any network model's data from OpenDSS. Pyomo needs several Python libraries to run the scripts without any error, such as numpy, pandas, random, math, matplotlib, pyomo, and sys. The package is Windows-based as it is dependent on OpenDSS (e.g., Win32 and Win64); therefore, it can interface with Windows COM. OpenDSS is compatible with other platforms, such as MATLAB, Excel, Python, and Julia [245]. The package can handle ''.csv'', ''.xlsx'' (i.e., Excel), ''.txt'', and ''.mat'' (i.e., MATLAB) files. The outputs of the software can result in several file types, such as ''.csv'', ''.xlsx'', and ''.mat'' files. The package has some basic documentation [377]–[379], which is not enough for beginner users. The package has one example using a real British LV network with domestic-scale PV systems as a test case [330].

Open-DSOPF can model the same components in OpenDSS environment. All the functions of the network components in OpenDSS can be imported as an object in any Python script, including the single- and three-phase PV systems, inverter models, and smart inverter control functions. For more information about the type of components that OpenDSS can model, the reader can refer to Subsubsection III-C1. The extracted admittance matrix of the network models and the parameters of the assets are used to define the OPF problem and initialize its variable. The OPF solution can be validated by sending the values of the controllable variables obtained by solving the OPF by Open-DSOPF to OpenDSS. Accordingly, OpenDSS solves the PF simulation using the received parameters, and comparing the state variables' values ensures a match [330].

The PF equations are derived based on the current mismatch method given in [169] for a 3-phase network with no explicit modeling of the neutral cable. The package considers equality constraints, such as current mismatch (i.e., should equal zero) and the voltage at the slack bus (i.e., should equal the specified value), and inequality constraints (i.e., network operational limits), such as voltage limit (i.e., the magnitude of the steady-state voltage at every node has to comply with the statutory voltage limits), line thermal limits (i.e., the current flow at each phase of each line cannot be in excess of the rated current) and transformer rating limits (i.e., the total apparent PF across every transformer cannot exceed its respective rating). Besides, the controllable variables for DERs (e.g., PV systems) are defined (i.e., PV active power control ($P_{control_{PV}}$) and $\tan(\cos^{-1}(\text{pf}))$ to control the active power curtailment [330]. Open-DSOPF supports two OPF solvers, Knitro and Ipopt. The user can select the solver by typing the solver name in the function ''optimizer=pyo.SolverFactory('solver_name')'', which can be found in the file name ''MAIN_Unbalanced_OPF_RUN.py'' [378].

- PowerModelsDistribution

  PowerModelsDistribution [380] is an open-source package developed by the Los Alamos National Laboratory's Advanced Network Science Initiative (ANSI) and other individual contributors, in 2018, as an extension to ''PowerModels.jl'' package [138]. PowerModelsDistribution was first implemented to focus on solving steady-state multi-conductor unbalanced distribution network optimization problems, including balanced and unbalanced PF and OPF problems [23]. Also, the package can handle other key problems, such as the maximal load delivery problem [381]. Therefore, PowerModelsDistribution is engineered to decouple problem specifications, such as PF (e.g., ACP, ACR, IVR, LinDist3Flow, NFA and DCP), OPF (e.g., ACP, ACR, IVR, LinDist3Flow, NFA and DCP), continuous load shed, minimum load delta (mld) (e.g., ACP, NFA and LinDist3Flow), and OPF with on-load tap-changer (OPF_OLTC) (e.g., ACP). This allows a large range of power network formulations to be defined and compared on common problem specifications [380]. The package includes non-convex non-linear forms (e.g., ACP, ACR and IVR), convex relaxations (e.g., semidefinite programming (SDP) BFM, second-order cone (SOC) BFM relaxation and SOC BIM relaxation), and linear approximations (e.g., LinDist3Flow, NFA and DCP) of the unbalanced PF equations (for an overview about the mentioned formulation, see [9].

  PowerModelsDistribution is written in Julia and developed on top of JuMP (i.e., a mathematical programming abstraction layer for optimization) [359]. This package supports OpenDSS ''.dss'' files as input to leverage OpenDSS existing mature data format to construct network cases for validation and further development. PowerModelsDistribution parser can ingest any valid OpenDSS file into a serializable data structure for further user processing. More details about the use of OpenDSS format are located in the documentation of PowerModelsDistribution [382]. The accuracy of the mathematical formulations for modeling the distribution networks and for solving balanced and unbalanced PF and OPF problems are validated by comparing the numerical results on IEEE distribution test cases [383] with that obtained by OpenDSS software [23]. The package is well documented, providing several examples, and a helper function for beginners and developers [382].

  PowerModelsDistribution represents the branch and bus based on the multi-conductor π-section model,

TABLE 6. Basic features and available equipment models in unbalanced OPF tools.

	Feature	Open-DSOPF	PowerModelsDistribution
Basic Features	OPF analysis for radial network	✓	✓
	OPF analysis for mesh/loop network	✓	✓
	OPF analysis for systems with unbalanced loads	✓	✓
	Multiple generation sources	✓	✓
	Three-phase OPF analysis	✓	✓
	Choosing the type of OPF solver	✓	✓
	Choosing the type of objective function	✓	✓
	Voltage regulation	✓	✓
	PV voltage regulation support in PF	✓	✓
Available Equipment Models	Distribution lines or cables (π-equivalent)	✓	✓
	Generators	✓	✓
	Three-phase transformers	✓	✓
	Models of PV generators	✓	✓
	Smart inverter control	✓	×
	Capacitors	✓	✓
	Switches	✓	✓
	Overcurrent devices	✓	✓
	Motors	✓	×
	Preloaded geographical PV insolation data	×	×
	Residential end-user models	×	×

supporting full matrices for series and shunt elements, by considering that the admittance shunts on either side are not necessarily identical at Γ-section. Accordingly, the package offers a set of component models, such as a bus model (i.e., many terminals (4+)), three-phase bus model (i.e., special case of the bus model), pi-model branch model for line and cable representation, transformer models (e.g., n-winding, n-phase, lossy transformers, asymmetric, lossless, and two-winding), switches, shunts, loads (e.g., power, current, impedance, exponential and ZIP), generators, generator cost model, PV systems, PV system cost model, wind turbine systems, storage, voltage sources, and fuses [382]. Although the package can model single- and three-phase PV systems, it does not support the smart inverter control strategies to mitigate the voltage issues in the distribution networks.

In PowerModelsDistribution, unbalanced OPF has well-defined semantics for a sizeable group of formulations (e.g., AC in polar coordinates, DC approximation, or SOC relaxation). The results for AC formulations can be obtained using Ipopt solver, while Mosek solver [348] is used to solve the SDP and SOC formulations [23]. To solve the OPF problem, the variables for branch and transformer flows, voltage, storage, and generators are firstly initialized based on the specified formulation. Secondly, the constraints (e.g., Ohm's Law, power balance, thermal limits, etc.) are employed. Finally, an objective function is included in the OPF problem. Details of every JuMP model alter based on the chosen formulation [138].

2) SUMMARY AND COMPARISON

Open-DSOPF and PowerModelsDistribution are the only tools which are able to perform unbalanced non-linear OPF analysis. These two tools are open-access. However, some commercial tools can handle linear OPF problems, such as Digsilent PowerFactory [226] and electrical transient analyzer program (ETAP) [384].

Each of the reviewed tools has one or multiple solvers to handle OPF problems. MATPOWER utilizes several solvers and optimizers, such as MINOS solver, Ipopt solver, MIPS solver, Knitro solver, GLPK, CLP solver and MP-Opt-Model. PYPOWER utilizes another set of solvers, such as MINOS solver, Ipopt solver, MIPS solver, and Knitro solver. Moreover, Open-DSOPF implements two solvers (i.e., Knitro and Ipopt) from which the users select. Furthermore, PowerModelsDistribution utilizes Ipopt solver for solving AC OPF formulations, and Mosek solver to solve the SDP and SOC OPF formulations.

Open-DSOPF and PowerModelsDistribution tools support the modeling of single- and three-phase PV systems. In contrast, MATPOWER/PAYPOWER do not support modeling the PV systems. Open-DSOPF implements distribution control strategies to manage the voltage levels and reactive PFs in the distribution networks by coordinating the behaviour of controllable devices (e.g., inverters) based on OpenDSS software, such as volt-var, volt-watt, fixed power factor,

combined mode (i.e., volt-var/volt-watt), and other advanced level inverter control characteristics [245]. In contrast, PowerModelsDistribution and MATPOWER/PAYPOWER tools do not support the smart inverter control strategies. More differences between the tools in terms of basic features and a model library for the majority of power components are summarized in Table 6.

Open-DSOPF and PowerModelsDistribution tools support several explicit models for the distribution networks, and they can solve unbalanced non-linear OPF problems. The development of the meta-heuristic-based optimization algorithms is still in progress to solve the OPF problems as efficiently as the existing algorithms and faster using parallel processing. In most cases, parallel processing is not a good solution, especially for the algorithms that mainly require iterative evaluation. In addition, meta-heuristic-based optimization algorithms need hyper-parameter tuning to improve their performance. However, development is still progressing to overcome these issues by applying them to the existing OPF solvers. Accordingly, Niu *et al.* [385] reviewed the applications of meta-heuristic-based optimization algorithms for solving OPF problems in modern power systems. Moreover, the efficiency improvements in meta-heuristic-based optimization algorithms for solving OPF problems are discussed in [386].

V. CONCLUSION

The increased growth of low-carbon technologies in the distribution networks is changing how the distribution network is exploited in real terms. This highlights the importance of the accuracy of modeling and analyzing the distribution systems to accommodate these technologies without adversely impacting the power quality or reliability for normal operation of the distribution network. In addition, these technologies can contribute to normalizing the operation of the network and provide flexibility and control capabilities. Accordingly, each feeder with its connected components must be modeled as accurately as possible to exploit existing infrastructure better to avoid any under- or over-estimation for the level of reliability predicted in the distribution networks.

As reviewed in this paper, a set of approximations and modifications are widely used to model the components in the distribution networks, which raise challenges in decision-making and control. These challenges reduce the accuracy of optimization problems. Therefore, in this paper the aim has been to review the exact models and best practices to model the LVDNs as accurately as possible and to conduct accurate PF and OPF analysis with the available tools. Achieving accurate models of the components in LVDNs requires gathering real-time data and representing the physical first principles. The crucial nature of modeling LVDNs components has been stressed in this paper. Here, the analysis results are suspect if there is no consideration of exact models that reflect the unbalanced nature of a distribution feeder. The first step to achieve accurate simulations and representations can be started by modeling the LVDNs as a steady-state system, including Kirchhoff's laws and multi-conductor line models. The lack of visibility of the LVDN data (in the suitable form) is the primary concern for most of the DNSPs in Australia and worldwide, which needs smart devices, with the appropriate privacy considerations.

The distribution network modeling, optimization, and control with accurate mathematical representations and using real-time data are not particularly suited for hand calculations but have been designed with simulation tools. In most contexts, these models incorporate non-linear equations, which introduces challenges from algorithmic solution standpoints and for implementing them using the simulation tools. Marked progress has been seen in developing high-quality simulation tools that support the accurate LVDNs models and (O)PF formulations useful in a variety of contexts. Some of these tools use less accurate models so as to include more detail elsewhere, such as longer data horizons or more minor time-step data. Therefore, the trade-off is between accuracy and computational time. However, it is challenging to actually establish the effect of particular simplifications (e.g., neglect of the phase unbalance). Armed with computer tools and using the models and techniques reviewed in this paper, finding solutions for contemporary problems and long-range planning studies can be carried out as accurately as possible. As reviewed in this paper, only two simulation tools can handle the unbalanced non-linear OPF problems and provide explicit models for the components in the LVDNs. These tools are still under development to address power system challenges.

Simultaneously, increasing the PV penetration levels in LVDNs has introduced several technical issues, including voltage violations, assets congestion, frequency, and harmonics issues. These impacts can limit the integration of new PV systems in LVDNs. Most DNSPs are more concerned about the voltage and over-heating issues which are the major factors that can limit the increase in PV penetration levels. Accordingly, several solutions have been proposed in the literature to mitigate these issues, in order to allow the network to accommodate more PV systems than the ''business as usual'' scenario. These solutions are categorized as traditional and non-traditional solutions. Some of these require extra investments, such as upgrading or replacing existing network assets (e.g., conductors and transformers), replacing the off-load tap changers with on-load tap changers, and installing storage batteries.

At the same time, other solutions require smart meter data and management of the asset congestion by installing smart controllers, such as adjustment of the on-load tap changer in zone-substation transformers, setting up on-load tap changer-fitted LV transformers with adaptive control, and a dynamic voltage target at the zone-substation on-load tap changer. However, the smart inverters control solution does not need any extra investments, which can make it the most cost-effective one. The most used smart inverters controls are the volt-watt and volt-var techniques. These techniques can

mitigate voltage issues and enable high PV penetration levels. Yet they have some limitations. Using only the volt-watt technique increases the active power curtailment. By just using the volt-var technique, this increases the current flows in the network assets and causes a poor power factor issue. A combination of both techniques still leads to the residual outcome of a poor power factor issue. The poor power factor issue can be solved by installing power factor correction units, which need extra investment from DNSPs. Therefore, a new control technique is needed to overcome these limitations without any extra investment.

With this in mind, a non-exhaustive overview of open questions and future research opportunities which arise from the investigations in this paper are as follows:

- *Extend the unbalanced three-phase network models in LV networks in terms of experimentation with optimal control.* It is noted that the progress that has been made in LV networks is less than that done in MV networks. The components modeling equations and PF representations have already been extended to consider unbalanced three-phase network models. In real applications, the networks can be 4-wire. This requires more advanced technologies (e.g., smart meters) to gather real-time data to model the networks accurately, which introduces more challenges and needs extra privacy considerations and regulations.
- *Develop accurate forecasting methods to represent the actual load data in LVDNs at the substation and household levels.*The load data has time-varying characteristics, which increases the complexity and uncertainty of the LVDNs. Accurate characterization of the load data is useful for power system operations, planning, and controlling the inverters efficiently. Therefore, more investigations are required to develop accurate forecasting methods to avoid under- or over-estimation of the PV penetration levels that the network can accommodate. This can increase the data available at the substation and household levels.
- *Develop accurate PV system models to reflect its actual behaviour with the availability of fewer data incorporating unbalanced network physics.*Further investigation is required using the available tools or others to develop a more accurate PV system's model, which can reflect the actual behaviour of the systems, including the uncertainty. The main idea is to implement these models to be as accurately as possible with fewer data and information requirements.
- *Develop inverter control strategy that can overcome the limitations of the existing smart inverter solutions (e.g., volt-watt and volt-var techniques) to enable high PV penetration levels.* Further investigation is required to develop an inverter operating mode that can enable high PV penetration with lower active power curtailment and a reduction in the current flow in the network assets to keep the voltage levels and power factor within predefined limits without any extra investment.
- *Develop centralized optimization algorithms with keeping distribution optimization algorithms as a backup considering the unbalanced network physics.* Centralized optimization algorithms show an outstanding performance in coordinating the controllable devices in the LVDNs (e.g., inverters). However, maintaining the privacy, security and reliability of these algorithms is considered challenging. Therefore, distribution optimization algorithms need more extension to back up the centralized algorithms to reduce or eliminate operational challenges in future power systems by sharing the computational tasks and communication burdens while maintaining privacy.
- *Consider different coordinates of the optimization algorithms at the various levels of the grid.* Expressing the PF variables in different coordinate systems at various grid levels (e.g., between MV and LV levels) may result in PF representations with differing characteristics. PF equations can be formulated in many coordinate systems (e.g., SOCP relaxations, quadratically constrained quadratics, etc.), yielding representations with desirable properties. Therefore, further study of alternative coordinate systems is deserving of effort.
- *Investigate the ability of machine and deep learning techniques to support voltage levels in LVDNs.* Machine and deep learning techniques show high performance in forecasting the characteristics of PV generation and load profiles. Therefore, these techniques can be implemented to coordinate controllable devices in LVDNs to mitigate voltage issues at high PV penetration. Accordingly, further studies are needed to investigate the capability of these techniques and the minimum required data to coordinate controllable devices in order to enable high PV penetration levels.
- *Explore the limitations of local solution algorithms and various PF representations to overcome them by developing global optimization approaches.* The PF representations reviewed in this paper have synergistic capabilities with local solution algorithms when applied for distribution network models. Further development of these algorithms and other such synergies is essential for future research as some local solvers can use the solutions to the PF representations considered in this paper to speed up computations and encourage convergence to a better solution.
- *Extend the use of unbalanced PF representations to cover more power system applications.* PF equations are the core of many power system optimization and control problems. In this paper, the PF representations are focused on OPF problems. Further research is required to extend PF representation to cover other applications, such as multi-objective problems, online (real-time) OPF, multi-period optimization with storage, stochastic optimization, state estimation, unit commitment, infrastructure planning, electricity pricing, transmission switching, distribution network reconfiguration,

system restoration, voltage stability margins, voltage constraint satisfaction, and contingency analysis.

- *Exploit alternatives to the existing convex optimization tools.* Several convex programming algorithms (e.g., LP, SOCP, and SDP formulations) are widely applied to various problems in power systems. Other convex programming tools (e.g., geometric programming) and linearization of the PF equations (e.g., iterative linearization as a solution method) have not yet found widespread applications in power systems and need future research.
- *Investigate the capability of meta-heuristic-based optimization methods to solve unbalanced (O)PF problems.* In this paper, meta-heuristic-based optimization methods to solve unbalanced (O)PF problems have not been considered. Therefore, further investigation is required to evaluate the effectiveness of meta-heuristic-based optimization methods to solve unbalanced (O)PF problems.
- *Develop a set of test cases and benchmark datasets, and study challenging test cases.* The lack of benchmark datasets and case studies that have gaps and challenges significantly slows the development and validation of the models and tools. The datasets for 3 and 4-wire MV and LV distribution networks are urgently needed. Here, the existing PF representations show promise for specific test cases, benchmark datasets, and applications (e.g., OPF problems for many of the IEEE test cases); however, there are a set of challenging problems deserving of further investigation (e.g., multi-period, to compare the optimality and feasibility of different optimization engines). Accordingly, PGLib [387] archives several gaps for various OPF test cases and applications [388], which are the topic of ongoing research. In addition, more investigation should be carried out about the feasible spaces of OPF problems and their relaxations to characterize both challenging and straightforward cases.
- *Investigate the current and future cybersecurity risks of using centralized control strategies.* The centralized control strategy may require an increase in the reliance on data sharing to enable LV management in an application such as DOEs. Thus, further investigations are needed to overview the cybersecurity risks in substations and PV systems communications in order to propose protection and planning tools to safeguard assets, customers, and DNSPs.

ACKNOWLEDGMENT

The authors would like to thank Frederik Geth from CSIRO for the thoughtful remarks and valuable feedbacks he gave on initial drafts of this work.

REFERENCES

[1] A. Dubey, A. Bose, M. Liu, and L. N. Ochoa, "Paving the way for advanced distribution management systems applications: Making the most of models and data," *IEEE Power Energy Mag.*, vol. 18, no. 1, pp. 63–75, Jan. 2020.

[2] F. Schweppe and J. Wildes, "Power system static-state estimation, Part I: Exact model," *IEEE Trans. Power App. Syst.*, vol. PAS-89, no. 1, pp. 120–125, Jan. 1970. [Online]. Available: http://ieeexplore.ieee.org/document/4074022/

[3] A. J. Urquhart, "Accuracy of low voltage distribution network modelling," Ph.D. dissertation, School Mech., Elect. Manuf. Eng., Loughborough Univ., Loughborough, U.K., 2016. [Online]. Available: https://repository.lboro.ac.uk/articles/thesis/9517922

[4] I. Leisse, O. Samuelsson, and J. Svensson, "Coordinated voltage control in medium and low voltage distribution networks with wind power and photovoltaics," in *Proc. IEEE Grenoble Conf.*, Jun. 2013, pp. 1–6. [Online]. Available: http://ieeexplore.ieee.org/document/6652349/

[5] S. Pfenninger, L. Hirth, I. Schlecht, E. Schmid, F. Wiese, T. Brown, C. Davis, M. Gidden, H. Heinrichs, C. Heuberger, S. Hilpert, U. Krien, C. Matke, A. Nebel, R. Morrison, B. Müller, G. Pleßmann, M. Reeg, J. C. Richstein, A. Shivakumar, I. Staffell, T. Tröndle, and C. Wingenbach, "Opening the black box of energy modelling: Strategies and lessons learned," *Energy Strategy Rev.*, vol. 19, pp. 63–71, Jan. 2018.

[6] S. Pfenninger, "Energy scientists must show their workings," *Nature News*, vol. 542, no. 7642, p. 393, 2017.

[7] R. C. Dugan and T. E. McDermott, "An open source platform for collaborating on smart grid research," in *Proc. IEEE Power Energy Soc. General Meeting*, Jul. 2011, pp. 1–7. [Online]. Available: https://ieeexplore.ieee.org/document/6039829/

[8] G. Wang and H. Hijazi, "Mathematical programming methods for microgrid design and operations: A survey on deterministic and stochastic approaches," *Comput. Optim. Appl.*, vol. 71, no. 2, pp. 553–608, Nov. 2018, doi: 10.1007/s10589-018-0015-1.

[9] D. K. Molzahn and I. A. Hiskens, "A survey of relaxations and approximations of the power flow equations," in *Foundations and Trends in Electric Energy Systems*, vol. 4. Delft, The Netherlands: Now, 2019.

[10] D. Bienstock, M. Escobar, C. Gentile, and L. Liberti, "Mathematical programming formulations for the alternating current optimal power flow problem," *4OR*, vol. 18, no. 3, pp. 249–292, Sep. 2020, doi: 10.1007/s10288-020-00455-w.

[11] T. Reindl, X. Kong, and A. Pathare, "UPDATE of the solar photovoltaic (PV) roadmap for Singapore," Sol. Energy Res. Inst., Singapore, Tech. Rep., 2020. [Online]. Available: https://www.nccs.gov.sg/docs/defaultsource/default-document-library/SolarPVRoadmapforSingapore2020.pdf

[12] O. Gandhi, D. S. Kumar, C. D. Rodríguez-Gallegos, and D. Srinivasan, "Review of power system impacts at high PV penetration Part I: Factors limiting PV penetration," *Sol. Energy*, vol. 210, pp. 181–201, Nov. 2020, doi: 10.1016/j.solener.2020.06.097.

[13] D. Sampath Kumar, O. Gandhi, C. D. Rodríguez-Gallegos, and D. Srinivasan, "Review of power system impacts at high PV penetration Part II: Potential solutions and the way forward," *Sol. Energy*, vol. 210, pp. 202–221, Nov. 2020, doi: 10.1016/j.solener.2020.08.047.

[14] W. H. Kersting, *Distribution System Modeling and Analysis*, 4th ed. Boca Raton, FL, USA: CRC Press, Aug. 2017. [Online]. Available: https://www.taylorfrancis.com/books/9781498772143

[15] H. L. Willis, *Power Distribution Planning Reference Book*. Boca Raton, FL, USA: CRC Press, Jun. 2004. [Online]. Available: https://www.taylorfrancis.com/books/9780824755386

[16] G. Cronshaw, "Earthing: Your questions answered," in *IET Wiring Matters*. London, U.K.: Inst. Eng. Technol., 2005, pp. 18–24. [Online]. Available: https://electrical.theiet.org/media/1698/earthing-your-questions-answered.pdf

[17] A. J. Urquhart and M. Thomson, "Series impedance of distribution cables with sector-shaped conductors," *IET Gener. Transmiss. Distrib.*, vol. 9, no. 16, pp. 2679–2685, Dec. 2015.

[18] J. R. Carson, "Wave propagation in overhead wires with ground return," *Bell Syst Tech. J.*, vol. 5, no. 4, pp. 539–554, Oct. 1926. [Online]. Available: https://ieeexplore.ieee.org/document/6768096

[19] D. Woodhouse, "On the theoretical basis of Carson's equations," in *Proc. IEEE Int. Conf. Power Syst. Technol. (POWERCON)*, Oct.,Nov. 2012, pp. 1–6. [Online]. Available: http://ieeexplore.ieee.org/document/6401356/

[20] F. Geth and H. Ergun, "Real-value power-voltage formulations of, and bounds for, three-wire unbalanced optimal power flow," 2021, *arXiv:2106.06186*. [Online]. Available: http://arxiv.org/abs/2106.06186

[21] F. Geth, S. Claeys, and G. Deconinck, "Current-voltage formulation of the unbalanced optimal power flow problem," in *Proc. 8th Workshop Model. Simul. Cyber-Phys. Energy Syst.*, Apr. 2020, pp. 1–6. [Online]. Available: https://ieeexplore.ieee.org/document/9133699/

[22] F. Geth, C. Coffrin, and D. Fobes, "A flexible storage model for power network optimization," in *Proc. 11th ACM Int. Conf. Future Energy Syst.*, New York, NY, USA, Jun. 2020, pp. 503–508. [Online]. Available: https://dl.acm.org/doi/10.1145/3396851.3402121

[23] D. M. Fobes, S. Claeys, F. Geth, and C. Coffrin, "Powermodelsdistribution.Jl: An open-source framework for exploring distribution power flow formulations," *Electr. Power Syst. Res.*, vol. 189, Dec. 2020, Art. no. 106664, doi: 10.1016/j.epsr.2020.106664.

[24] E. Lakervi and E. J. Holmes, *Electricity Distribution Network Design*, 2nd ed. London, U.K.: Institution of Engineering and Technology, Jan. 2003. [Online]. Available: https://digital-library.theiet.org/content/books/po/pbpo021e

[25] I. Sharma, K. Bhattacharya, and C. Cañizares, "Smart distribution system operations with price-responsive and controllable loads," *IEEE Trans. Smart Grid*, vol. 6, no. 2, pp. 795–807, Mar. 2015.

[26] Y. Liu, J. Li, and L. Wu, "Coordinated optimal network reconfiguration and voltage regulator/DER control for unbalanced distribution systems," *IEEE Trans. Smart Grid*, vol. 10, no. 3, pp. 2912–2922, May 2019.

[27] Q. Nguyen, H. V. Padullaparti, K.-W. Lao, S. Santoso, X. Ke, and N. Samaan, "Exact optimal power dispatch in unbalanced distribution systems with high PV penetration," *IEEE Trans. Power Syst.*, vol. 34, no. 1, pp. 718–728, Jan. 2019.

[28] L. Gutierrez-Lagos and L. F. Ochoa, "OPF-based CVR operation in PV-rich MV–LV distribution networks," *IEEE Trans. Power Syst.*, vol. 34, no. 4, pp. 2778–2789, Jul. 2019.

[29] M. Bazrafshan, N. Gatsis, and H. Zhu, "Optimal power flow with step-voltage regulators in multi-phase distribution networks," *IEEE Trans. Power Syst.*, vol. 34, no. 6, pp. 4228–4239, Nov. 2019. [Online]. Available: https://ieeexplore.ieee.org/document/8710279/

[30] W. G. Sunderman, R. C. Dugan, and D. S. Dorr, "The neutral-to-Earth voltage (NEV) test case and distribution system analysis," in *Proc. IEEE Power Energy Soc. Gen. Meeting-Convers. Del. Electr. Energy 21st Century*, Jul. 2008, pp. 1–6. [Online]. Available: http://ieeexplore.ieee.org/document/4596812/

[31] T.-H. Chen and Y.-L. Chang, "Integrated models of distribution transformers and their loads for three-phase power flow analyses," *IEEE Trans. Power Del.*, vol. 11, no. 1, pp. 507–513, Jan. 1996.

[32] M. Thomson and D. G. Infield, "Network power-flow analysis for a high penetration of distributed generation," *IEEE Trans. Power Syst.*, vol. 22, no. 3, pp. 1157–1162, Aug. 2007. [Online]. Available: http://ieeexplore.ieee.org/document/1709489/ and [Online]. Available: http://ieeexplore.ieee.org/document/4282058/

[33] I. Richardson, M. Thomson, D. Infield, and A. Delahunty, "A modelling framework for the study of highly distributed power systems and demand side management," in *Proc. Int. Conf. Sustain. Power Gener. Supply*, Apr. 2009, pp. 1–6. [Online]. Available: http://ieeexplore.ieee.org/document/5348274/

[34] N. Tleis, *Power Systems Modelling and Fault Analysis*, 2nd ed. Amsterdam, The Netherlands: Elsevier, 2019. [Online]. Available: https://linkinghub.elsevier.com/retrieve/pii/C20170022620

[35] M. H. Rashid, *Electric Renewable Energy Systems*. Amsterdam, The Netherlands: Elsevier, 2016. [Online]. Available: https://linkinghub.elsevier.com/retrieve/pii/C20130144327

[36] S. Claeys, G. Deconinck, and F. Geth, "Decomposition of n-winding transformers for unbalanced optimal power flow," *IET Gener., Transmiss. Distrib.*, vol. 14, no. 24, pp. 5961–5969, Dec. 2020. [Online]. Available: https://onlinelibrary.wiley.com/doi/10.1049/iet-gtd.2020.0776

[37] R. Dugan, "A perspective on transformer modeling for distribution system analysis," in *Proc. IEEE Power Eng. Soc. Gen. Meeting*, vol. 1, Jul. 2003, pp. 114–119. [Online]. Available: http://ieeexplore.ieee.org/document/1267146/

[38] R. R. Jha, A. Dubey, C.-C. Liu, and K. P. Schneider, "Bi-level volt-VAR optimization to coordinate smart inverters with voltage control devices," *IEEE Trans. Power Syst.*, vol. 34, no. 3, pp. 1801–1813, May 2019. [Online]. Available: https://ieeexplore.ieee.org/document/8598813/

[39] M. Thomson, "Automatic voltage control relays and embedded generation," *Power Eng. J.*, vol. 14, no. 2, pp. 71–76, Apr. 2000. [Online]. Available: https://digital-library.theiet.org/content/journals/10.1049/pe_20000208

[40] *Smart-Grid Smart-City Customer Trial Data*, Australian Government-Department of Industry, Science, Energy and Resources, Canberra, ACT, Australia, 2018. [Online]. Available: https://data.gov.au/data/dataset/4e21dea3-9b87-4610-94c7-15a8a77907ef

[41] I. Richardson, M. Thomson, D. Infield, and C. Clifford, "Domestic electricity use: A high-resolution energy demand model," *Energy Buildings*, vol. 42, no. 10, pp. 1878–1887, 2010. [Online]. Available: http://dx.doi.org/10.1016/j.enbuild.2010.05.023

[42] A. Navarro-Espinosa and L. F. Ochoa, "Probabilistic impact assessment of low carbon technologies in LV distribution systems," *IEEE Trans. Power Syst.*, vol. 31, no. 3, pp. 2192–2203, May 2016.

[43] I. Richardson and M. Thomson. (Jan. 2011). *Integrated Domestic Electricity Demand and PV Micro-Generation Model*. [Online]. Available: https://hdl.handle.net/2134/7773

[44] T. Cutsem and C. Vournas, *Voltage Stability of Electric Power Systems*. Boston, MA, USA: Springer, 1998. [Online]. Available: http://link.springer.com/10.1007/978-0-387-75536-6

[45] Y. Liu, J. Li, and L. Wu, "ACOPF for three-phase four-conductor distribution systems: Semidefinite programming based relaxation with variable reduction and feasible solution recovery," *IET Gener., Transmiss. Distrib.*, vol. 13, no. 2, pp. 266–276, Jan. 2019. [Online]. Available: https://onlinelibrary.wiley.com/doi/10.1049/iet-gtd.2018.5033

[46] E. Dall'Anese, G. B. Giannakis, and B. F. Wollenberg, "Optimization of unbalanced power distribution networks via semidefinite relaxation," in *Proc. North Amer. Power Symp. (NAPS)*, Sep. 2012, pp. 1–6. [Online]. Available: http://ieeexplore.ieee.org/document/6336350/

[47] J. S. Giraldo, J. C. Lopez, J. A. Castrillon, M. J. Rider, and C. A. Castro, "Probabilistic OPF model for unbalanced three-phase electrical distribution systems considering robust constraints," *IEEE Trans. Power Syst.*, vol. 34, no. 5, pp. 3443–3454, Sep. 2019.

[48] F. Meng, B. Chowdhury, and M. Chamanamcha, "Three-phase optimal power flow for market-based control and optimization of distributed generations," *IEEE Trans. Smart Grid*, vol. 9, no. 4, pp. 3691–3700, Jul. 2018.

[49] L. Gan and S. H. Low, "Convex relaxations and linear approximation for optimal power flow in multiphase radial networks," in *Proc. 18th Power Syst. Comput. Conf.*, Aug. 2014, pp. 1–9. [Online]. Available: http://ieeexplore.ieee.org/document/7038399/

[50] A. Gastalver-Rubio, E. Romero-Ramos, and J. M. Maza-Ortega, "Improving the performance of low voltage networks by an optimized unbalance operation of three-phase distributed generators," *IEEE Access*, vol. 7, pp. 177504–177516, 2019.

[51] J. Wang, N. Zhou, Y. Ran, and Q. Wang, "Optimal operation of active distribution network involving the unbalance and harmonic compensation of converter," *IEEE Trans. Smart Grid*, vol. 10, no. 5, pp. 5360–5373, Sep. 2019. [Online]. Available: https://ieeexplore.ieee.org/document/8528512/

[52] F. Geth, S. Claeys, and G. Deconinck, "Nonconvex lifted unbalanced branch flow model: Derivation, implementation and experiments," *Electr. Power Syst. Res.*, vol. 189, Dec. 2020, Art. no. 106558. [Online]. Available: https://linkinghub.elsevier.com/retrieve/pii/S037877962030362X, doi: 10.1016/j.epsr.2020.106558.

[53] Electric Power Research Institute, "OpenDSS PV system element model," Washington, DC, USA, Tech. Rep., 2011. [Online]. Available: https://sourceforge.net/p/electricdss/discussion/861977/thread/7cc53d82/d60d/attachment/OpenDSS PVSystem Model.pdf

[54] D. K. Molzahn, F. Dörfler, H. Sandberg, S. H. Low, S. Chakrabarti, R. Baldick, and J. Lavaei, "A survey of distributed optimization and control algorithms for electric power systems," *IEEE Trans. Smart Grid*, vol. 8, no. 6, pp. 2941–2962, Nov. 2017.

[55] K. E. Antoniadou-Plytaria, I. N. Kouveliotis-Lysikatos, P. S. Georgilakis, and N. D. Hatziargyriou, "Distributed and decentralized voltage control of smart distribution networks: Models, methods, and future research," *IEEE Trans. Smart Grid*, vol. 8, no. 6, pp. 2999–3008, Nov. 2017.

[56] M. Yao and J. L. Mathieu, "Overcoming the practical challenges of applying steinmetz circuit design to mitigate voltage unbalance using distributed solar PV," *Electr. Power Syst. Res.*, vol. 188, Nov. 2020, Art. no. 106563, doi: 10.1016/j.epsr.2020.106563.

[57] M. Oshiro, K. Tanaka, T. Senjyu, S. Toma, A. Yona, A. Y. Saber, T. Funabashi, and C.-H. Kim, "Optimal voltage control in distribution systems using PV generators," *Int. J. Electr. Power Energy Syst.*, vol. 33, no. 3, pp. 485–492, Mar. 2011, doi: 10.1016/j.ijepes.2010.11.002.

[58] S. Jashfar and S. Esmaeili, "Volt/VAR/THD control in distribution networks considering reactive power capability of solar energy conversion," *Int. J. Electr. Power Energy Syst.*, vol. 60, pp. 221–233, Sep. 2014, doi: 10.1016/j.ijepes.2014.02.038.

[59] V. Calderaro, G. Conio, V. Galdi, G. Massa, and A. Piccolo, "Optimal decentralized voltage control for distribution systems with inverter-based distributed generators," *IEEE Trans. Power Syst.*, vol. 29, no. 1, pp. 230–241, Jan. 2014.

[60] C. G. Bajo, S. Hashemi, S. B. Kjsar, G. Yang, and J. Ostergaard, "Voltage unbalance mitigation in LV networks using three-phase PV systems," in *Proc. IEEE Int. Conf. Ind. Technol. (ICIT)*, Mar. 2015, pp. 2875–2879.

[61] M. Yao, I. A. Hiskens, and J. L. Mathieu, "Mitigating voltage unbalance using distributed solar photovoltaic inverters," *IEEE Trans. Power Syst.*, vol. 36, no. 3, pp. 2642–2651, May 2021.

[62] *AS/NZS 4777.2:2015: Grid Connection of Energy Systems Via Inverters—Part 2: Inverter Requirements*, Standards Australia, Sydney, NSW, Australia, 2015.

[63] A. T. Procopiou, K. Petrou, and L. N. Ochoa, "Advanced planning of PV-rich distribution networks–deliverable 3: Traditional solutions," Univ. Melbourne, Parkville VIC, Australia, Tech. Rep. UoM-AusNet-2018ARP135-Deliverable3_v02, Feb. 2020.

[64] P. Chaudhary and M. Rizwan, "Voltage regulation mitigation techniques in distribution system with high PV penetration: A review," *Renew. Sustain. Energy Rev.*, vol. 82, pp. 3279–3287, Feb. 2018. [Online]. Available: https://linkinghub.elsevier.com/retrieve/pii/S1364032117313989

[65] J. D. Watson, N. R. Watson, D. Santos-Martin, A. R. Wood, S. Lemon, and A. J. Miller, "Impact of solar photovoltaics on the low-voltage distribution network in New Zealand," *IET Gener., Transmiss. Distrib.*, vol. 10, no. 1, pp. 1–9, 2016.

[66] S. Singh, V. B. Pamshetti, A. K. Thakur, and S. P. Singh, "Multistage multiobjective volt/VAR control for smart grid-enabled CVR with solar PV penetration," *IEEE Syst. J.*, vol. 15, no. 2, pp. 2767–2778, Jun. 2021. [Online]. Available: https://ieeexplore.ieee.org/document/9099637/

[67] X. Su, M. A. S. Masoum, and P. J. Wolfs, "Optimal PV inverter reactive power control and real power curtailment to improve performance of unbalanced four-wire LV distribution networks," *IEEE Trans. Sustain. Energy*, vol. 5, no. 3, pp. 967–977, Jul. 2014. [Online]. Available: http://ieeexplore.ieee.org/document/6804647/

[68] J. H. Braslavsky, L. D. Collins, and J. K. Ward, "Voltage stability in a grid-connected inverter with automatic volt-watt and volt-VAR functions," *IEEE Trans. Smart Grid*, vol. 10, no. 1, pp. 84–94, Jan. 2019.

[69] R. Tonkoski, L. A. C. Lopes, and T. H. M. El-Fouly, "Coordinated active power curtailment of grid connected PV inverters for overvoltage prevention," *IEEE Trans. Sustain. Energy*, vol. 2, no. 2, pp. 139–147, Apr. 2011.

[70] M. Z. Liu, A. T. Procopiou, K. Petrou, L. F. Ochoa, T. Langstaff, J. Harding, and J. Theunissen, "On the fairness of PV curtailment schemes in residential distribution networks," *IEEE Trans. Smart Grid*, vol. 11, no. 5, pp. 4502–4512, Sep. 2020.

[71] S. Weckx, C. Gonzalez, and J. Driesen, "Combined central and local active and reactive power control of PV inverters," *IEEE Trans. Sustain. Energy*, vol. 5, no. 3, pp. 776–784, Jul. 2014.

[72] S. Ghosh, S. Rahman, and M. Pipattanasomporn, "Distribution voltage regulation through active power curtailment with PV inverters and solar generation forecasts," *IEEE Trans. Sustain. Energy*, vol. 8, no. 1, pp. 13–22, Jan. 2017.

[73] L. B. Perera, G. Ledwich, and A. Ghosh, "Multiple distribution static synchronous compensators for distribution feeder voltage support," *IET Gener., Transmiss. Distrib.*, vol. 6, no. 4, p. 285, 2012. https://digital-library.theiet.org/content/journals/10.1049/iet-gtd.2011.0197

[74] K. De Brabandere, B. Bolsens, J. Van den Keybus, A. Woyte, J. Driesen, R. Belmans, and K. U. Leuven, "A voltage and frequency droop control method for parallel inverters," in *Proc. IEEE 35th Annu. Power Electron. Spec. Conf.*, Jun. 2004, pp. 2501–2507. [Online]. Available: http://ieeexplore.ieee.org/document/1355222/

[75] T. R. Ricciardi, K. Petrou, J. F. Franco, and L. F. Ochoa, "Defining customer export limits in PV-rich low voltage networks," *IEEE Trans. Power Syst.*, vol. 34, no. 1, pp. 87–97, Jan. 2019. [Online]. Available: https://ieeexplore.ieee.org/document/8413150/

[76] M. Aydin, A. Navarro, and L. Ochoa, "Investigating the benefits of meshing real UK LV networks," in *Proc. 23rd Int. Conf. Electr. Distrib. (CIRED)*, Jun. 2015, pp. 1–5.

[77] C. V. T. Cabral, D. O. Filho, A. S. A. C. Diniz, J. H. Martins, O. M. Toledo, and L. D. V. B. Machado Neto, "A stochastic method for stand-alone photovoltaic system sizing," *Sol. Energy*, vol. 84, no. 9, pp. 1628–1636, Sep. 2010.

[78] M. Lee, D. Soto, and V. Modi, "Cost versus reliability sizing strategy for isolated photovoltaic micro-grids in the developing world," *Renew. Energy*, vol. 69, pp. 16–24, Sep. 2014. [Online]. Available: http://dx.doi.org/10.1016/j.renene.2014.03.019

[79] F. Spertino, P. Di Leo, V. Cocina, and G. M. Tina, "Storage sizing procedure and experimental verification of stand-alone photovoltaic systems," in *Proc. IEEE Int. Energy Conf. Exhib. (ENERGYCON)*, Sep. 2012, pp. 464–468.

[80] A. Bouabdallah, J. C. Olivier, S. Bourguet, M. Machmoum, and E. Schaeffer, "Safe sizing methodology applied to a standalone photovoltaic system," *Renew. Energy*, vol. 80, pp. 266–274, Aug. 2015, doi: 10.1016/j.renene.2015.02.007.

[81] S. Norbu and S. Bandyopadhyay, "Power pinch analysis for optimal sizing of renewable-based isolated system with uncertainties," *Energy*, vol. 135, pp. 466–475, Sep. 2017, doi: 10.1016/j.energy.2017.06.147.

[82] A. Sadio, I. Fall, and S. Mbodji, "New numerical sizing approach of a standalone photovoltaic power at Ngoundiane, Senegal," *EAI Endorsed Trans. Energy Web*, vol. 5, no. 16, pp. 1–12, 2018.

[83] R. Dufo-López, J. M. Lujano-rojas, and J. L. Bernal-Agustín, "Comparison of different lead–acid battery lifetime prediction models for use in simulation of stand-alone photovoltaic systems," *Appl. Energy*, vol. 115, pp. 242–253, Feb. 2014.

[84] N. D. Nordin and H. Abdul Rahman, "A novel optimization method for designing stand alone photovoltaic system," *Renew. Energy*, vol. 89, pp. 706–715, Apr. 2016, doi: 10.1016/j.renene.2015.12.001.

[85] I. A. Ibrahim, T. Khatib, and A. Mohamed, "Optimal sizing of a standalone photovoltaic system for remote housing electrification using numerical algorithm and improved system models," *Energy*, vol. 126, pp. 392–403, May 2017, doi: 10.1016/j.energy.2017.03.053.

[86] S. Semaoui, A. H. Arab, S. Bacha, and B. Azoui, "Optimal sizing of a stand-alone photovoltaic system with energy management in isolated areas," *Energy Proc.*, vol. 36, pp. 358–368, Feb. 2013.

[87] I. A. Ibrahim, M. J. Hossain, B. C. Duck, and C. J. Fell, "An adaptive wind-driven optimization algorithm for extracting the parameters of a single-diode PV cell model," *IEEE Trans. Sustain. Energy*, vol. 11, no. 2, pp. 1054–1066, Apr. 2020.

[88] D. H. Muhsen, A. B. Ghazali, T. Khatib, and I. A. Abed, "A comparative study of evolutionary algorithms and adapting control parameters for estimating the parameters of a single-diode photovoltaic module's model," *Renew. Energy*, vol. 96, pp. 377–389, Oct. 2016.

[89] M. Abd Elaziz, S. B. Thanikanti, I. A. Ibrahim, S. Lu, B. Nastasi, M. A. Alotaibi, M. A. Hossain, and D. Yousri, "Enhanced marine predators algorithm for identifying static and dynamic photovoltaic models parameters," *Energy Convers. Manage.*, vol. 236, May 2021, Art. no. 113971. [Online]. Available: https://linkinghub.elsevier.com/retrieve/pii/S0196890421001473

[90] I. A. Ibrahim, M. J. Hossain, B. C. Duck, and M. Nadarajah, "An improved wind driven optimization algorithm for parameters identification of a triple-diode photovoltaic cell model," *Energy Convers. Manage.*, vol. 213, Jun. 2020, Art. no. 112872.

[91] F. Chenlo, F. Fabero, and M. Alonso, "A comparative study between indoor and outdoor measurements; final report of project: Testing, norms, reliability and harmonisation. Joule II—Contract no," Spain, Tech. Rep. JOU2-CT92-0178, 1995.

[92] A. Hadj Arab, F. Chenlo, and M. Benghanem, "Loss-of-load probability of photovoltaic water pumping systems," *Sol. Energy*, vol. 76, no. 6, pp. 713–723, 2004.

[93] S. Claeys, G. Deconinck, and F. Geth, "Voltage-dependent load models in unbalanced optimal power flow using power cones," *IEEE Trans. Smart Grid*, vol. 12, no. 4, pp. 2890–2902, Jul. 2021.

[94] W. H. Kersting and R. C. Dugan, "Recommended practices for distribution system analysis," in *Proc. IEEE PES Power Syst. Conf. Expo.*, 2006, pp. 499–504. [Online]. Available: http://ieeexplore.ieee.org/document/4075803/

[95] A. O'Connell, D. Flynn, and A. Keane, "Rolling multi-period optimization to control electric vehicle charging in distribution networks," *IEEE Trans. Power Syst.*, vol. 29, no. 1, pp. 340–348, Sep. 2014.

[96] B. Stott, "Review of load-flow calculation methods," *Proc. IEEE*, vol. 62, no. 7, pp. 916–929, Jul. 1974. http://ieeexplore.ieee.org/document/6581918/ and [Online]. Available: https://ieeexplore.ieee.org/document/1451474

[97] D. Mehta, D. K. Molzahn, and K. Turitsyn, "Recent advances in computational methods for the power flow equations," in *Proc. Amer. Control Conf. (ACC)*, Jul. 2016, pp. 1753–1765. [Online]. Available: http://ieeexplore.ieee.org/document/7525170/

[98] H. H. Happ, "Optimal power dispatch A comprehensive survey," *IEEE Trans. Power App. Syst.*, vol. PAS-96, no. 3, pp. 841–854, May 1977. [Online]. Available: http://ieeexplore.ieee.org/document/1601999/

[99] S. N. Talukdar and F. F. Wu, "Computer-aided dispatch for electric power systems," *Proc. IEEE*, vol. 69, no. 10, pp. 1212–1231, Oct. 1981.

[100] J. Carpentier, "Optimal power flows: Uses, methods and developments," *IFAC Proc. Volumes*, vol. 18, no. 7, pp. 11–21, Jul. 1985. [Online]. Available: https://linkinghub.elsevier.com/retrieve/pii/S1474667017604105, doi: 10.1016/S1474-6670(17)60410-5.

[101] M. Huneault and F. D. Galiana, "A survey of the optimal power flow literature," *IEEE Trans. Power Syst.*, vol. 6, no. 2, pp. 762–770, May 1991. [Online]. Available: http://ieeexplore.ieee.org/document/76723/

[102] J. A. Momoh, R. Adapa, and M. E. El-Hawary, "A review of selected optimal power flow literature to 1993. I. Nonlinear and quadratic programming approaches," *IEEE Trans. Power Syst.*, vol. 14, no. 1, pp. 96–104, Feb. 1999.

[103] J. A. Momoh, M. E. El-Hawary, and R. Adapa, "A review of selected optimal power flow literature to 1993. II. Newton, linear programming and interior point methods," *IEEE Trans. Power Syst.*, vol. 14, no. 1, pp. 105–111, Feb. 1999.

[104] Z. Qiu, G. Deconinck, and R. Belmans, "A literature survey of optimal power flow problems in the electricity market context," in *Proc. IEEE/PES Power Syst. Conf. Expo.*, Mar. 2009, pp. 1–6.

[105] S. Frank, I. Steponavice, and S. Rebennack, "Optimal power flow: A bibliographic survey I," *Energy Syst.*, vol. 3, no. 3, pp. 221–258, Sep. 2012. [Online]. Available: http://link.springer.com/10.1007/s12667-012-0056-y

[106] S. Frank, I. Steponavice, and S. Rebennack, "Optimal power flow: A bibliographic survey II Non-deterministic and hybrid methods," *Energy Syst.*, vol. 3, no. 3, pp. 259–289, 2012.

[107] A. Castillo and R. P. O'Neill, "Survey of approaches to solving the ACOPF (OPF Paper 4)," U.S. Federal Energy Regulatory Commission, Washington, DC, USA, Tech. Rep., 2013.

[108] P. Panciatici, M. C. Campi, S. Garatti, S. H. Low, D. K. Molzahn, A. X. Sun, and L. Wehenkel, "Advanced optimization methods for power systems," in *Proc. Power Syst. Comput. Conf.*, Aug. 2014, pp. 1–18.

[109] J. A. Taylor, *Convex Optimization of Power Systems*. Cambridge, U.K.: Cambridge Univ. Press, 2015.

[110] S. Frank and S. Rebennack, "An introduction to optimal power flow: Theory, formulation, and examples," *IIE Trans.*, vol. 48, no. 12, pp. 1172–1197, Aug. 2016. [Online]. Available: http://dx.doi.org/10.1080/0740817X.2016.1189626

[111] H. Abdi, S. D. Beigvand, and M. L. Scala, "A review of optimal power flow studies applied to smart grids and microgrids," *Renew. Sustain. Energy Rev.*, vol. 71, pp. 742–766, May 2017, doi: 10.1016/j.rser.2016.12.102.

[112] M. Yazdanian and A. Mehrizi-Sani, "Distributed control techniques in microgrids," *IEEE Trans. Smart Grid*, vol. 5, no. 6, pp. 2901–2909, Nov. 2014. https://linkinghub.elsevier.com/retrieve/pii/B9780081017531000024 and [Online]. Available: http://ieeexplore.ieee.org/document/6870484/

[113] H. Han, X. Hou, J. Yang, J. Wu, M. Su, and J. M. Guerrero, "Review of power sharing control strategies for islanding operation of AC microgrids," *IEEE Trans. Smart Grid*, vol. 7, no. 1, pp. 200–215, Jan. 2016.

[114] A. Kargarian, J. Mohammadi, J. Guo, S. Chakrabarti, M. Barati, G. Hug, S. Kar, and R. Baldick, "Toward distributed/decentralized DC optimal power flow implementation in future electric power systems," *IEEE Trans. Smart Grid*, vol. 9, no. 4, pp. 2574–2594, Jul. 2018. [Online]. Available: https://ieeexplore.ieee.org/document/7581042/

[115] C. W. Taylor, "Modelling of voltage collapse including dynamic phenoma," CIGRE Task Force, Paris, France, Tech. Rep. 38.02.11, 1993. [Online]. Available: https://e-cigre.org/publication/075-modelling-of-voltage-collapse-including-dynamic-phenomena

[116] N. D. Hatziargyriou and T. Van Cutsem, "Indices predicting voltage collapse including dynamic phenomena," CIGRE Task Force, Paris, France, Tech. Rep. 38.02.11, 1994. [Online]. Available: https://e-cigre.org/publication/091-indices-predicting-voltage-collapse-including-dynamic-phenomena

[117] C. W. Taylor, *Power System Voltage Stability*. New York, NY, USA: McGraw-Hill, 1994.

[118] I. Dobson, T. V. Cutsem, C. Vournas, C. L. DeMarco, M. Venkatasubramanian, and T. J. Overbye, *Voltage Stability Assessment: Concepts, Practices Tools*. Piscataway, NJ, USA: IEEE Power Engineering Society, 2002.

[119] S. Sen and D. P. Kothari, "Optimal thermal generating unit commitment: A review," *Int. J. Electr. Power Energy Syst.*, vol. 20, no. 7, pp. 443–451, Oct. 1998. http://ieeexplore.ieee.org/document/4074522/ and [Online]. Available: https://linkinghub.elsevier.com/retrieve/pii/S0142061598000131

[120] N. P. Padhy, "Unit commitment-a bibliographical survey," *IEEE Trans. Power Syst.*, vol. 19, no. 2, pp. 1196–1205, May 2004. [Online]. Available: http://ieeexplore.ieee.org/document/1295033/

[121] M. Tahanan, W. van Ackooij, A. Frangioni, and F. Lacalandra, "Large-scale unit commitment under uncertainty," *4OR*, vol. 13, no. 2, pp. 115–171, Jun. 2015. [Online]. Available: http://link.springer.com/10.1007/s10288-014-0279-y

[122] W. van Ackooij, I. Danti Lopez, A. Frangioni, F. Lacalandra, and M. Tahanan, "Large-scale unit commitment under uncertainty: An updated literature survey," *Ann. Oper. Res.*, vol. 271, no. 1, pp. 11–85, Dec. 2018. [Online]. Available: http://link.springer.com/10.1007/s10479-018-3003-z and doi: 10.1007/s10479-018-3003-z.

[123] F. F. Wu, "Power system state estimation: A survey," *Int. J. Elect. Power Energy Syst.*, vol. 12, no. 2, pp. 80–87, 1990. [Online]. Available: https://www.sciencedirect.com/science/article/pii/014206159090003T

[124] A. Monticelli, *State Estimation in Electric Power Systems*. Norwell, MA, USA: Kluwer, 1999.

[125] A. Abur and A. G. Expósito, *Power System State Estimation: Theory and Implementation*. New York, NY, USA: Marcel Dekker, 2004.

[126] V. Kekatos, G. Wang, H. Zhu, and G. B. Giannakis, "PSSE redux: Convex relaxation, decentralized, robust, and dynamic approaches," 2017, *arXiv:1708.03981*. [Online]. Available: http://arxiv.org/abs/1708.03981

[127] S. Abhyankar, G. Geng, M. Anitescu, X. Wang, and V. Dinavahi, "Solution techniques for transient stability-constrained optimal power flow—Part I," *IET Gener., Transmiss. Distrib.*, vol. 11, no. 12, pp. 3177–3185, Aug. 2017. [Online]. Available: https://onlinelibrary.wiley.com/doi/10.1049/iet-gtd.2017.0345

[128] G. Geng, S. Abhyankar, X. Wang, and V. Dinavahi, "Solution techniques for transient stability-constrained optimal power flow—Part II," *IET Gener., Transmiss. Distrib.*, vol. 11, no. 12, pp. 3186–3193, Aug. 2017. [Online]. Available: https://onlinelibrary.wiley.com/doi/10.1049/iet-gtd.2017.0346

[129] B. Stott, O. Alsac, and A. J. Monticelli, "Security analysis and optimization," *Proc. IEEE*, vol. 75, no. 12, pp. 1623–1644, Dec. 1987.

[130] F. Capitanescu, J. L. M. Ramos, P. Panciatici, D. Kirschen, A. M. Marcolini, P. Platbrood, and L. Wehenkel, "State-of-the-art, challenges, and future trends in security constrained optimal power flow," *Electr. Power Syst. Res.*, vol. 81, no. 8, pp. 1731–1741, Aug. 2011. [Online]. Available: https://linkinghub.elsevier.com/retrieve/pii/S0378779611000885, doi: 10.1016/j.epsr.2011.04.003.

[131] B. Stott and O. Alsaç, "Optimal power flow-basic requirements for real-life problems and their solutions (white paper)," in *Proc. 12th Symp. Spec. Electr. Oper. Expansion Planning (SEPOPE)*, Rio de Janeiro, Brazil, 2012, pp. 1866–1876. [Online]. Available: http://www.ieee.hr/_download/repository/Stott-Alsac-OPF-White-Paper.pdf

[132] F. Capitanescu, "Critical review of recent advances and further developments needed in AC optimal power flow," *Electr. Power Syst. Res.*, vol. 136, pp. 57–68, Jul. 2016. [Online]. Available: https://linkinghub.elsevier.com/retrieve/pii/S0378779616300141 and doi: 10.1016/j.epsr.2016.02.008.

[133] M. Vaiman, K. Bell, Y. Chen, B. Chowdhury, I. Dobson, P. Hines, M. Papic, S. Miller, and P. Zhang, "Risk assessment of cascading outages: Methodologies and challenges," *IEEE Trans. Power Syst.*, vol. 27, no. 2, pp. 631–641, May 2012. [Online]. Available: http://ieeexplore.ieee.org/document/6112807

[134] K. W. Hedman, S. S. Oren, and R. P. O'Neill, "A review of transmission switching and network topology optimization," in *Proc. IEEE Power Energy Soc. Gen. Meeting*, Jul. 2011, pp. 1–7. [Online]. Available: https://ieeexplore.ieee.org/document/6039857/

[135] G. A. Pagani and M. Aiello, "The power grid as a complex network: A survey," *Phys. A, Stat. Mech. Appl.*, vol. 392, no. 11, pp. 2688–2700, 2013. [Online]. Available: http://dx.doi.org/10.1016/j.physa.2013.01.023

[136] P. W. Sauer and M. A. Pai, *Power System Dynamics and Stability*, 1st ed. Upper Saddle River, NJ, USA: Prentice-Hall, 1998.

[137] R. D. Zimmerman, C. E. Murillo-Sánchez, and R. J. Thomas, "MATPOWER: Steady-state operations, planning, and analysis tools for power systems research and education," *IEEE Trans. Power Syst.*, vol. 26, no. 1, pp. 12–19, Feb. 2011. [Online]. Available: http://ieeexplore.ieee.org/document/5491276/
[138] C. Coffrin, R. Bent, K. Sundar, Y. Ng, and M. Lubin, "PowerModels. JL: An open-source framework for exploring power flow formulations," in *Proc. Power Syst. Comput. Conf. (PSCC)*, Jun. 2018, pp. 1–8. [Online]. Available: https://ieeexplore.ieee.org/document/8442948/
[139] D. Bienstock and A. Verma, "Strong NP-hardness of AC power flows feasibility," *Oper. Res. Lett.*, vol. 47, no. 6, pp. 494–501, Nov. 2019, doi: 10.1016/j.orl.2019.08.009.
[140] K. Lehmann, A. Grastien, and P. Van Hentenryck, "AC-feasibility on tree networks is NP-hard," *IEEE Trans. Power Syst.*, vol. 31, no. 1, pp. 798–801, Jan. 2016. [Online]. Available: http://ieeexplore.ieee.org/document/7063278/
[141] W. A. Bukhsh, A. Grothey, K. I. M. McKinnon, and P. A. Trodden, "Local solutions of the optimal power flow problem," *IEEE Trans. Power Syst.*, vol. 28, pp. 4780–4788, Nov. 2013. [Online]. Available: http://ieeexplore.ieee.org/document/6581918/
[142] B. Lesieutre and D. Wu, "An efficient method to locate all the load flow solutions–revisited," in *Proc. 53rd Annu. Allerton Conf. Commun., Control, Comput. (Allerton)*, Sep. 2015, pp. 381–388. [Online]. Available: http://ieeexplore.ieee.org/document/7447029/
[143] D. Wu, D. K. Molzahn, B. C. Lesieutre, and K. Dvijotham, "A deterministic method to identify multiple local extrema for the ac optimal power flow problem," *IEEE Trans. Power Syst.*, vol. 33, no. 1, pp. 654–668, Jan. 2018. [Online]. Available: http://ieeexplore.ieee.org/document/7933222/
[144] Y. C. Chen and S. V. Dhople, "Power divider," *IEEE Trans. Power Syst.*, vol. 31, no. 6, pp. 5135–5143, Nov. 2016. [Online]. Available: http://ieeexplore.ieee.org/document/7399775/
[145] Y. C. Chen, A. Al-Digs, and S. V. Dhople, "Mapping nodal power injections to branch flows in connected LTI electrical networks," in *Proc. IEEE Int. Symp. Circuits Syst. (ISCAS)*, May 2016, pp. 2146–2149. [Online]. Available: https://ieeexplore.ieee.org/document/7539005
[146] D. Cheverez-Gonzalez and C. L. DeMarco, "Characterization of feasible LMPs: Inclusion of losses and reactive power," in *Proc. 39th North Amer. Power Symp.*, Sep. 2007, pp. 440–447. [Online]. Available: http://ieeexplore.ieee.org/document/4402347/
[147] J. Lin and D. Cheverez-Gonzalez, "Network-driven dynamic congestion based on mutually orthogonal LMP decomposition," in *Proc. VIII Symp. Bulk Power Syst. Dyn. Control (IREP)*, Aug. 2010, pp. 1–8. [Online]. Available: http://ieeexplore.ieee.org/document/5563300/
[148] M. E. Baran and F. F. Wu, "Optimal capacitor placement on radial distribution systems," *IEEE Trans. Power Del.*, vol. 4, no. 1, pp. 725–734, Jan. 1989. [Online]. Available: http://ieeexplore.ieee.org/document/19265/
[149] M. E. Baran and F. F. Wu, "Optimal sizing of capacitors placed on a radial distribution system," *IEEE Trans. Power Del.*, vol. 4, no. 1, pp. 735–743, Jan. 1989. [Online]. Available: http://ieeexplore.ieee.org/document/19266/
[150] B. Park, J. Netha, M. C. Ferris, and C. L. DeMarco, "Sparse tableau formulation for optimal power flow applications," 2017, *arXiv:1706.01372*. [Online]. Available: http://arxiv.org/abs/1706.01372
[151] R. P. O'Neill, A. Castillo, and M. B. Cain, "The IV formulation and linear approximations of the AC optimal power flow problem (OPF Paper 2)," U.S. Federal Energy Regulatory Commission, Washington, DC, USA, Tech. Rep., Dec. 2012. [Online]. Available: http://www.ferc.gov/industries/electric/indus-act/market-planning/opf-papers/acopf-2-iv-linearization.pdf
[152] D. M. Bromberg, M. Jereminov, X. Li, G. Hug, and L. Pileggi, "An equivalent circuit formulation of the power flow problem with current and voltage state variables," in *Proc. IEEE Eindhoven PowerTech*, Jun. 2015, pp. 1–6. [Online]. Available: http://ieeexplore.ieee.org/document/7232632/
[153] A. Castillo, P. Lipka, J.-P. Watson, S. S. Oren, and R. P. O'Neill, "A successive linear programming approach to solving the IV-ACOPF," *IEEE Trans. Power Syst.*, vol. 31, no. 4, pp. 2752–2763, Jul. 2016. [Online]. Available: http://ieeexplore.ieee.org/document/7299702/
[154] A. Pandey, M. Jereminov, X. Li, G. Hug, and L. Pileggi, "Unified power system analyses and models using equivalent circuit formulation," in *Proc. IEEE Power Energy Soc. Innov. Smart Grid Technol. Conf. (ISGT)*, Sep. 2016, pp. 1–5. [Online]. Available: http://ieeexplore.ieee.org/document/7781182/
[155] M. Jereminov, D. M. Bromberg, A. Pandey, X. Li, G. Hug, and L. Pileggi, "An equivalent circuit formulation for three-phase power flow analysis of distribution systems," in *Proc. IEEE/PES Transmiss. Distrib. Conf. Expo. (T&D)*, May 2016, pp. 1–5. [Online]. Available: http://ieeexplore.ieee.org/document/7519894/
[156] M. Jereminov, D. M. Bromberg, X. Li, G. Hug, and L. Pileggi, "Improving robustness and modeling generality for power flow analysis," in *Proc. IEEE/PES Transmiss. Distrib. Conf. Expo. (T&D)*, May 2016, pp. 1–5. [Online]. Available: http://ieeexplore.ieee.org/document/7520067/
[157] S. Misra, L. Roald, M. Vuffray, and M. Chertkov, "Fast and robust determination of power system emergency control actions," 2017, *arXiv:1707.07105*. [Online]. Available: http://arxiv.org/abs/1707.07105
[158] A. Trias, "HELM: The holomorphic embedding load-flow method. Foundations and implementations," *Found. Trends, Electr. Energy Syst.*, vol. 3, nos. 3–4, pp. 140–370, 2018. [Online]. Available: http://www.nowpublishers.com/article/Details/EES-015
[159] T. Chen and D. Mehta, "On the network topology dependent solution count of the algebraic load flow equations," *IEEE Trans. Power Syst.*, vol. 33, no. 2, pp. 1451–1460, Mar. 2018.
[160] Y. V. Makarov, D. J. Hill, and I. A. Hiskens, "Properties of quadratic equations and their application to power system analysis," *Int. J. Electr. Power Energy Syst.*, vol. 22, no. 5, pp. 313–323, Jun. 2000.
[161] C. Coffrin, H. L. Hijazi, and P. Van Hentenryck, "DistFlow extensions for AC transmission systems," pp. 1–20, May 2018, *arXiv:1506.04773v2* . [Online]. Available: https://arxiv.org/abs/1506.04773v2
[162] J. Baillieul and C. Byrnes, "Geometric critical point analysis of lossless power system models," *IEEE Trans. Circuits Syst.*, vol. 29, no. 11, pp. 724–737, Nov. 1982.
[163] D. K. Molzahn, D. Mehta, and M. Niemerg, "Toward topologically based upper bounds on the number of power flow solutions," in *Proc. Amer. Control Conf. (ACC)*, Jul. 2016, pp. 5927–5932. [Online]. Available: http://ieeexplore.ieee.org/document/7526599/
[164] O. Coss, J. D. Hauenstein, H. Hong, and D. K. Molzahn, "Locating and counting equilibria of the Kuramoto model with rank-one coupling," *SIAM J. Appl. Algebra Geometry*, vol. 2, no. 1, pp. 45–71, 2018.
[165] W. Ma and J. S. Thorp, "An efficient algorithm to locate all the load flow solutions," *IEEE Trans. Power Syst.*, vol. 8, no. 3, pp. 1077–1083, Aug. 1993.
[166] D. Mehta, H. D. Nguyen, and K. Turitsyn, "Numerical polynomial homotopy continuation method to locate all the power flow solutions," *IET Gener., Transmiss. Distrib.*, vol. 10, no. 12, pp. 2972–2980, 2016. [Online]. Available: https://onlinelibrary.wiley.com/doi/10.1049/iet-gtd.2015.1546
[167] A. Zachariah, Z. Charles, N. Boston, and B. Lesieutre, "Distributions of the number of solutions to the network power flow equations," in *Proc. IEEE Int. Symp. Circuits Syst. (ISCAS)*, May 2018, pp. 1–5. [Online]. Available: https://ieeexplore.ieee.org/document/8351675/
[168] K. Balamurugan and D. Srinivasan, "Review of power flow studies on distribution network with distributed generation," in *Proc. IEEE 9th Int. Conf. Power Electron. Drive Syst.*, Dec. 2011, pp. 411–417. [Online]. Available: http://ieeexplore.ieee.org/document/6147281/
[169] P. A. N. Garcia, J. L. R. Pereira, S. Carneiro, V. M. da Costa, and N. Martins, "Three-phase power flow calculations using the current injection method," *IEEE Trans. Power Syst.*, vol. 15, no. 2, pp. 508–514, May 2000. [Online]. Available: http://ieeexplore.ieee.org/document/867133/
[170] J. E. V. Ness, "Iteration methods for digital load flow studies," *Trans. Amer. Inst. Electr. Engineers. Part III, Power App. Syst.*, vol. 78, no. 3, pp. 583–586, Apr. 1959. [Online]. Available: http://ieeexplore.ieee.org/document/4500383/
[171] N. Sato and W. F. Tinney, "Techniques for exploiting the sparsity or the network admittance matrix," *IEEE Trans. Power App. Syst.*, vol. 82, no. 69, pp. 944–950, Dec. 1963. [Online]. Available: http://ieeexplore.ieee.org/document/4072891/
[172] W. F. Tinney and C. E. Hart, "Power flow solution by Newton's method," *IEEE Trans. Power App. Syst.*, vol. PAS-86, no. 11, pp. 1449–1460, Nov. 1967. [Online]. Available: http://ieeexplore.ieee.org/document/4073219/
[173] J. S. Thorp and S. A. Naqavi, "Load flow fractals," in *Proc. 28th IEEE Conf. Decis. Control*, Dec. 1989, pp. 1822–1827. [Online]. Available: http://ieeexplore.ieee.org/document/70472/
[174] J. S. Thorp, S. A. Naqavi, and H.-D. Chiang, "More load flow fractals," in *Proc. 29th IEEE Conf. Decis. Control*, 1990, pp. 3028–3030. [Online]. Available: http://ieeexplore.ieee.org/document/203339/

[175] J.-J. Deng and H.-D. Chiang, "Convergence region of Newton iterative power flow method: Numerical studies," *J. Appl. Math.*, vol. 2013, Nov. 2013, Art. no. 509496. [Online]. Available: http://www.hindawi.com/journals/jam/2013/509496/

[176] J. E. Tate and T. J. Overbye, "A comparison of the optimal multiplier in polar and rectangular coordinates," *IEEE Trans. Power Syst.*, vol. 20, no. 4, pp. 1667–1674, Nov. 2005.

[177] P. Xiao, D. C. Yu, and W. Yan, "A unified three-phase transformer model for distribution load flow calculations," *IEEE Trans. Power Syst.*, vol. 21, no. 1, pp. 153–159, Feb. 2006.

[178] V. H. Quintana and N. Müller, "Studies of load flow methods in polar and rectangular coordinates," *Electric Power Syst. Res.*, vol. 20, no. 3, pp. 225–235, Mar. 1991. [Online]. Available: https://linkinghub.elsevier.com/retrieve/pii/037877969190067W

[179] B. Stott and O. Alsac, "Fast decoupled load flow," *IEEE Trans. Power App. Syst.*, vol. PAS-93, no. 3, pp. 859–869, May 1974. [Online]. Available: http://ieeexplore.ieee.org/document/4075431/

[180] F. F. Wu, "Theoretical study of the convergence of the fast decoupled load flow," *IEEE Trans. Power App. Syst.*, vol. 96, no. 1, pp. 268–275, Jan. 1977. [Online]. Available: http://ieeexplore.ieee.org/document/1601936/

[181] J. Nanda, D. P. Kothari, and S. C. Srivastava, "Some important observations on fast decoupled load flow algorithm," *Proc. IEEE*, vol. 75, no. 5, pp. 732–733, May 1987. [Online]. Available: http://ieeexplore.ieee.org/document/1458056/

[182] A. Trias, "The holomorphic embedding load flow method," in *Proc. IEEE Power Energy Soc. Gen. Meeting*, Jul. 2012, pp. 1–8. [Online]. Available: http://ieeexplore.ieee.org/document/6344759/

[183] D. Shirmohammadi, H. W. Hong, A. Semlyen, and G. X. Luo, "A compensation-based power flow method for weakly meshed distribution and transmission networks," *IEEE Trans. Power Syst.*, vol. 3, no. 2, pp. 753–762, May 1988. [Online]. Available: http://ieeexplore.ieee.org/document/192932/

[184] C. S. Cheng and D. Shirmohammadi, "A three-phase power flow method for real-time distribution system analysis," *IEEE Trans. Power Syst.*, vol. 10, no. 2, pp. 671–679, May 1995. [Online]. Available: http://ieeexplore.ieee.org/document/387902/

[185] E. Bompard, E. Carpaneto, G. Chicco, and R. Napoli, "Convergence of the backward/forward sweep method for the load-flow analysis of radial distribution systems," *Int. J. Electr. Power Energy Syst.*, vol. 22, no. 7, pp. 521–530, Oct. 2000. [Online]. Available: https://linkinghub.elsevier.com/retrieve/pii/S0142061500000090

[186] C. González-Morán, P. Arboleya, and B. Mohamed, "Matrix backward forward sweep for unbalanced power flow in $\alpha\beta 0$ frame," *Electr. Power Syst. Res.*, vol. 148, pp. 273–281, Jul. 2017. [Online]. Available: https://linkinghub.elsevier.com/retrieve/pii/S0378779617301268, doi: 10.1016/j.epsr.2017.03.026.

[187] K. Mahmoud and N. Yorino, "Robust quadratic-based BFS power flow method for multi-phase distribution systems," *IET Gener., Transmiss. Distrib.*, vol. 10, no. 9, pp. 2240–2250, 2016. [Online]. Available: https://onlinelibrary.wiley.com/doi/10.1049/iet-gtd.2015.1518

[188] F. Hameed, M. Al Hosani, and H. H. Zeineldin, "A modified backward/forward sweep load flow method for islanded radial microgrids," *IEEE Trans. Smart Grid*, vol. 10, no. 1, pp. 910–918, Jan. 2019. [Online]. Available: https://ieeexplore.ieee.org/document/8047263/

[189] P. Fortenbacher, M. Zellner, and G. Andersson, "Optimal sizing and placement of distributed storage in low voltage networks," in *Proc. Power Syst. Comput. Conf. (PSCC)*, Jun. 2016, pp. 1–7. [Online]. Available: http://ieeexplore.ieee.org/document/7540850/

[190] P. M. De Oliveira-De Jesus, "A simplified formulation for the Backward/Forward sweep power flow method," 2020, *arXiv:2010.06389*. [Online]. Available: http://arxiv.org/abs/2010.06389

[191] C. E. Lemke, "Pathways to solutions, fixed points, and equilibria (C. B. Garcia and W. J. Zangwill)," *SIAM Rev.*, vol. 26, no. 3, pp. 445–446, Jul. 1984. [Online]. Available: http://epubs.siam.org/doi/10.1137/1026093

[192] G. B. Price, "A generalized circle diagram approach for global analysis of transmission system performance," *IEEE Trans. Power App. Syst.*, vol. PAS-103, no. 10, pp. 2881–2890, Oct. 1984. [Online]. Available: http://ieeexplore.ieee.org/document/4112389/

[193] V. Ajjarapu and C. Christy, "The continuation power flow: A tool for steady state voltage stability analysis," *IEEE Trans. Power Syst.*, vol. 7, no. 1, pp. 416–423, Feb. 1992. [Online]. Available: http://ieeexplore.ieee.org/document/141737/

[194] C. A. Canizares and F. L. Alvarado, "Point of collapse and continuation methods for large AC/DC systems," *IEEE Trans. Power Syst.*, vol. 8, no. 1, pp. 1–8, Feb. 1993. [Online]. Available: http://ieeexplore.ieee.org/document/221241/

[195] I. A. Hiskens and R. J. Davy, "Exploring the power flow solution space boundary," *IEEE Trans. Power Syst.*, vol. 16, no. 3, pp. 389–395, Aug. 2001. [Online]. Available: http://ieeexplore.ieee.org/document/932273/

[196] H. Dommel, W. Tinney, and W. Powell, "Further developments in Newton's method for power system applications," in *Proc. IEEE Winter Power Meeting*, Jan. 1970, pp. 1–13.

[197] W. Tinney, "A presentation to the workshop in engineering mathematics and computer sciences," in *Proc. Workshop Adv. Math. Comput. Sci. Power Syst. Anal.*, 1991, p. 1.

[198] V. M. D. Costa, N. Martins, and J. L. R. Pereira, "Developments in the Newton Raphson power flow formulation based on current injections," *IEEE Trans. Power Syst.*, vol. 14, no. 4, pp. 1320–1326, Nov. 1999. [Online]. Available: http://ieeexplore.ieee.org/document/801891/

[199] K. Sunderland, M. Coppo, M. Conlon, and R. Turri, "A correction current injection method for power flow analysis of unbalanced multiple-grounded 4-wire distribution networks," *Electr. Power Syst. Res.*, vol. 132, pp. 30–38, Mar. 2016. [Online]. Available: https://linkinghub.elsevier.com/retrieve/pii/S0378779615003235, doi: 10.1016/j.epsr.2015.10.027.

[200] H. Stahl, "On the convergence of generalized Padé approximants," *Construct. Approximation*, vol. 5, no. 1, pp. 221–240, 1989. [Online]. Available: http://link.springer.com/10.1007/BF01889608

[201] H. Stahl, "The convergence of Padé approximants to functions with branch points," *J. Approximation Theory*, vol. 91, no. 2, pp. 139–204, 1997. [Online]. Available: https://linkinghub.elsevier.com/retrieve/pii/S0021904597931415

[202] M. K. Subramanian, Y. Feng, and D. Tylavsky, "PV bus modeling in a holomorphically embedded power-flow formulation," in *Proc. North Amer. Power Symp. (NAPS)*, Sep. 2013, pp. 1–6. [Online]. Available: http://ieeexplore.ieee.org/document/6666940/

[203] L. Sun, Y. Ju, L. Yang, S. Ge, Q. Fang, and J. Wang, "Holomorphic embedding load flow modeling of the three-phase active distribution network," in *Proc. Int. Conf. Power Syst. Technol. (POWERCON)*, Nov. 2018, pp. 488–495. [Online]. Available: https://ieeexplore.ieee.org/document/8602144/

[204] S. Rao, Y. Feng, D. J. Tylavsky, and M. K. Subramanian, "The holomorphic embedding method applied to the power-flow problem," *IEEE Trans. Power Syst.*, vol. 31, no. 5, pp. 3816–3828, Sep. 2016. [Online]. Available: http://ieeexplore.ieee.org/document/7352383/

[205] H.-D. Chiang, A. J. Flueck, K. S. Shah, and N. Balu, "CPFLOW: A practical tool for tracing power system steady-state stationary behavior due to load and generation variations," *IEEE Trans. Power Syst.*, vol. 10, no. 2, pp. 623–634, May 1995. [Online]. Available: http://ieeexplore.ieee.org/document/387897/

[206] A. Trias and J. L. Marín, "The holomorphic embedding loadflow method for dc power systems and nonlinear DC circuits," *IEEE Trans. Circuits Syst. I, Reg. Papers*, vol. 63, no. 2, pp. 322–333, Feb. 2016. [Online]. Available: http://ieeexplore.ieee.org/document/7393554/

[207] H.-D. Chiang, T. Wang, and H. Sheng, "A novel fast and flexible holomorphic embedding power flow method," *IEEE Trans. Power Syst.*, vol. 33, no. 3, pp. 2551–2562, May 2018. [Online]. Available: https://ieeexplore.ieee.org/document/8031027/

[208] S. Sadeghi Baghsorkhi and S. Pavlovich Suetin, "Embedding AC power flow in the complex plane Part I: Modelling and mathematical foundation," 2016, *arXiv:1604.03425*. [Online]. Available: http://arxiv.org/abs/1604.03425

[209] S. S. Baghsorkhi and S. P. Suetin, "Embedding AC power flow in the complex plane Part II: A reliable framework for voltage collapse analysis," 2016, *arXiv:1609.01211*. [Online]. Available: http://arxiv.org/abs/1609.01211

[210] M. Basiri-Kejani and E. Gholipour, "Holomorphic embedding load-flow modeling of thyristor-based FACTS controllers," *IEEE Trans. Power Syst.*, vol. 32, no. 6, pp. 4871–4879, Nov. 2017. [Online]. Available: http://ieeexplore.ieee.org/document/7878687/

[211] D. K. Asl, M. Mohammadi, and A. R. Seifi, "Holomorphic embedding load flow for unbalanced radial distribution networks with DFIG and tap-changer modelling," *IET Gener., Transmiss. Distrib.*, vol. 13, no. 19, pp. 4263–4273, Oct. 2019. [Online]. Available: https://onlinelibrary.wiley.com/doi/10.1049/iet-gtd.2018.6239

[212] S. D. Rao, D. J. Tylavsky, and Y. Feng, "Estimating the saddle-node bifurcation point of static power systems using the holomorphic embedding method," *Int. J. Elect. Power Energy Syst.*, vol. 84, pp. 1–12, Jan. 2017. [Online]. Available: http://dx.doi.org/10.1016/j.ijepes.2016.04.045

[213] C. Liu, B. Wang, F. Hu, K. Sun, and C. L. Bak, "Online voltage stability assessment for load areas based on the holomorphic embedding method," *IEEE Trans. Power Syst.*, vol. 33, no. 4, pp. 3720–3734, Jul. 2018. [Online]. Available: https://ieeexplore.ieee.org/document/8100989/

[214] S. Rao and D. Tylavsky, "Nonlinear network reduction for distribution networks using the holomorphic embedding method," in *Proc. North Amer. Power Symp. (NAPS)*, Sep. 2016, pp. 1–6. [Online]. Available: http://ieeexplore.ieee.org/document/7747978/

[215] Y. Zhu and D. Tylavsky, "Bivariate holomorphic embedding applied to the power flow problem," in *Proc. North Amer. Power Symp. (NAPS)*, Sep. 2016, pp. 1–6. [Online]. Available: http://ieeexplore.ieee.org/document/7747975/

[216] C. Liu, B. Wang, X. Xu, K. Sun, D. Shi, and B. C. L. Bak, "A multi-dimensional holomorphic embedding method to solve ac power flows," *IEEE Access*, vol. 5, pp. 25270–25285, 2017.

[217] U. Sur, A. Biswas, J. N. Bera, and G. Sarkar, "A modified holomorphic embedding method based hybrid AC-DC microgrid load flow," *Electr. Power Syst. Res.*, vol. 182, May 2020, Art. no. 106267. [Online]. Available: https://linkinghub.elsevier.com/retrieve/pii/S0378779620300742 and doi: 10.1016/j.epsr.2020.106267.

[218] R. Dugan, "Open distribution simulations system workshop: Using open dss for smart distribution simulations," in *Proc. PQ Smart Distrib. Conf. Exhib. (EPRI)*, 2010, pp. 14–17.

[219] D. P. Chassin, K. Schneider, and C. Gerkensmeyer, "GridLAB-D: An open-source power systems modeling and simulation environment," in *Proc. IEEE/PES Transmiss. Distrib. Conf. Expo.*, Apr. 2008, pp. 1–5. [Online]. Available: http://ieeexplore.ieee.org/document/4517260/

[220] D. P. Chassin, J. C. Fuller, and N. Djilali, "GridLAB-D: An agent-based simulation framework for smart grids," *J. Appl. Math.*, vol. 2014, Jun. 2014, Art. no. 492320. [Online]. Available: http://www.hindawi.com/journals/jam/2014/492320/

[221] T. Morstyn, K. A. Collett, A. Vijay, M. Deakin, S. Wheeler, S. M. Bhagavathy, F. Fele, and M. D. McCulloch, "OPEN: An open-source platform for developing smart local energy system applications," *Appl. Energy*, vol. 275, Oct. 2020, Art. no. 115397, doi: 10.1016/j.apenergy.2020.115397.

[222] L. Thurner, A. Scheidler, F. Schafer, J.-H. Menke, J. Dollichon, F. Meier, S. Meinecke, and M. Braun, "Pandapower—An open-source python tool for convenient modeling, analysis, and optimization of electric power systems," *IEEE Trans. Power Syst.*, vol. 33, no. 6, pp. 6510–6521, Nov. 2018. [Online]. Available: https://ieeexplore.ieee.org/document/8344496/

[223] D. W. Gao, E. Muljadi, T. Tian, and M. Miller, "Software comparison for renewable energy deployment in a distribution network," NREL, Golden, CO, USA, Tech. Rep. NREL/TP-5D00-64228, 2017. [Online]. Available: https://www.nrel.gov/docs/fy17osti/64228.pdf

[224] R. M. Czekster, "Tools for modelling and simulating the smart grid," 2020, *arXiv:2011.07968*. [Online]. Available: http://arxiv.org/abs/2011.07968

[225] University of Melbourne. (2021). *Advanced Planning of PV-Rich Distribution Networks*. [Online]. Available: https://arena.gov.au/projects/advanced-planning-of-pv-rich-distribution-networks-study/

[226] DIgSILENT GmbH. (2021). *PowerFactory*. [Online]. Available: https://www.digsilent.de/en/powerfactory.html

[227] F. M. Gonzalez-Longatt and J. L. Rueda, Eds., *PowerFactory Applications for Power System Analysis* (Power Systems). Cham, Switzerland: Springer, 2014. [Online]. Available: http://link.springer.com/10.1007/978-3-319-12958-7

[228] DIgSILENT GmbH. (2021). *PowerFactory: Data converter*. [Online]. Available: https://www.digsilent.de/en/data-converter.html

[229] D. GmbH, "PowerFactory 2021 Brochure," DIgSILENT GmbH, Gomaringen, Germany, Tech. Rep., 2021. [Online]. Available: https://www.digsilent.de/en/downloads.html?downloadkey=2A6AA670118821591D9A0869087E8A9A

[230] DIgSILENT GmbH. (2021). *PowerFactory: Power Equipment Models*.[Online]. Available: https://www.digsilent.de/en/power-equipment-models.html

[231] DIgSILENT GmbH. (2021). *PowerFactory: Load Flow Analysis*. [Online]. Available: https://www.digsilent.de/en/load-flow-analysis.html

[232] K. Purchala, L. Meeus, D. Van Dommelen, and R. Belmans, "Usefulness of DC power flow for active power flow analysis," in *Proc. IEEE Power Eng. Soc. Gen. Meeting*, vol. 1, Jun. 2005, pp. 2457–2462. [Online]. Available: http://ieeexplore.ieee.org/document/1489581/

[233] D. Van Hertem, "Usefulness of DC power flow for active power flow analysis with flow controlling devices," in *Proc. 8th IEE Int. Conf. AC DC Power Transmiss. (ACDC)*, 2006, pp. 58–62. https://digital-library.theiet.org/content/conferences/10.1049/cp_20060013

[234] DDIgSILENT GmbH. (2021). *PowerFactory: Distribution Network Tools*. [Online]. Available: https://www.digsilent.de/en/distribution-network-tools.html

[235] Siemens AG. (2021). *PSS SINCAL*. [Online]. Available: https://new.siemens.com/global/en/products/energy/energy-automation-and-smart-grid/pss-software/pss-sincal.html

[236] Siemens AG, "PSS SINCAL: All-in-one simulation software for the analysis and planning of power networks," Siemens AG, Erlangen, Germany, Tech. Rep., 2018. [Online]. Available: https://assets.new.siemens.com/siemens/assets/api/uuid:31ece3a2-e9cc-4528-b9f9-6bf61b613de2/ref-no-69-ps-c-pss-sincal-brochure-hires-intl-sept2018.pdf

[237] Siemens AG. (2021). *PSS SINCAL Platform Electricity Modules*. [Online]. Available: https://new.siemens.com/global/en/products/energy/energy-automation-and-smart-grid/pss-software/pss-sincal/pss-sincal-electricity.html

[238] EATON. (2020). *CYMDIST*. [Online]. Available: https://www.cyme.com/software/cymdist/

[239] EATON. (2020). *Low-Voltage Secondary Distribution Modeling and Analysis*. [Online]. Available: https://www.cyme.com/software/cymelvdn/

[240] EATON. (2020). *Enhanced Substation Modeling*. [Online]. Available: https://www.cyme.com/software/cymdistsub/

[241] Y. Tang, X. Mao, and R. Ayyanar, "Distribution system modeling using CYMDIST for study of high penetration of distributed solar photovoltaics," in *Proc. North Amer. Power Symp. (NAPS)*, Sep. 2012, pp. 1–6.

[242] EATON and CYME International T&D, "Reliable modeling, analytic and planning tools to improve the performance of the distribution system," EATON, Dublin, Ireland, Tech. Rep. BR917045EN, 2018. [Online]. Available: https://cyme.com/software/cymdist/BR917045EN-Distribution.pdf

[243] D. Rizy and R. Staunton, "Evaluation of distribution analysis software for DER applications," Oak Ridge Nat. Lab., Oak Ridge, TN, USA, Tech. Rep. ORNL/TM-2001/215, 2002.

[244] Source Forge. (2021). *OpenDSS*. [Online]. Available: https://sourceforge.net/projects/electricdss/

[245] R. C. Dugan and D. Montenegro, "Reference guide: The open distribution system simulator (OpenDSS)," Electr. Power Res. Inst., CA, USA, Tech. Rep., 2020, pp. 1–177. [Online]. Available: http://svn.code.sf.net/p/electricdss/code/trunk/Distrib/Doc/OpenDSSManual.pdf

[246] J. Smith, "Modeling high-penetration PV for distribution interconnection studies," Electric Power Research Institute (EPRI), Washington, DC, USA, Tech. Rep. 3002002271, 2013.

[247] P. Radatz, C. Rocha, W. Sunderman, M. Rylander, and J. Peppanen, "OpenDSS PV system and in V control element models," Electr. Power Res. Inst., CA, USA, Tech. Rep., 2020, pp. 1–30. [Online]. Available: https://sourceforge.net/projects/electricdss/files/

[248] Electric Power Research Institute (EPRI). (2013). *OpenDSS-G*. [Online]. Available: https://sourceforge.net/projects/dssimpc/

[249] Electric Power Research Institute (EPRI). (2020). *OpenDSS-G*. [Online]. Available: https://www.youtube.com/channel/UCGe58SDH3Iq-EGvnxEOuWaQ

[250] Battelle Memorial Institute. (2021). *Power Flow User Guide*. [Online]. Available: http://gridlab-d.shoutwiki.com/wiki/Power_Flow_User_Guide##Volt-VAr_Control

[251] Battelle Memorial Institute. (2021). *Powerflow*. [Online]. Available: http://gridlab-d.shoutwiki.com/wiki/Powerflow

[252] J. Grainger and W. Stevenson, *Power System Analysis*. New York, NY, USA: McGraw-Hill, 1994.

[253] Battelle Memorial Institute. (2021). *Solar*. [Online]. Available: http://gridlab-d.shoutwiki.com/wiki/Solar

[254] Battelle Memorial Institute. (2021). *Inverter DYN*. [Online]. Available: http://gridlab-d.shoutwiki.com/wiki/Inverter_dyn

[255] V. Borozan, M. E. Baran, and D. Novosel, "Integrated volt/VAr control in distribution systems," in *Proc. IEEE Power Eng. Soc. Winter Meeting. Conf.*, Jan./Feb. 2001, pp. 1485–1490. [Online]. Available: http://ieeexplore.ieee.org/document/917328/

[256] M. A. Al Faruque and F. Ahourai, "GridMat: MATLAB toolbox for GridLAB-D to analyze grid impact and validate residential microgrid level energy management algorithms," in *Proc. ISGT*, Feb. 2014, pp. 1–5. [Online]. Available: http://ieeexplore.ieee.org/document/6816479/

[257] Energy and Power Group-University of Oxford. (2020). *OPEN*. [Online]. Available: https://github.com/EPGOxford/OPEN

[258] A. Bernstein, C. Wang, E. Dall'Anese, J.-Y. Le Boudec, and C. Zhao, "Load flow in multiphase distribution networks: Existence, uniqueness, non-singularity and linear models," *IEEE Trans. Power Syst.*, vol. 33, no. 6, pp. 5832–5843, Nov. 2018. [Online]. Available: https://ieeexplore.ieee.org/document/8332975/

[259] M. Bazrafshan and N. Gatsis, "Comprehensive modeling of three-phase distribution systems via the bus admittance matrix," *IEEE Trans. Power Syst.*, vol. 33, no. 2, pp. 2015–2029, Mar. 2018. [Online]. Available: http://ieeexplore.ieee.org/document/7995066/

[260] D. Montenegro, M. Hernandez, and G. A. Ramos, "Real time OpenDSS framework for distribution systems simulation and analysis," in *Proc. 6th IEEE/PES Transmiss. Distribution: Latin Amer. Conf. Expo. (T&D-LA)*, Sep. 2012, pp. 1–5. [Online]. Available: http://ieeexplore.ieee.org/document/6319069/

[261] J. Travis and J. Kring, *LabVIEW for Everyone: Graphical Programming Made Easy and Fun*, 3rd ed. Upper Saddle River, NJ, USA: Prentice-Hall, 2006.

[262] X. Sun, Y. Chen, J. Liu, and S. Huang, "A co-simulation platform for smart grid considering interaction between information and power systems," in *Proc. ISGT*, Feb. 2014, pp. 1–6. [Online]. Available: http://ieeexplore.ieee.org/document/6816423/

[263] OPNET. (2021). *OPNET Modeler*. https://support.riverbed.com/content/support/software/opnet-model/modeler.html

[264] E. de Souza, O. Ardakanian, and I. Nikolaidis, "A co-simulation platform for evaluating cyber security and control applications in the smart grid," in *Proc. IEEE Int. Conf. Commun. (ICC)*, Jun. 2020, pp. 1–7. [Online]. Available: https://ieeexplore.ieee.org/document/9149212/

[265] G. F. Riley and T. R. Henderson, "The *ns*-3 network simulator," in *Modeling and Tools for Network Simulation*, K. Wehrle, M. Günes, and J. Gross, Eds. Berlin, Germany: Springer, 2010, pp. 15–34, doi: 10.1007/978-3-642-12331-3_2.

[266] Nsnam. (2021). *NS-3: Network Simulator*. [Online]. Available: https://www.nsnam.org/

[267] S. Schutte, S. Scherfke, and M. Troschel, "Mosaik: A framework for modular simulation of active components in smart grids," in *Proc. IEEE 1st Int. Workshop Smart Grid Modeling Simulation (SGMS)*, Oct. 2011, pp. 55–60. [Online]. Available: http://ieeexplore.ieee.org/document/6089027/

[268] D. Bytschkow, M. Zellner, and M. Duchon, "Combining SCADA, CIM, GridLab-D and AKKA for smart grid co-simulation," in *Proc. IEEE Power Energy Soc. Innov. Smart Grid Technol. Conf. (ISGT)*, Feb. 2015, pp. 1–5. [Online]. Available: http://ieeexplore.ieee.org/document/7131872/

[269] Lightbend. (2021). *AKKA*. [Online]. Available: https://akka.io/

[270] T. M. Hansen, B. Palmintier, S. Suryanarayanan, A. A. Maciejewski, and H. J. Siegel, "Bus.Py: A GridLAB-D communication interface for smart distribution grid simulations," in *Proc. IEEE Power Energy Soc. Gen. Meeting*, Jul. 2015, pp. 1–5. [Online]. Available: http://ieeexplore.ieee.org/document/7286003/

[271] S. Ciraci, J. Daily, J. Fuller, A. Fisher, L. Marinovici, and K. Agarwal, "FNCS: A framework for power system and communication networks co-simulation," in *Proc. Symp. Theory Modeling Simulation (DEVS Integrative)*, 2014, pp. 1–8.

[272] R. Huang, R. Fan, J. Daily, A. Fisher, and J. Fuller, "Open-source framework for power system transmission and distribution dynamics co-simulation," *IET Gener., Transmiss. Distrib.*, vol. 11, no. 12, pp. 3152–3162, Sep. 2017. [Online]. Available: https://onlinelibrary.wiley.com/doi/10.1049/iet-gtd.2016.1556

[273] B. Palmintier, D. Krishnamurthy, P. Top, S. Smith, J. Daily, and J. Fuller, "Design of the HELICS high-performance transmission-distribution-communication-market co-simulation framework," in *Proc. Workshop Modeling Simulation Cyber-Phys. Energy Syst. (MSCPES)*, Apr. 2017, pp. 1–6. [Online]. Available: https://ieeexplore.ieee.org/document/8064542/

[274] Q. Huang, T. E. McDermott, Y. Tang, A. Makhmalbaf, D. J. Hammerstrom, A. R. Fisher, L. D. Marinovici, and T. Hardy, "Simulation-based valuation of transactive energy systems," *IEEE Trans. Power Syst.*, vol. 34, no. 5, pp. 4138–4147, Sep. 2019. [Online]. Available: https://ieeexplore.ieee.org/document/8360969/

[275] Battelle Memorial Institute. (2020). *Transactive Energy Simulation Platform (TESP)*. [Online]. Available: https://github.com/pnnl/tesp/

[276] D. B. Crawley, L. K. Lawrie, F. C. Winkelmann, W. Buhl, Y. Huang, C. O. Pedersen, R. K. Strand, R. J. Liesen, D. E. Fisher, M. J. Witte, and J. Glazer, "Energyplus: Creating a new-generation building energy simulation program," *Energy Buildings*, vol. 33, no. 4, pp. 319–331, 2001. [Online]. Available: https://linkinghub.elsevier.com/retrieve/pii/S0378778800001146

[277] F. Zhao, J. Si, and J. Wang, "Research on optimal schedule strategy for active distribution network using particle swarm optimization combined with bacterial foraging algorithm," *Int. J. Electr. Power Energy Syst.*, vol. 78, pp. 637–646, Jun. 2016, doi: 10.1016/j.ijepes.2015.11.112.

[278] J. L. Carpentier, "Contribution a l'étude du dispatching économique," *Bull. de la Societe Francoise des Electriciens*, vol. 8, no. 3, pp. 431–447, 1962.

[279] S. Claeys, M. Vanin, F. Geth, and G. Deconinck, "Applications of optimization models for electricity distribution networks," *WIREs Energy Environ.*, vol. 10, no. 5, pp. 1–35, May 2021. [Online]. Available: https://onlinelibrary.wiley.com/doi/10.1002/wene.401

[280] J. Y. Jackson, "Interpretation and use of generator reactive capability diagrams," *IEEE Trans. Ind. General Appl.*, vols. IGA–7, no. 6, pp. 729–732, Nov. 1971. [Online]. Available: http://ieeexplore.ieee.org/document/4181375/

[281] D. Kosterev, A. Meklin, J. Undrill, B. Lesieutre, W. Price, D. Chassin, R. Bravo, and S. Yang, "Load modeling in power system studies: WECC progress update," in *Proc. IEEE Power Energy Soc. Gen. Meeting Convers. Del. Electr. Energy 21st Century*, Jul. 2008, pp. 1–8. [Online]. Available: http://ieeexplore.ieee.org/document/4596557/

[282] R. D. Zimmerman, "AC power flows, generalized OPF costs and their derivatives using complex matrix notation," Power Syst. Eng. Res. Center (PSERC), New York, NY, USA, Tech. Rep., 2019. [Online]. Available: http://www.pserc.cornell.edu/matpower/TN2-OPF-Derivatives.pdf

[283] R. Madani, S. Sojoudi, and J. Lavaei, "Convex relaxation for optimal power flow problem: Mesh networks," *IEEE Trans. Power Syst.*, vol. 30, no. 1, pp. 199–211, Jan. 2015. [Online]. Available: http://ieeexplore.ieee.org/document/6822653/

[284] B. Park, L. Tang, M. C. Ferris, and C. L. DeMarco, "Examination of three different ACOPF formulations with generator capability curves," *IEEE Trans. Power Syst.*, vol. 32, no. 4, pp. 2913–2923, Jul. 2017. [Online]. Available: http://ieeexplore.ieee.org/document/7737062/

[285] A. M. Sasson and H. M. Merrill, "Some applications of optimization techniques to power systems problems," *Proc. IEEE*, vol. 62, no. 7, pp. 959–972, Jul. 1974. [Online]. Available: https://ieeexplore.ieee.org/document/1451478

[286] A. J. Wood, B. F. Wollenberg, and G. B. Sheblé, *Power Generation, Operation, and Control*. Hoboken, NJ, USA: Wiley, 2013.

[287] J. A. Momoh, *Electric Power System Applications of Optimization*. Boca Raton, FL, USA: CRC Press, 2017.

[288] L. R. Araujo, D. R. R. Penido, S. Carneiro, and J. L. R. Pereira, "A three-phase optimal power-flow algorithm to mitigate voltage unbalance," *IEEE Trans. Power Del.*, vol. 28, no. 4, pp. 2394–2402, Oct. 2013. [Online]. Available: http://ieeexplore.ieee.org/document/6596521/

[289] M. Vanin, H. Ergun, R. D'hulst, and D. Van Hertem, "Comparison of linear and conic power flow formulations for unbalanced low voltage network optimization," *Electr. Power Syst. Res.*, vol. 189, Dec. 2020, Art. no. 106699, doi: 10.1016/j.epsr.2020.106699.

[290] P. Richardson, D. Flynn, and A. Keane, "Optimal charging of electric vehicles in low-voltage distribution systems," *IEEE Trans. Power Syst.*, vol. 27, no. 1, pp. 268–279, Feb. 2012. [Online]. Available: http://ieeexplore.ieee.org/document/5929499/

[291] L. Bai, J. Wang, C. Wang, C. Chen, and F. Li, "Distribution locational marginal pricing (DLMP) for congestion management and voltage support," *IEEE Trans. Power Syst.*, vol. 33, no. 4, pp. 4061–4073, Jul. 2017.

[292] Y. Liu, J. Li, and L. Wu, "Distribution system restructuring: Distribution LMP via unbalanced ACOPF," *IEEE Trans. Smart Grid*, vol. 9, no. 5, pp. 4038–4048, Sep. 2018. [Online]. Available: https://ieeexplore.ieee.org/document/7805301/

[293] B. C. Lesieutre and I. A. Hiskens, "Convexity of the set of feasible injections and revenue adequacy in FTR markets," *IEEE Trans. Power Syst.*, vol. 20, no. 4, pp. 1790–1798, Nov. 2005. [Online]. Available: http://ieeexplore.ieee.org/document/1525108/

[294] Y. V. Makarov, Z. Yang Dong, and D. J. Hill, "On convexity of power flow feasibility boundary," *IEEE Trans. Power Syst.*, vol. 23, no. 2, pp. 811–813, May 2008. [Online]. Available: http://ieeexplore.ieee.org/document/4470566/

[295] D. K. Molzahn, B. C. Lesieutre, and C. L. DeMarco, "Investigation of non-zero duality gap solutions to a semidefinite relaxation of the optimal power flow problem," in *Proc. 47th Hawaii Int. Conf. Syst. Sci.*, Jan. 2014, pp. 2325–2334. [Online]. Available: http://ieeexplore.ieee.org/document/6758891/

[296] J. Lavaei, D. Tse, and B. Zhang, "Geometry of power flows and optimization in distribution networks," *IEEE Trans. Power Syst.*, vol. 29, no. 2, pp. 572–583, Mar. 2014. [Online]. Available: http://ieeexplore.ieee.org/document/6624135/

[297] S. Chandra, D. Mehta, and A. Chakrabortty, "Equilibria analysis of power systems using a numerical homotopy method," in *Proc. IEEE Power Energy Soc. Gen. Meeting*, Jul. 2015, pp. 1–5. [Online]. Available: http://ieeexplore.ieee.org/document/7285823/

[298] B. Polyak and E. Gryazina, "Convexity/nonconvexity certificates for power flow analysis," in *Advances in Energy System Optimization*, V. Bertsch, W. Fichtner, V. Heuveline, and T. Leibfried, Eds. Cham, Switzerland: Springer, 2017, pp. 221–230.

[299] D. K. Molzahn, "Computing the feasible spaces of optimal power flow problems," *IEEE Trans. Power Syst.*, vol. 32, no. 6, pp. 4752–4763, Nov. 2017. [Online]. Available: http://ieeexplore.ieee.org/document/7879340/

[300] H.-D. Chiang and C.-Y. Jiang, "Feasible region of optimal power flow: Characterization and applications," *IEEE Trans. Power Syst.*, vol. 33, no. 1, pp. 236–244, Jan. 2018. [Online]. Available: http://ieeexplore.ieee.org/document/7913722/

[301] M. R. Narimani, D. K. Molzahn, D. Wu, and M. L. Crow, "Empirical investigation of non-convexities in optimal power flow problems," in *Proc. Annu. Amer. Control Conf. (ACC)*, Jun. 2018, pp. 3847–3854. [Online]. Available: https://ieeexplore.ieee.org/document/8431760/

[302] D. K. Molzahn, "Identifying and characterizing non-convexities in feasible spaces of optimal power flow problems," *IEEE Trans. Circuits Syst. II, Exp. Briefs*, vol. 65, no. 5, pp. 672–676, May 2018. [Online]. Available: https://ieeexplore.ieee.org/document/8332512/

[303] A. Dymarsky, E. Gryazina, S. Volodin, and B. Polyak, "Geometry of quadratic maps via convex relaxation," 2018, *arXiv:1810.00896*. [Online]. Available: http://arxiv.org/abs/1810.00896

[304] A. Dymarsky and K. Turitsyn, "Convexity of solvability set of power distribution networks," *IEEE Control Syst. Lett.*, vol. 3, no. 1, pp. 222–227, Jan. 2019. [Online]. Available: https://ieeexplore.ieee.org/document/8502879/

[305] K. Bestuzheva and H. Hijazi, "Invex optimization revisited," *J. Global Optim.*, vol. 74, no. 4, pp. 753–782, Aug. 2019, doi: 10.1007/s10898-018-0650-1.

[306] J. Nocedal and S. Wright, *Numerical Optimization*. New York, NY, USA: Springer, 2006.

[307] A. Wächter, "Nonlinear optimization algorithms," in *Advances and Trends in Optimization With Engineering Applications*, T. Terlaky, M. F. Anjos, and S. Ahmed, Eds. Philadelphia, PA, USA: Society for Industrial and Applied Mathematics, Apr. 2017, pp. 221–235. [Online]. Available: https://doi.org/10.1137/1.9781611974683.ch17 and [Online]. Available: http://epubs.siam.org/doi/10.1137/1.9781611974683.ch17

[308] V. Rigoni and A. Keane. (2020). *Open-DSOPF*. [Online]. Available: https://github.com/ValentinRigoni/Open-DSOPF

[309] X. Cao, J. Wang, and B. Zeng, "A study on the strong duality of conic relaxation of AC optimal power flow in radial networks," 2018, *arXiv:1807.08785*. [Online]. Available: http://arxiv.org/abs/1807.08785

[310] M. Slater, "Lagrange multipliers revisited," in *Traces and Emergence of Nonlinear Programming*, G. Giorgi and T. H. Kjeldsen, Eds. Basel, Switzerland: Springer, 2014, pp. 293–306, doi: 10.1007/978-3-0348-0439-4_14.

[311] A. Hauswirth, S. Bolognani, G. Hug, and F. Dorfler, "Generic existence of unique Lagrange multipliers in AC optimal power flow," *IEEE Control Syst. Lett.*, vol. 2, no. 4, pp. 791–796, Oct. 2018. [Online]. Available: https://ieeexplore.ieee.org/document/8391733/

[312] D. W. Peterson, "A review of constraint qualifications in finite-dimensional spaces," *SIAM Rev.*, vol. 15, no. 3, pp. 639–654, Jul. 1973. [Online]. Available: http://epubs.siam.org/doi/10.1137/1015075

[313] K. C. Almeida and F. D. Galiana, "Critical cases in the optimal power flow," *IEEE Trans. Power Syst.*, vol. 11, no. 3, pp. 1509–1518, Aug. 1996. [Online]. Available: http://ieeexplore.ieee.org/document/535692/

[314] Y.-C. Wu, A. S. Debs, and R. E. Marsten, "A direct nonlinear predictor-corrector primal-dual interior point algorithm for optimal power flows," *IEEE Trans. Power Syst.*, vol. 9, no. 2, pp. 876–883, May 1994. [Online]. Available: http://ieeexplore.ieee.org/document/317660/

[315] S. Granville, "Optimal reactive dispatch through interior point methods," *IEEE Trans. Power Syst.*, vol. 9, no. 1, pp. 136–146, Feb. 1994. [Online]. Available: http://ieeexplore.ieee.org/document/317548/

[316] G. D. Irisarri, X. Wang, J. Tong, and S. Mokhtari, "Maximum loadability of power systems using interior point nonlinear optimization method," *IEEE Trans. Power Syst.*, vol. 12, no. 1, pp. 162–172, Feb. 1997. [Online]. Available: http://ieeexplore.ieee.org/document/574936/

[317] G. L. Torres and V. H. Quintana, "An interior-point method for nonlinear optimal power flow using voltage rectangular coordinates," *IEEE Trans. Power Syst.*, vol. 13, no. 4, pp. 1211–1218, Nov. 1998. [Online]. Available: http://ieeexplore.ieee.org/document/736231/

[318] K. Clement, "An interior point algorithm for weighted least absolute value power system state estimation," PWRS, New York, NY, USA, Tech. Rep. 91 WM 235-2, 1991.

[319] K. Ponnambalam, V. H. Quintana, and A. Vannelli, "A fast algorithm for power system optimization problems using an interior point method," *IEEE Trans. Power Syst.*, vol. 7, no. 2, pp. 892–899, May 1992.

[320] H. Wei, H. Sasaki, and R. Yokoyama, "An application of interior point quadratic programming algorithm to power system optimization problems," *IEEE Trans. Power Syst.*, vol. 11, no. 1, pp. 260–266, Feb. 1996. [Online]. Available: http://ieeexplore.ieee.org/document/486104/

[321] H. Wang, C. E. Murillo-Sanchez, R. D. Zimmerman, and R. J. Thomas, "On computational issues of market-based optimal power flow," *IEEE Trans. Power Syst.*, vol. 22, no. 3, pp. 1185–1193, Aug. 2007. [Online]. Available: http://ieeexplore.ieee.org/document/4282060/

[322] F. Capitanescu and L. Wehenkel, "Experiments with the interior-point method for solving large scale optimal power flow problems," *Electr. Power Syst. Res.*, vol. 95, pp. 276–283, Feb. 2013, doi: 10.1016/j.epsr.2012.10.001.

[323] A. Forsgren, "On warm starts for interior methods," in *Proc. IFIP Conf. Syst. Modeling Optim.* New York, NY, USA: Springer, 2005, pp. 51–66.

[324] A. Forsgren, P. E. Gill, and M. H. Wright, "Interior methods for nonlinear optimization," *SIAM Rev.*, vol. 44, no. 4, pp. 525–597, Apr. 2002. [Online]. Available: http://epubs.siam.org/doi/10.1137/S0036144502414942

[325] F. Capitanescu, M. Glavic, D. Ernst, and L. Wehenkel, "Interior-point based algorithms for the solution of optimal power flow problems," *Electric Power Syst. Res.*, vol. 77, nos. 5–6, pp. 508–517, Apr. 2007.

[326] N. Gould, D. Orban, and P. Toint, "Numerical methods for large-scale nonlinear optimization," *Acta Numer.*, vol. 14, pp. 299–361, May 2005. https://www.cambridge.org/core/product/identifier/S0962492904000248/type/journal_article

[327] R. J. Vanderbei, "LOQO: An interior point code for quadratic programming," *Optim. Methods Softw.*, vol. 11, nos. 1–4, pp. 451–484, 1999.

[328] R. H. Byrd, J. Nocedal, and R. A. Waltz, "Knitro: An integrated package for nonlinear optimization," in *Large-Scale Nonlinear Optimization*, G. Di Pillo and M. Roma, Eds. Boston, MA: Springer, 2006, pp. 35–59, doi: 10.1007/0-387-30065-1_4.

[329] A. Wächter and L. T. Biegler, "On the implementation of an interior-point filter line-search algorithm for large-scale nonlinear programming," *Math. Program.*, vol. 106, no. 1, pp. 25–57, May 2006. [Online]. Available: http://dx.doi.org/10.1007/s10107-004-0559-y

[330] V. Rigoni and A. Keane, "Open-DSOPF: An open-source optimal power flow formulation integrated with OpenDSS," in *Proc. IEEE Power Energy Soc. Gen. Meeting (PESGM)*, Aug. 2020, pp. 1–5. [Online]. Available: https://ieeexplore.ieee.org/document/9282125/

[331] R. Lincoln. (2010). *PYPOWER*. [Online]. Available: https://pypi.org/project/PYPOWER/

[332] COIN-OR Foundation. (2005). *Ipopt*. [Online]. Available: https://github.com/coin-or/Ipopt

[333] A. Wächter, "An interior point algorithm for large-scale nonlinear optimization with applications in process engineering," Ph.D. dissertation, Dept. Chem. Eng., Carnegie Mellon Univ., Pittsburgh, PA, USA, 2002. [Online]. Available: http://users.iems.northwestern.edu/~andreasw/pubs/waechter_thesis.pdf

[334] A. Wächter and L. T. Biegler, "Line search filter methods for nonlinear programming: Local convergence," *SIAM J. Optim.*, vol. 16, no. 1, pp. 32–48, Jan. 2005. [Online]. Available: http://epubs.siam.org/doi/10.1137/S1052623403426544

[335] A. Wächter and L. T. Biegler, "Line search filter methods for nonlinear programming: Motivation and global convergence," *SIAM J. Optim.*, vol. 16, no. 1, pp. 1–31, 2005. http://epubs.siam.org/doi/10.1137/S1052623403426544. [Online]. Available: http://epubs.siam.org/doi/10.1137/S1052623403426556

[336] J. Nocedal, A. Wächter, and R. A. Waltz, "Adaptive barrier update strategies for nonlinear interior methods," *SIAM J. Optim.*, vol. 19, no. 4, pp. 1674–1693, Jan. 2009. [Online]. Available: http://epubs.siam.org/doi/10.1137/060649513

[337] R. C. Burchett, H. H. Happ, and D. R. Vierath, "Quadratically convergent optimal power flow," *IEEE Trans. Power App. Syst.*, vol. PAS-103, no. 11, pp. 3267–3275, Nov. 1984. [Online]. Available: http://ieeexplore.ieee.org/document/4112441/

[338] P. E. Gill, W. Murray, and M. A. Saunders, "SNOPT: An SQP algorithm for large-scale constrained optimization," *SIAM J. Optim.*, vol. 12, no. 4, pp. 979–1006, 2002. [Online]. Available: http://epubs.siam.org/doi/10.1137/S1052623499350013

[339] R. Fletcher and S. Leyffer, "Nonlinear programming without a penalty function," *Math. Program.*, vol. 91, no. 2, pp. 239–269, Jan. 2002. [Online]. Available: http://link.springer.com/10.1007/s101070100244

[340] S. Boyd and L. Vandenberghe, *Convex Optimization*. Cambridge, U.K.: Cambridge Univ. Press, Mar. 2004. [Online]. Available: https://www.cambridge.org/core/product/identifier/9780511804441/type/book

[341] G. Strang, *Linear Algebra and Its Applications*, 3rd ed. Orlando, FL, USA: Harcourt Brace Jovanovich, 1988.

[342] M. S. Lobo, L. Vandenberghe, S. Boyd, and H. Lebret, "Applications of second-order cone programming," *Linear Algebra Appl.*, vol. 284, nos. 1–3, pp. 193–228, Nov. 1998. [Online]. Available: https://linkinghub.elsevier.com/retrieve/pii/S0024379598100320

[343] J. C. Gilbert and C. Josz, "Plea for a semidefinite optimization solver in complex numbers," LAAS-Laboratoire d'analyse et d'architecture des systèmes, Toulouse, France, Tech. Rep. hal-01497173, 2017. [Online]. Available: http://www.optimization-online.org/DB_FILE/2017/03/5929.pdf

[344] C. Josz and D. K. Molzahn, "Lasserre hierarchy for large scale polynomial optimization in real and complex variables," *SIAM J. Optim.*, vol. 28, no. 2, pp. 1017–1048, Jan. 2018. [Online]. Available: https://epubs.siam.org/doi/10.1137/15M1034386

[345] C. Josz and D. K. Molzahn, "Moment/sum-of-squares hierarchy for complex polynomial optimization," 2015, *arXiv:1508.02068*. [Online]. Available: http://arxiv.org/abs/1508.02068

[346] D. K. Molzahn, I. A. Hiskens, C. Josz, and P. Panciatici, "Computational analysis of sparsity-exploiting moment relaxations of the OPF problem," in *Proc. Power Syst. Comput. Conf. (PSCC)*, Jun. 2016, pp. 1–7. [Online]. Available: http://ieeexplore.ieee.org/document/7540831/

[347] R. Y. Zhang, C. Josz, and S. Sojoudi, "Conic optimization theory: Convexification techniques and numerical algorithms," in *Proc. Annu. Amer. Control Conf. (ACC)*, Jun. 2018, pp. 798–815. [Online]. Available: https://ieeexplore.ieee.org/document/8430887/

[348] MOSEK ApS. (2021). *MOSEK Modeling Cookbook Release 3.2.2*. [Online]. Available: https://docs.mosek.com/MOSEKModelingCookbook-letter.pdf

[349] J. Löfberg, "YALMIP: A toolbox for modeling and optimization in MATLAB," in *Proc. IEEE Int. Conf. Robot. Automat.*, Sep. 2004, pp. 284–289.

[350] M. Grant and S. Boyd. (2020). *CVX: MATLAB Software for Disciplined Convex Programming, Version 2.2*. [Online]. Available: http://cvxr.com/cvx/

[351] M. Kočvara and M. Stingl. (2006). *PENSDP User's Guide (Version 2.2)*. [Online]. Available: http://www.penopt.com/doc/pensdp2_2.pdf

[352] M. Yamashita, K. Fujisawa, M. Fukuda, K. Kobayashi, K. Nakata, and M. Nakata, "Latest developments in the sdpa family for solving large-scale sdps," in *Handbook on Semidefinite, Conic and Polynomial Optimization*, M. F. Anjos and J. B. Lasserre, Eds. Boston, MA, USA: Springer, 2012, pp. 687–713, doi: 10.1007/978-1-4614-0769-0_24.

[353] R. H. Tutuncu, K. C. Toh, and M. J. Todd, "Solving semidefinite-quadratic-linear programs using SDPT3," *Math. Program.*, vol. 95, no. 2, pp. 189–217, 2003.

[354] B. Borchers, "CSDP, AC library for semidefinite programming," *Optim. Methods Softw.*, vol. 11, nos. 1–4, pp. 613–623, 1999.

[355] J. F. Sturm, "Using SeDuMi 1.02, a MATLAB toolbox for optimization over symmetric cones," *Optim. Methods Softw.*, vol. 11, nos. 1–4, pp. 625–653, 1999.

[356] T. Gally, M. E. Pfetsch, and S. Ulbrich, "A framework for solving mixed-integer semidefinite programs," *Optim. Methods Softw.*, vol. 33, no. 3, pp. 594–632, May 2018.

[357] M. Lubin, E. Yamangil, R. Bent, and J. P. Vielma, "Extended formulations in mixed-integer convex programming," in *Proc. Int. Conf. Integer Program. Combinat. Optim.* Cham, Switzerland: Springer, 2016, pp. 102–113.

[358] J. Löfberg. (2021). *Solvers*. [Online]. Available: https://yalmip.github.io/allsolvers/

[359] I. Dunning, J. Huchette, and M. Lubin, "JuMP: A modeling language for mathematical optimization," *SIAM Rev.*, vol. 59, no. 2, pp. 295–320, 2017. [Online]. Available: https://epubs.siam.org/doi/10.1137/15M1020575

[360] W. E. Hart, J.-P. Watson, and D. L. Woodruff, "Pyomo: Modeling and solving mathematical programs in python," *Math. Program. Comput.*, vol. 3, no. 3, pp. 219–260, 2011.

[361] O. Kröger, C. Coffrin, H. Hijazi, and H. Nagarajan, "Juniper: An open-source nonlinear branch-and-bound solver in Julia," in *Integration of Constraint Programming, Artificial Intelligence, and Operations Research*, W.-J. van Hoeve, Ed. Cham, Switzerland: Springer, 2018, pp. 377–386.

[362] MATPOWER. (2010). *MATPOWER*. [Online]. Available: https://matpower.org/

[363] R. Lincoln. (2010). *oct2Pypower*. [Online]. Available: https://github.com/rwl/oct2pypower

[364] R. D. Zimmerman and C. E. Murillo-Sánchez. (2011). *Matpower 4.1, User's Manual*. [Online]. Available: https://matpower.org/docs/MATPOWER-manual-4.1.pdf

[365] R. D. Zimmerman and C. E. Murillo-Sánchez. (2020). *MATPOWER User's Manual, Version 7.1*. [Online]. Available: https://matpower.org/docs/MATPOWER-manual.pdf

[366] MATPOWER. (2020). *MATPOWER Based Web Application*. [Online]. Available: https://matpower.app/

[367] R. D. Zimmerman, C. E. Murillo-Sánchez, and R. J. Thomas, "MATPOWER's extensible optimal power flow architecture," in *Proc. IEEE Power Energy Soc. Gen. Meeting*, Jul. 2009, pp. 1–7. [Online]. Available: http://ieeexplore.ieee.org/document/5275967/

[368] C. E. Murillo-Sánchez. (1997). *BPMPD_MEX*. [Online]. Available: https://www.pserc.cornell.edu/bpmpd/

[369] C. Mészáros, "The efficient implementation of interior point methods for linear programming and their applications," Ph.D. dissertation, Comput. Automat. Res. Inst., Univ. Sci. Eötvös Loránd, Budapest, Hungary1996.

[370] B. A. Murtagh, "MINOS 5.5 user's guide," Systems Optim. Lab., Stanford Univ., Stanford, CA, USA, Tech. Rep. SOL 83-20R, 1998. [Online]. Available: http://www.sbsi-sol-optimize.com/asp/sol_product_minos.htm

[371] C. E. Murillo-Ssánchez. (2007). *MINOPF*. [Online]. Available: https://www.pserc.cornell.edu/minopf/

[372] H. Wang and R. D. Zimmerman, "Matpower interior point solver, MIPS 1.4, user's manual," Power Syst. Eng. Res. Center (PSERC), New York, NY, USA, Tech. Rep., 2020. [Online]. Available: https://github.com/MATPOWER/mips/blob/master/docs/MIPS-manual.pdf

[373] Gurobi Optimization. (2016). *Gurobi Optimizer Reference Manual*. [Online]. Available: https://www.gurobi.com/

[374] A. Makhorin. (2000). *GLPK (GNU Linear Programming Kit)*. [Online]. Available: https://www.gnu.org/software/glpk/

[375] COIN-OR Foundation. (2002). *COIN-OR Linear Programming (CLP) Solver*. [Online]. Available: https://github.com/coin-or/Clp

[376] R. D. Zimmerman, "MP-opt-model user's manual, version 3.0," Power Syst. Eng. Res. Center (PSERC), Tech. Rep., 2020. [Online]. Available: https://github.com/MATPOWER/mp-opt-model/blob/master/docs/MP-Opt-Model-manual.pdf

[377] V. Rigoni and A. Keane. (2020). *Getting Started*. Univ. College Dublin, Dublin, Ireland. [Online]. Available: https://github.com/ValentinRigoni/Open-DSOPF/blob/master/Tutorial/Getting started.pdf

[378] V. Rigoni and A. Keane. (2020). *Publicly Available Networks*. [Online]. Available: https://github.com/ValentinRigoni/Open-DSOPF/blob/master/Tutorial/Publicly available networks.pdf

[379] V. Rigoni and A. Keane. (2020). *Solvers—IPOPT*. [Online]. Available: https://github.com/ValentinRigoni/Open-DSOPF/blob/master/Tutorial/Solvers-IPOPT.pdf
[380] Los Alamos ANSI. (2018). *PowerModelsDistribution.Jl*. [Online]. Available: https://github.com/lanl-ansi/PowerModelsDistribution.jl
[381] C. Coffrin, R. Bent, B. Tasseff, K. Sundar, and S. Backhaus, "Relaxations of AC maximal load delivery for severe contingency analysis," *IEEE Trans. Power Syst.*, vol. 34, no. 2, pp. 1450–1458, Mar. 2019. [Online]. Available: https://ieeexplore.ieee.org/document/8494809/
[382] Los Alamos ANSI. (2020). *PowerModelsDistribution.jl Documentation*. [Online]. Available: https://lanl-ansi.github.io/PowerModelsDistribution.jl/stable/
[383] K. P. Schneider, B. A. Mather, B. C. Pal, C. W. Ten, G. J. Shirek, H. Zhu, J. C. Fuller, J. L. Pereira, L. F. Ochoa, L. R. De Araujo, R. C. Dugan, S. Matthias, S. Paudyal, T. E. McDermott, and W. Kersting, "Analytic considerations and design basis for the IEEE distribution test feeders," *IEEE Trans. Power Syst.*, vol. 33, no. 3, pp. 3181–3188, Oct. 2017.
[384] Operation Technology. (2021). *ETAP*. [Online]. Available: https://etap.com/?msclkid=d3847d7e7b8c1923600d1df7534ea17f
[385] M. Niu, C. Wan, and Z. Xu, "A review on applications of heuristic optimization algorithms for optimal power flow in modern power systems," *J. Mod. Power Syst. Clean Energy*, vol. 2, no. 4, pp. 289–297, Dec. 2014. [Online]. Available: http://link.springer.com/10.1007/s40565-014-0089-4
[386] S. S. Reddy and P. R. Bijwe, "Efficiency improvements in meta-heuristic algorithms to solve the optimal power flow problem," *Int. J. Elect. Power Energy Syst.*, vol. 82, pp. 288–302, Nov. 2016. [Online]. Available: http://dx.doi.org/10.1016/j.ijepes.2016.03.028
[387] IEEE PES-Power Grid Lib. (2021). *Benchmarks for the Optimal Power Flow Problem*. [Online]. Available: https://github.com/power-grid-lib/pglib-opf
[388] IEEE PES-Power Grid Lib. (2021). *A Library of IEEE PES Power Grid Benchmarks*. [Online]. Available: https://github.com/power-grid-lib

IBRAHIM ANWAR IBRAHIM (Member, IEEE) received the B.Sc. degree in electrical engineering from An-Najah National University, Nablus, Palestine, in 2014, and the M.Sc. degree in electrical, electronic and systems engineering from Universiti Kebangsaan Malaysia, Bangi, Malaysia, in 2016. He is currently pursuing the Ph.D. degree with the School of Engineering, Macquarie University, Sydney, Australia.

He is also a Visiting Ph.D. Scholar with the CSIRO Energy Centre, Newcastle, Australia. His research interests include photovoltaic (PV) systems modeling and optimization, renewable energy integration, power quality, micro grids, smart grids, and artificial intelligence and machine learning applications for solar energy and PV systems. He is a member of the Institute of Electrical and Electronics Engineers, the Institution of Engineering and Technology, the International Solar Energy Society, the Australian Institute of Energy, the Electric Energy Society of Australia, the Engineers Without Borders Australia, the Australian Meteorological and Oceanographic Society, and the Jordanian Engineers Association.

M. J. HOSSAIN (Senior Member, IEEE) received the B.Sc. and M.Sc.Eng. degrees in electrical and electronic engineering from the Rajshahi University of Engineering & Technology (RUET), Bangladesh, in 2001 and 2005, respectively, and the Ph.D. degree in electrical and electronic engineering from the University of New South Wales, in 2010, Australia. He also received the Graduate Certificate in Higher Education degree from Griffith University, in 2014.

He is currently an Associate Professor with the School of Electrical and Data Engineering, University of Technology Sydney, Australia. Before joining there, he served as an Associate Professor with the School of Engineering, Macquarie University, for three and a half years, a Senior Lecturer and a Lecturer with the Griffith School of Engineering, Griffith University, Australia, for five years, and as a Research Fellow with the School of Information Technology and Electrical Engineering, University of Queensland, Brisbane, Australia. Previously, he worked as a Lecturer and an Assistant Professor at the Rajshahi University of Engineering & Technology, Bangladesh, for six years. His research interests include renewable energy integration and stabilization, voltage stability, micro grids and smart grids, robust control, electric vehicles, building energy management systems, and energy storage systems.